# TeV Halos and Searches for Dark Matter

TIM LINDEN

Satellites

Galactic Center

Milky Way Halo

Galaxy Clusters

Isotropic contributions

Features in γ-ray and cosmic-ray spectra
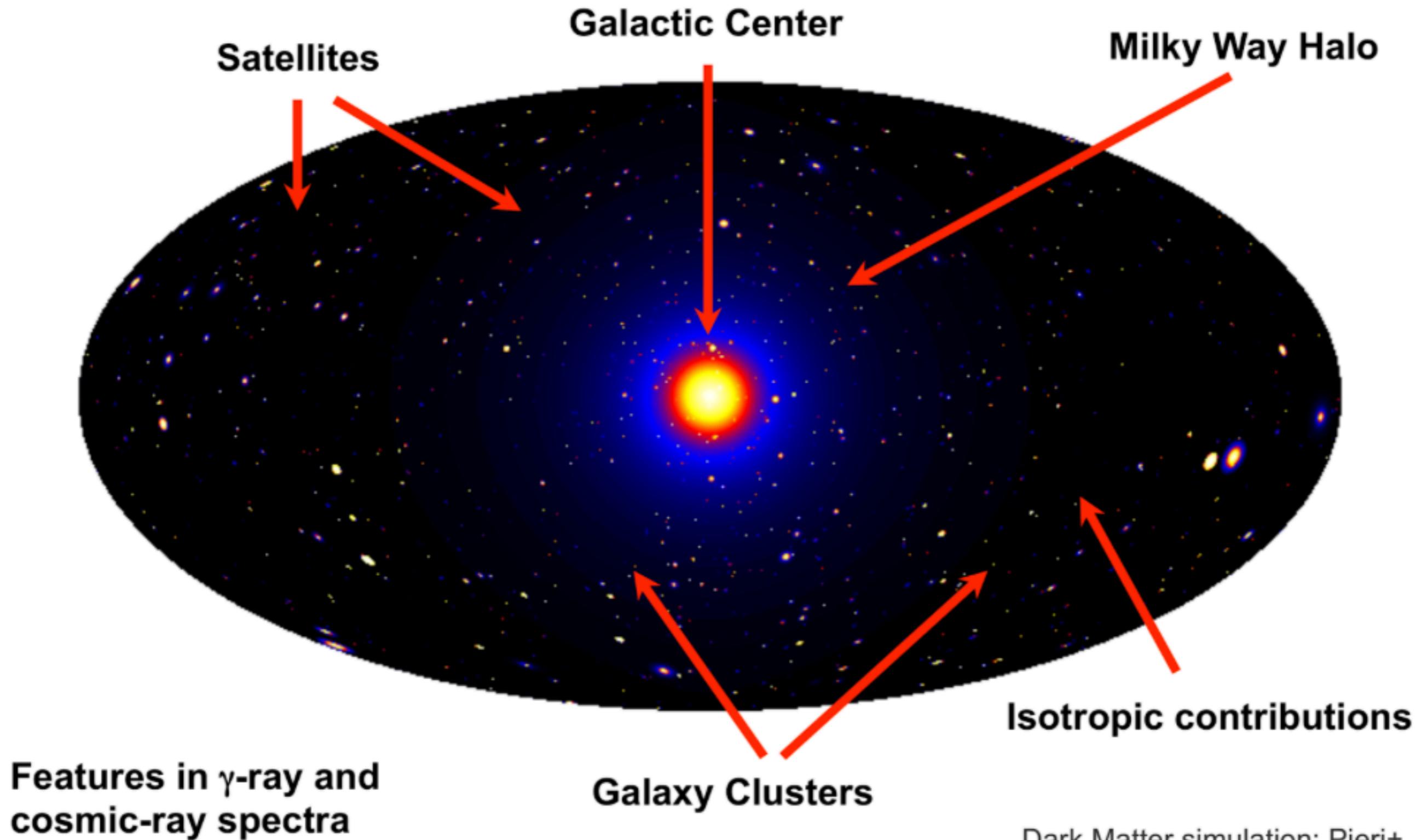
Dark Matter simulation: Pieri+ 2011PhRvD..83b3518P

▸ High Angular Resolution
  ▸ Point source separation and identification

▸ Long energy-lever arm (20 GeV — 100 TeV)
  ▸ Compare with Fermi: 100 MeV - 100 GeV

▸ Bifurcation in electron/proton morphology
  ▸ $D_{\text{proton}} \propto E^{\delta/2}$
  ▸ $D_{\text{electron}} \propto E^{\delta/2-1}$

▸ Difficulties: cosmic-ray background, inhomogeneous exposure.

▸ TeV Halos (Observationally):

    ▸ Bright at TeV energies

    ▸ Hard gamma-ray spectrum

    ▸ Surround young/middle-aged pulsars

    ▸ Relatively common

    ▸ Spatially extended

       ▸ Profile is diffusive



Geminga

Abeysekara et al. (2017; 1711.06223)
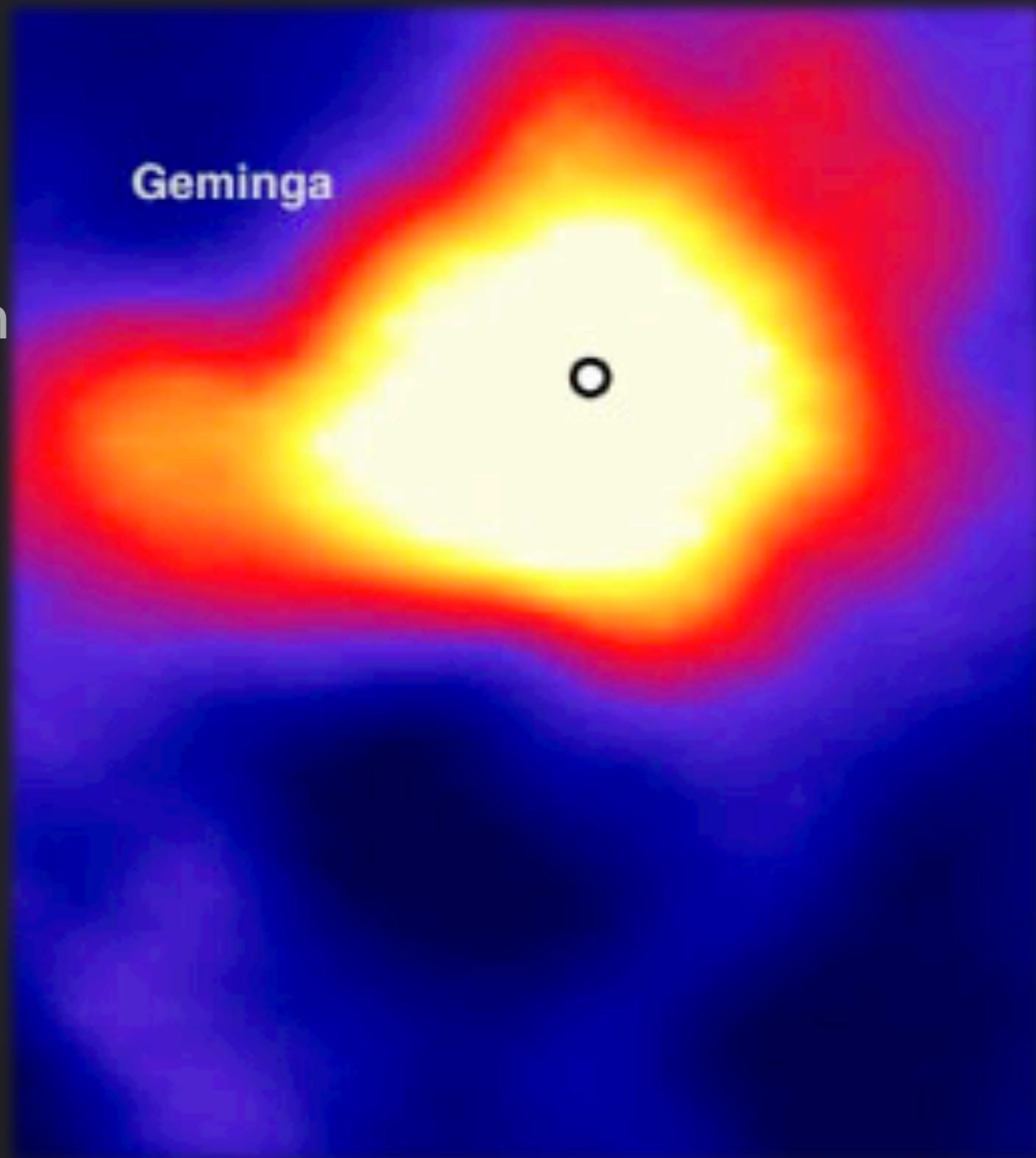
▸ Emission Profile is consistent with particle diffusion through the ISM.

▸ Strong evidence that particles are propagating through turbulent magnetic fields.
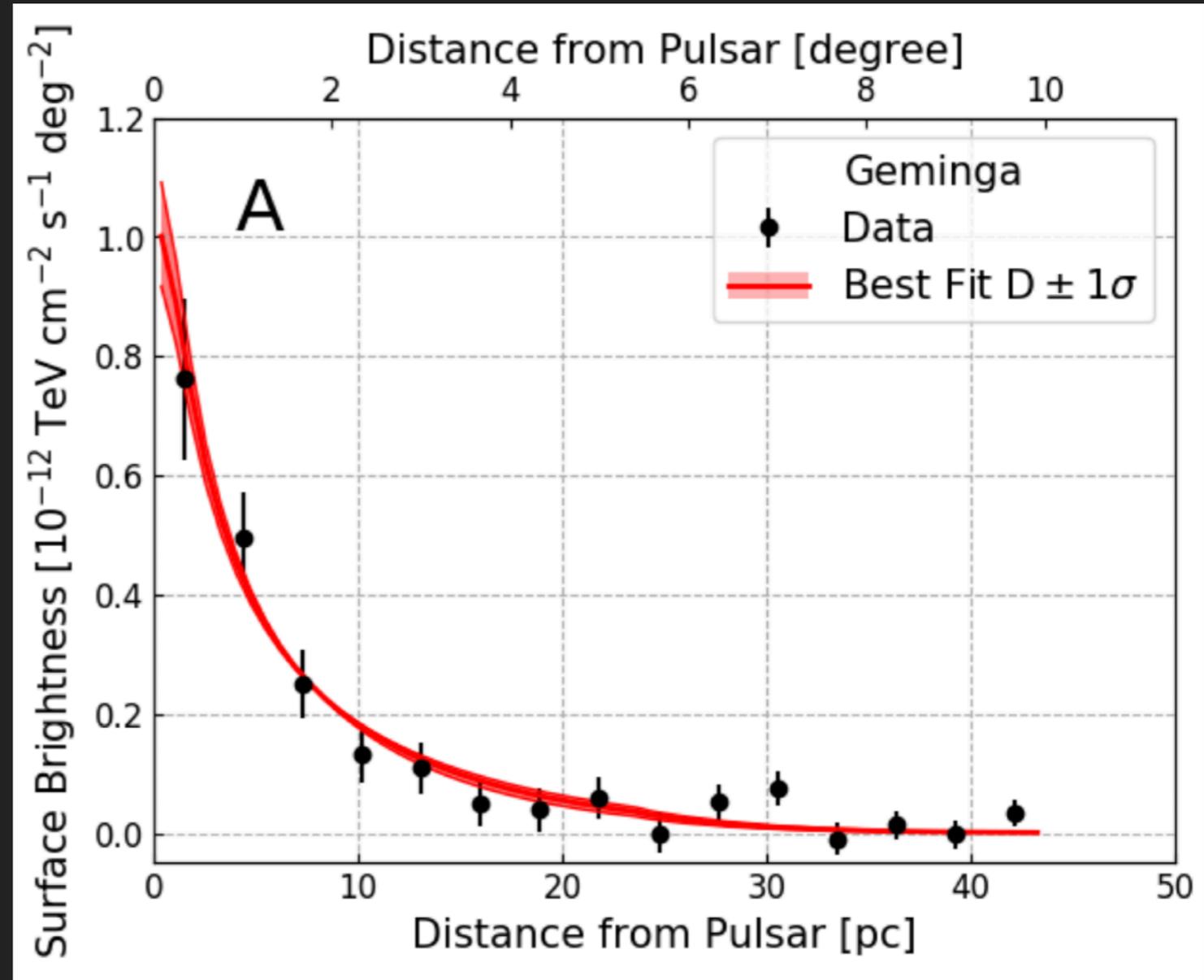
▸ But diffusion coefficient 2-orders of magnitude smaller than ISM!

▸ TeV Halos (Observationally):

  ▸ At least 7 detected systems

  ▸ Detected by all instruments (HAWC, LHAASO, HESS, VERITAS)

  ▸ Detected systems are nearby, or have high spin down power.
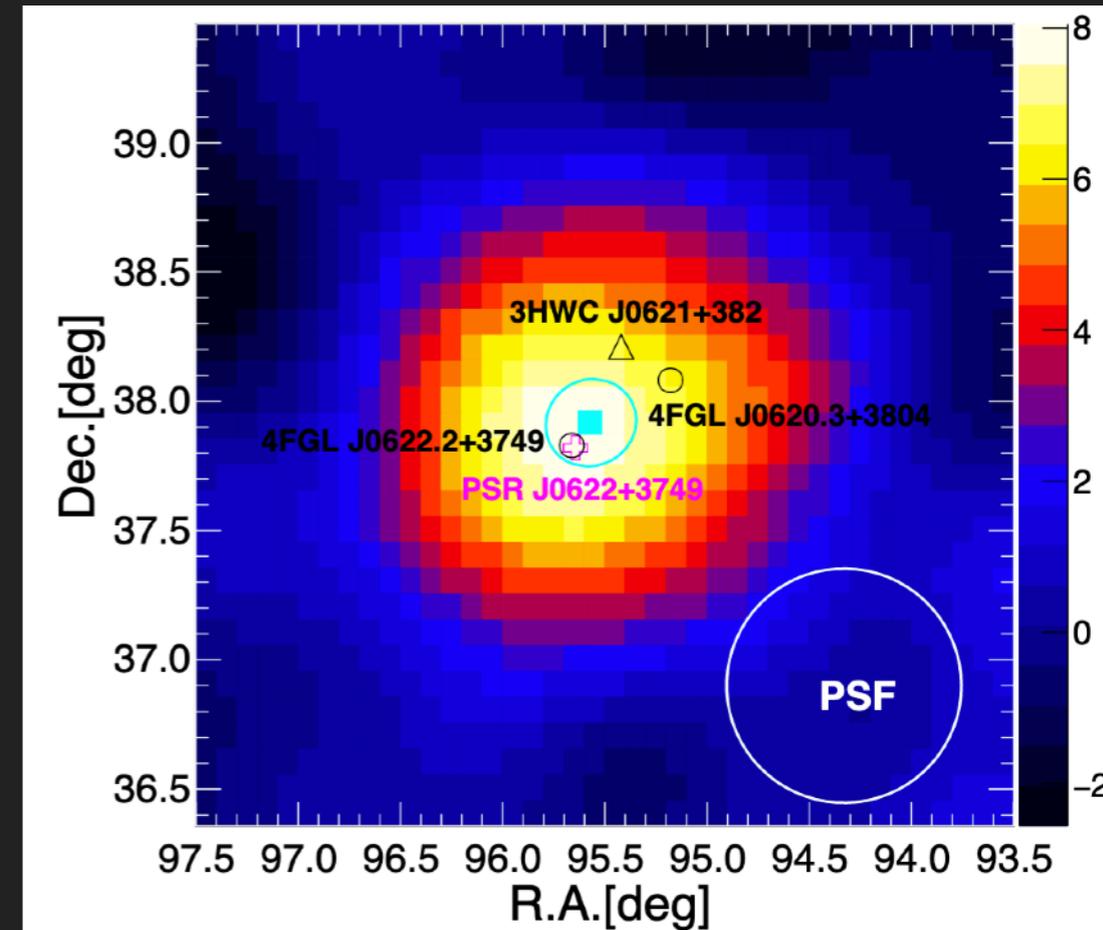


| ATNF Name | Dec. (°) | Distance (kpc) | Age (kyr) | Spindown Lum. (erg s$^{-1}$) | Spindown Flux (erg s$^{-1}$ kpc$^{-2}$) | 2HWC |
|---|---|---|---|---|---|---|
| J0633+1746 | 17.77 | 0.25 | 342 | 3.2e34 | 4.1e34 | 2HWC J0631+169 |
| B0656+14 | 14.23 | 0.29 | 111 | 3.8e34 | 3.6e34 | 2HWC J0700+143 |
| B1951+32 | 32.87 | 3.00 | 107 | 3.7e36 | 3.3e34 | — |
| J1740+1000 | 10.00 | 1.23 | 114 | 2.3e35 | 1.2e34 | — |
| J1913+1011 | 10.18 | 4.61 | 169 | 2.9e36 | 1.1e34 | 2HWC J1912+099 |
| J1831-0952 | -9.86 | 3.68 | 128 | 1.1e36 | 6.4e33 | 2HWC J1831-098 |
| J2032+4127 | 41.45 | 1.70 | 181 | 1.7e35 | 4.7e33 | 2HWC J2031+415 |
| B1822-09 | -9.58 | 0.30 | 232 | 4.6e33 | 4.1e33 | — |
| B1830-08 | -8.45 | 4.50 | 147 | 5.8e35 | 2.3e33 | — |
| J1913+0904 | 9.07 | 3.00 | 147 | 1.6e35 | 1.4e33 | — |
| B0540+23 | 23.48 | 1.56 | 253 | 4.1e34 | 1.4e33 | — |

- If TeV halo power is connected to pulsar spin down power, we can build a model of the full TeV sky.

- This means that many young systems should also produce even brighter TeV halo activity!

| # | PSRJ | P0 (s) | P1 | DIST (kpc) | AGE (Yr) | BSURF (G) | EDOT (ergs/s) |
|---|------|--------|-----|------------|----------|-----------|---------------|
| 1 | J0537−6910 | 0.016122 | 5.18e−14 | 49.700 | 4.93e+03 | 9.25e+11 | 4.88e+38 |
| 2 | J0534+2200 | 0.033392 | 4.21e−13 | 2.000 | 1.26e+03 | 3.79e+12 | 4.46e+38 |
| 3 | J0540−6919 | 0.050570 | 4.79e−13 | 49.700 | 1.67e+03 | 4.98e+12 | 1.46e+38 |
| 4 | J1813−1749 | 0.044741 | 1.27e−13 | 4.700 | 5.58e+03 | 2.41e+12 | 5.60e+37 |
| 5 | J1400−6325 | 0.031182 | 3.89e−14 | 7.000 | 1.27e+04 | 1.11e+12 | 5.07e+37 |
| 6 | J1747−2809 | 0.052153 | 1.56e−13 | 8.141 | 5.31e+03 | 2.88e+12 | 4.33e+37 |
| 7 | J1833−1034 | 0.061884 | 2.02e−13 | 4.100 | 4.85e+03 | 3.58e+12 | 3.37e+37 |
| 8 | J2022+3842 | 0.048579 | 8.61e−14 | 10.000 | 8.94e+03 | 2.07e+12 | 2.96e+37 |
| 9 | J0205+6449 | 0.065716 | 1.94e−13 | 3.200 | 5.37e+03 | 3.61e+12 | 2.70e+37 |
| 10 | J2229+6114 | 0.051624 | 7.83e−14 | 3.000 | 1.05e+04 | 2.03e+12 | 2.25e+37 |
| 11 | J1513−5908 | 0.151582 | 1.53e−12 | 4.400 | 1.57e+03 | 1.54e+13 | 1.73e+37 |
| 12 | J1617−5055 | 0.069357 | 1.35e−13 | 4.743 | 8.13e+03 | 3.10e+12 | 1.60e+37 |
| 13 | J1124−5916 | 0.135477 | 7.53e−13 | 5.000 | 2.85e+03 | 1.02e+13 | 1.19e+37 |
| 14 | J1930+1852 | 0.136855 | 7.51e−13 | 7.000 | 2.89e+03 | 1.03e+13 | 1.16e+37 |
| 15 | J1023−5746 | 0.111472 | 3.84e−13 | 2.080 | 4.60e+03 | 6.62e+12 | 1.09e+37 |
| 16 | J1420−6048 | 0.068180 | 8.32e−14 | 5.632 | 1.30e+04 | 2.41e+12 | 1.04e+37 |
| 17 | J1410−6132 | 0.050052 | 3.20e−14 | 13.510 | 2.48e+04 | 1.28e+12 | 1.01e+37 |
| 18 | J1849−0001 | 0.038523 | 1.42e−14 | * | 4.31e+04 | 7.47e+11 | 9.78e+36 |
| 19 | J1402+13 | 0.005890 | 4.83e−17 | * | 1.93e+06 | 1.71e+10 | 9.34e+36 |
| 20 | J1846−0258 | 0.326571 | 7.11e−12 | 5.800 | 7.28e+02 | 4.88e+13 | 8.06e+36 |
| 21 | J0835−4510 | 0.089328 | 1.25e−13 | 0.280 | 1.13e+04 | 3.38e+12 | 6.92e+36 |
| 22 | J1811−1925 | 0.064667 | 4.40e−14 | 5.000 | 2.33e+04 | 1.71e+12 | 6.42e+36 |
| 23 | J1111−6039 | 0.106670 | 1.95e−13 | * | 8.66e+03 | 4.62e+12 | 6.35e+36 |
| 24 | J1813−1246 | 0.048072 | 1.76e−14 | 2.635 | 4.34e+04 | 9.30e+11 | 6.24e+36 |
| 25 | J1838−0537 | 0.145708 | 4.72e−13 | * | 4.89e+03 | 8.39e+12 | 6.02e+36 |
| 26 | J1838−0655 | 0.070498 | 4.92e−14 | 6.600 | 2.27e+04 | 1.89e+12 | 5.55e+36 |
| 27 | J1418−6058 | 0.110573 | 1.69e−13 | 1.885 | 1.03e+04 | 4.38e+12 | 4.95e+36 |
| 28 | J1935+2025 | 0.080118 | 6.08e−14 | 4.598 | 2.09e+04 | 2.23e+12 | 4.66e+36 |
| 29 | J1856+0245 | 0.080907 | 6.21e−14 | 6.318 | 2.06e+04 | 2.27e+12 | 4.63e+36 |
| 30 | J1112−6103 | 0.064962 | 3.15e−14 | 4.500 | 3.27e+04 | 1.45e+12 | 4.53e+36 |
| 31 | J1640−4631 | 0.206443 | 9.76e−13 | 12.750 | 3.35e+03 | 1.44e+13 | 4.38e+36 |
| 32 | J1844−0346 | 0.112855 | 1.55e−13 | * | 1.16e+04 | 4.23e+12 | 4.25e+36 |
| 33 | J1952+3252 | 0.039531 | 5.84e−15 | 3.000 | 1.07e+05 | 4.86e+11 | 3.74e+36 |
| 34 | J1826−1256 | 0.110224 | 1.21e−13 | 1.550 | 1.44e+04 | 3.70e+12 | 3.58e+36 |
| 35 | J1709−4429 | 0.102459 | 9.30e−14 | 2.600 | 1.75e+04 | 3.12e+12 | 3.41e+36 |
| 36 | J2021+3651 | 0.103741 | 9.57e−14 | 1.800 | 1.72e+04 | 3.19e+12 | 3.38e+36 |
| 37 | J1524−5625 | 0.078219 | 3.90e−14 | 3.378 | 3.18e+04 | 1.77e+12 | 3.21e+36 |
| 38 | J1357−6429 | 0.166108 | 3.60e−13 | 3.100 | 7.31e+03 | 7.83e+12 | 3.10e+36 |
| 39 | J1913+1011 | 0.035909 | 3.37e−15 | 4.613 | 1.69e+05 | 3.52e+11 | 2.87e+36 |
| 40 | J1826−1334 | 0.101487 | 7.53e−14 | 3.606 | 2.14e+04 | 2.80e+12 | 2.84e+36 |
| 41 | J1907+0602 | 0.106633 | 8.68e−14 | 2.370 | 1.95e+04 | 3.08e+12 | 2.83e+36 |
| 42 | J1801−2451 | 0.124924 | 1.28e−13 | 3.803 | 1.55e+04 | 4.04e+12 | 2.59e+36 |
| 43 | J1016−5857 | 0.107386 | 8.08e−14 | 3.163 | 2.10e+04 | 2.98e+12 | 2.58e+36 |
| 44 | J1747−2958 | 0.098814 | 6.13e−14 | 2.520 | 2.55e+04 | 2.49e+12 | 2.51e+36 |
| 45 | J1105−6107 | 0.063202 | 1.58e−14 | 2.360 | 6.32e+04 | 1.01e+12 | 2.48e+36 |
| 46 | J1119−6127 | 0.407963 | 4.02e−12 | 8.400 | 1.61e+03 | 4.10e+13 | 2.34e+36 |
| 47 | J1824−2452A | 0.003054 | 1.62e−18 | 5.500 | 2.99e+07 | 2.25e+09 | 2.24e+36 |
| 48 | J1803−2137 | 0.133667 | 1.34e−13 | 4.400 | 1.58e+04 | 4.29e+12 | 2.22e+36 |
| 49 | J1135−6055 | 0.114943 | 7.93e−14 | * | 2.30e+04 | 3.05e+12 | 2.06e+36 |
| 50 | J1048−5832 | 0.123725 | 9.61e−14 | 2.900 | 2.04e+04 | 3.49e+12 | 2.00e+36 |

Di Mauro, Manconi, Donato (2019; 1908.03216)
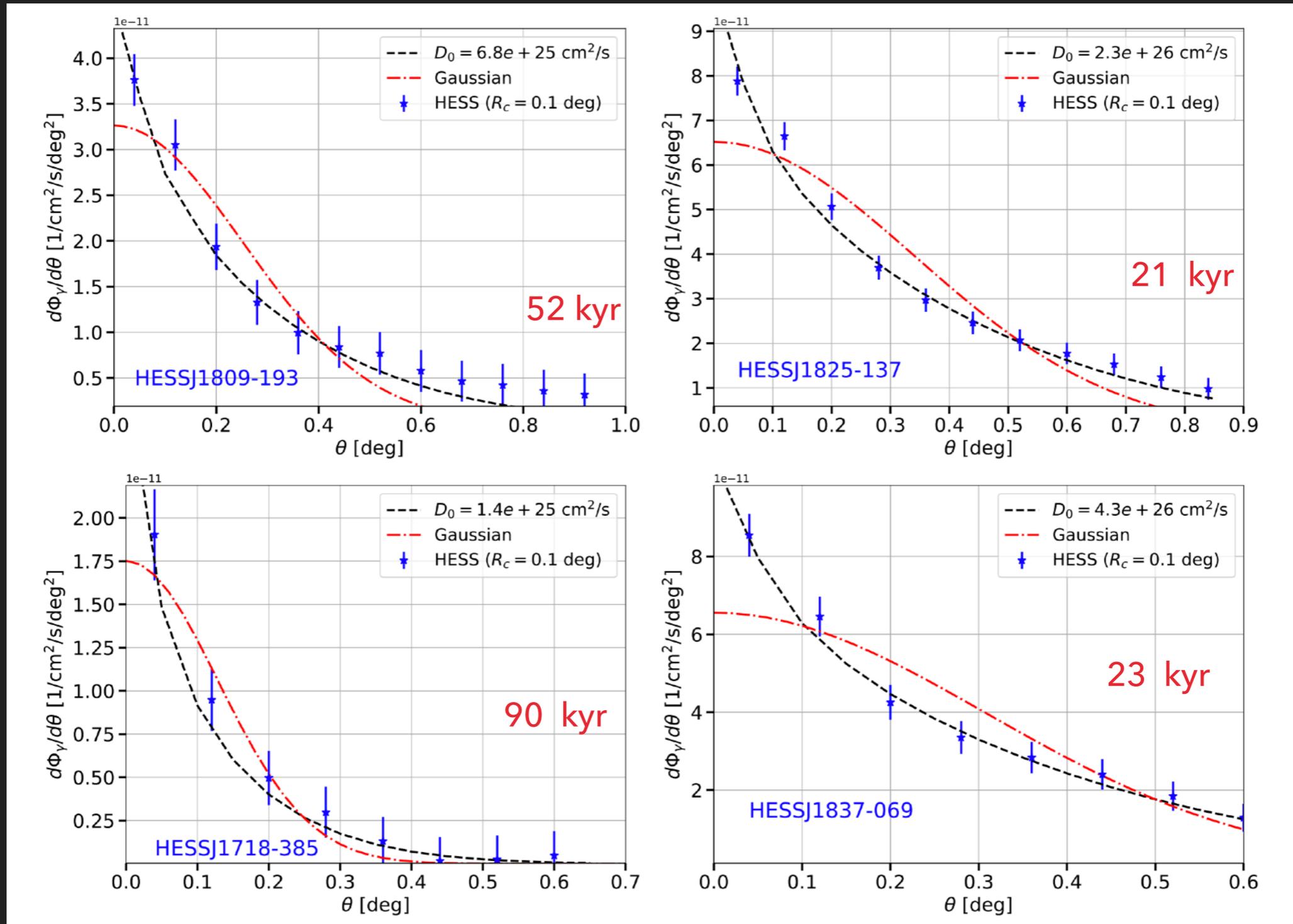


▸ Younger systems produce extended, diffusive halos

Sudoh, TL, Hooper (2021; 2101.11026)

▸ 8 out of 9 HAWC sources above 56 TeV are consistent with pulsars.

▸ Most have spectra more consistent with leptonic, rather than hadronic, emission.
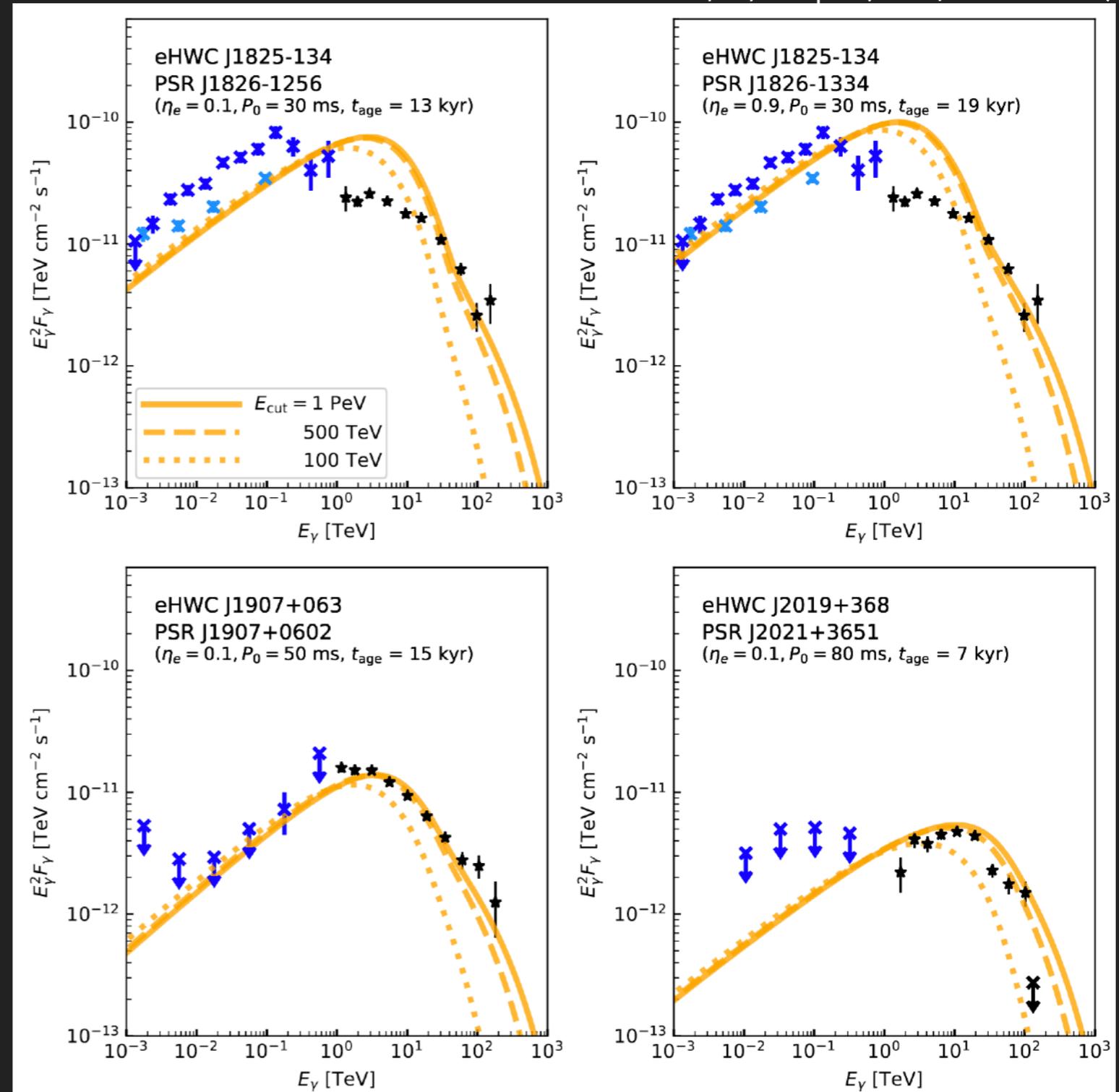


▸ The youngest systems produce very bright emission

▸ In addition to being much larger – the evolution of the TeV halo morphology is very different

PWN in the ISM have a radius that is proportional to spindown power.

$$R_{\mathrm{PWN}} \simeq 1.5 \left( \frac{\dot{E}}{10^{35}\,\mathrm{erg/s}} \right)^{1/2} \times$$
$$\left( \frac{n_{\mathrm{gas}}}{1\,\mathrm{cm}^{-3}} \right)^{-1/2} \left( \frac{v}{100\,\mathrm{km/s}} \right)^{-3/2} \mathrm{pc}$$
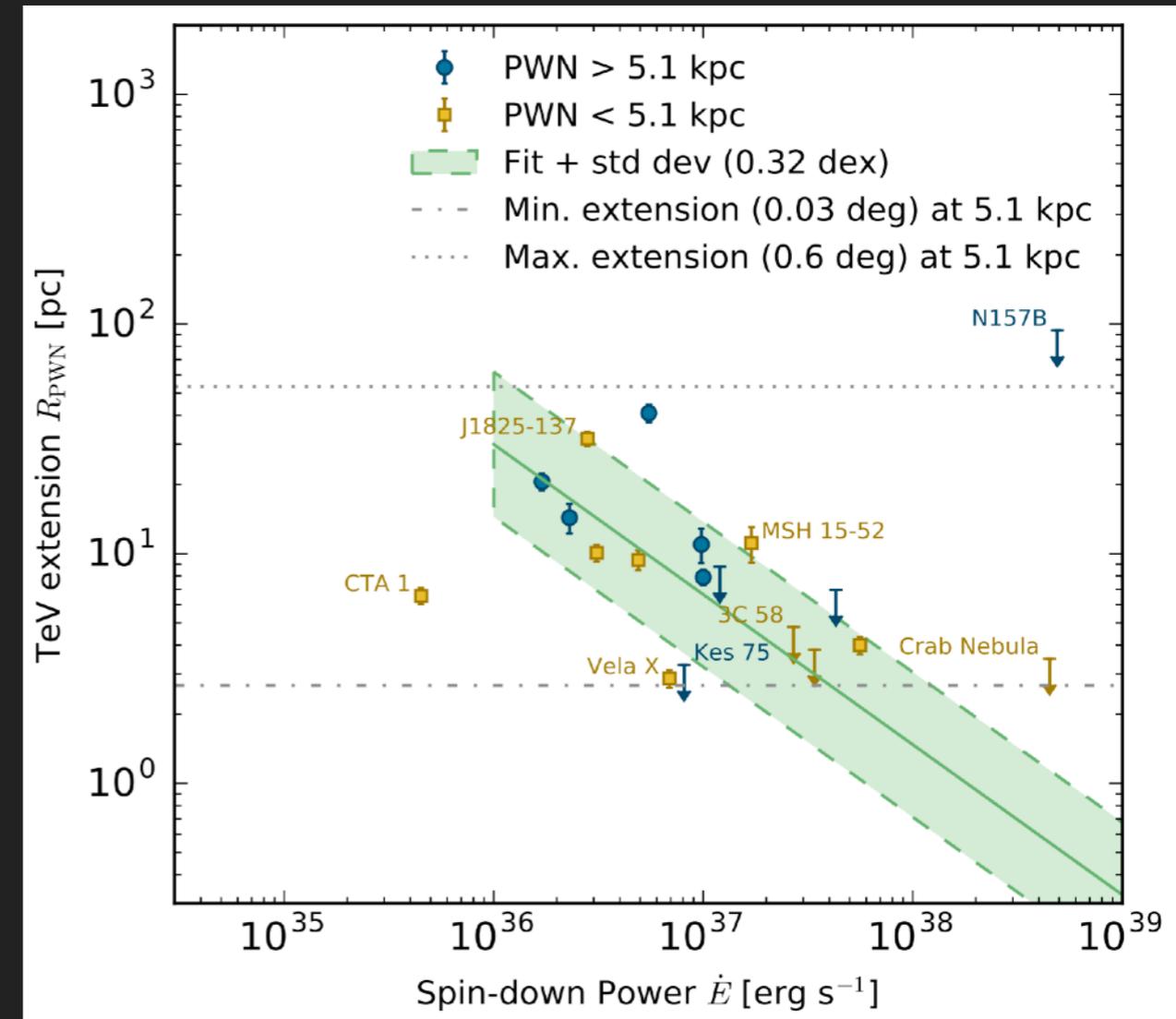


TeV Halos have an extension that is inversely proportional to spindown power (perhaps, proportional to age).

- An alternative definition of a "TeV halo" has been used by Giacinti et al. 2019 (1907.12121)

- Linden et al. (2017) - A TeV halo is a leptonic gamma-ray source surrounding a pulsar, where the electrons are diffusing through the medium (rather than being driven by convective pulsar winds).

- Giacinti et al. (2019) - A TeV halo is a leptonic gamma-ray source surrounding a pulsar, where the emission stems from a region where the electron density falls below the ambient ISM electron density.

▸ This Distinction Creates Confusion:

▸ Key Questions:

▸ Do pulsars convert a large fraction of their spin down power to e+e- pairs?

▸ Do these e+e- cool via synchrotron or ICS?

▸ Are these electrons confined near the pulsar?

▸ Do these electrons dominate turbulence in the ISM?
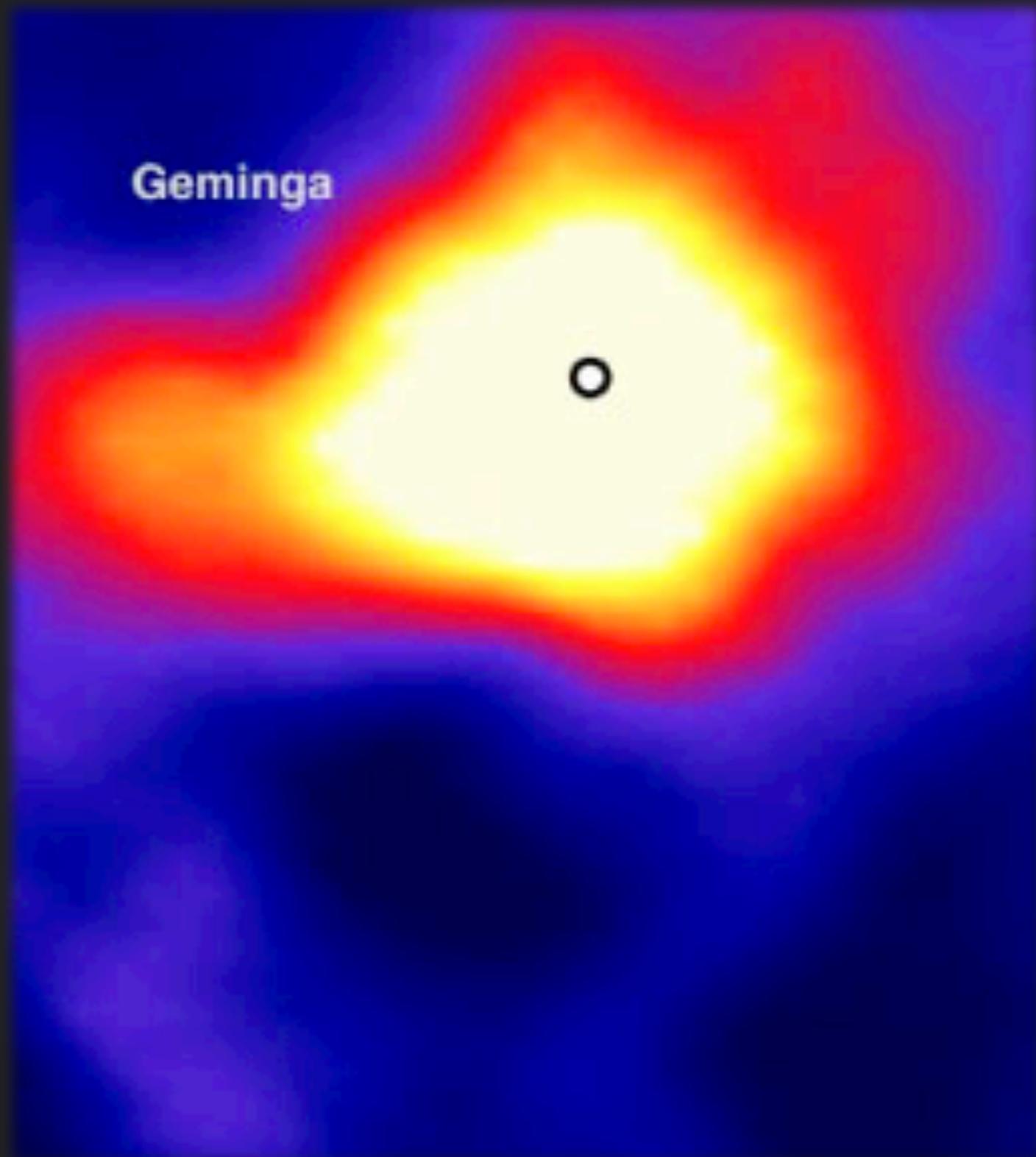


Geminga

‣ What were the uncertainties in pulsar models?

  ‣ **I: The e⁺e⁻ production efficiency?**

Profumo (0812.4457); Malyshev et al. (0903.1310)

%. A quantitative discussion of plausible values for $f_{e\pm}$ was recently given in Ref. [38]. We shall not review their discussion here, but Ref. [38] argues (see in particular their very informative App. B and C) that in the context of a standard model for the pulsar wind nebulae, a reasonable range for $f_{e\pm}$ falls between 1% and 30%.

  ‣ II: The e⁺e⁻ spectrum.

- What were the uncertainties in pulsar models?

  - I: The e⁺e⁻ production efficiency?

  - **II: The e⁺e⁻ spectrum.**

Hooper et al. (2008; 0810.1527)

part of their energy adiabatically because of the expansion of the wind. The energy spectrum injected by a single pulsar depends on the environmental parameters of the pulsar, but some attempts to calculate the average spectrum injected by a population of mature pulsars suggest that the spectrum may be relatively hard, having a slope of ~1.5-1.6 [18]. This spectrum, however, results from a complex interplay of individual pulsar spectra, of the spatial and age distributions of pulsars in the Galaxy, and on the assumption that the chief channel for pulsar spin down is magnetic dipole radiation. Due to the related uncertainties, variations from this injection spectra cannot be ruled out. Typically, one concentrates the attention on pulsars of age $\sim 10^5$ years because younger pulsars are likely to still

- TeV Halos answer both of these questions!

Hooper, Cholis, TL, Fang (2017; 1702.08436)

- Can use gamma-ray flux at the source to determine the total e⁺e⁻ energy!

- In agreement with models of the positron excess!
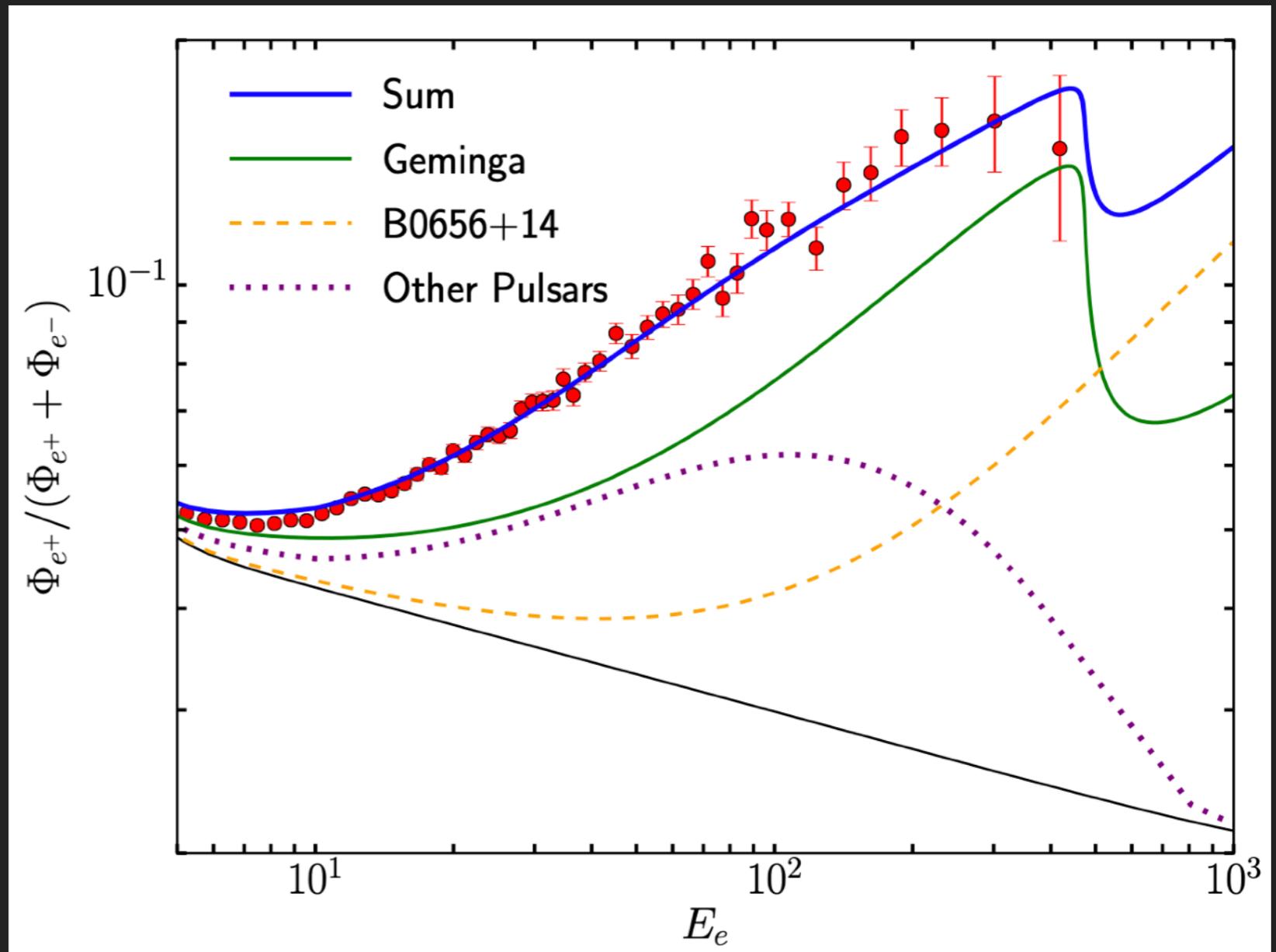
- Normalizing this to the positron data, we find that pulsars produce the majority of the positron excess.

- We can use this to set strong limits on dark matter annihilation.

- Better normalization of pulsar efficiencies will strengthen these limits (especially for soft DM spectra).
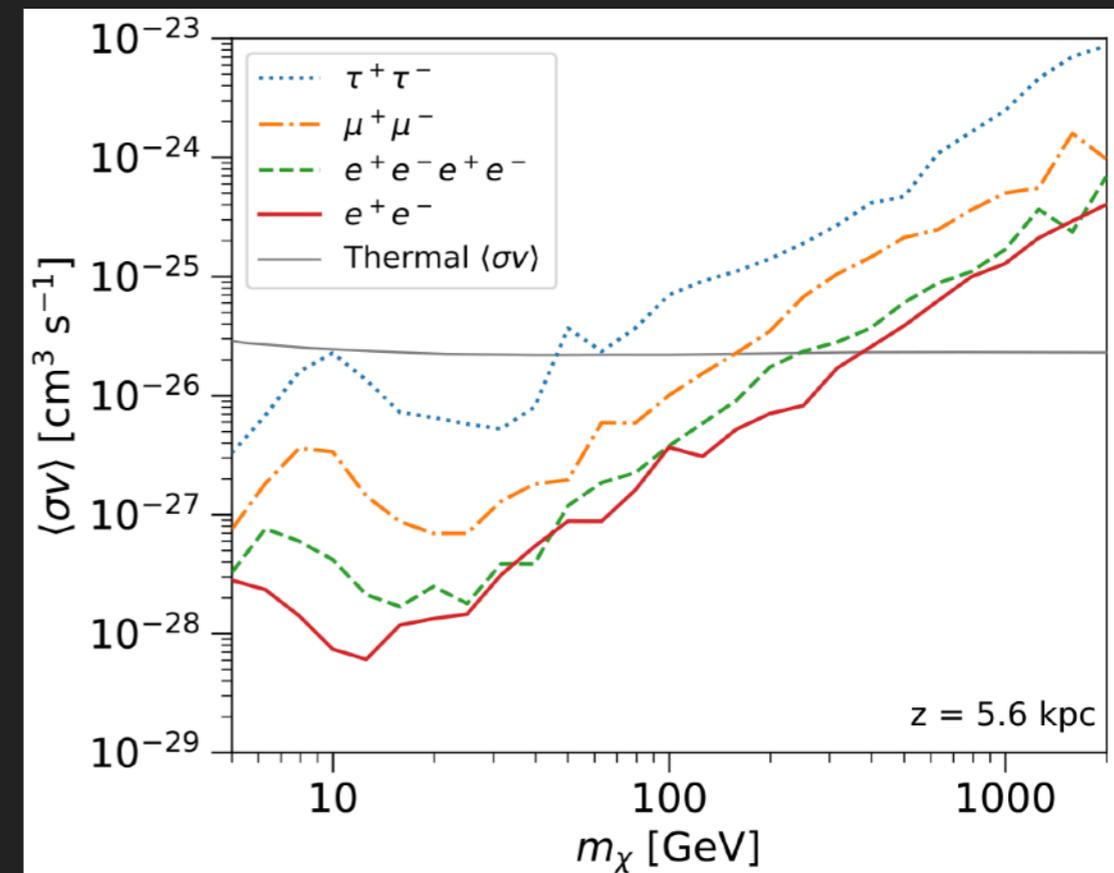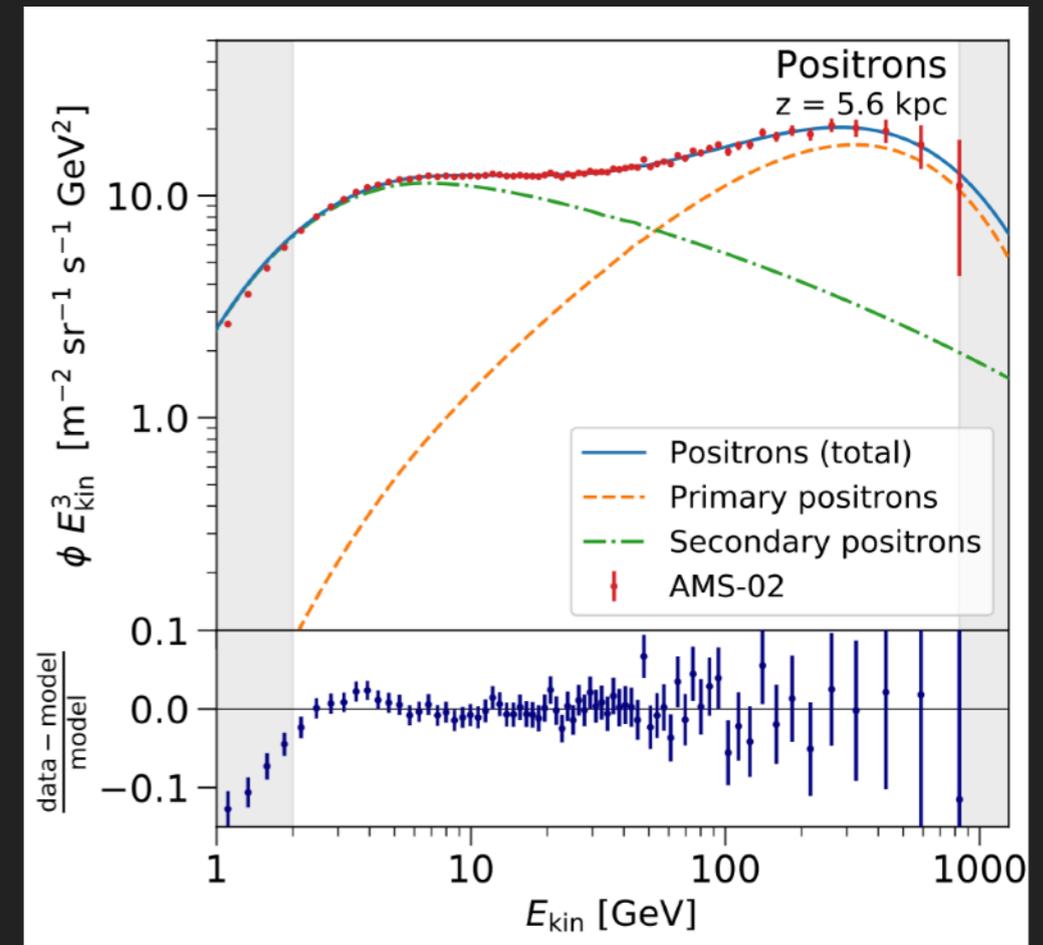
Turner & Wilczek (1989)

Orusa et al. (2021; 2107.06300)
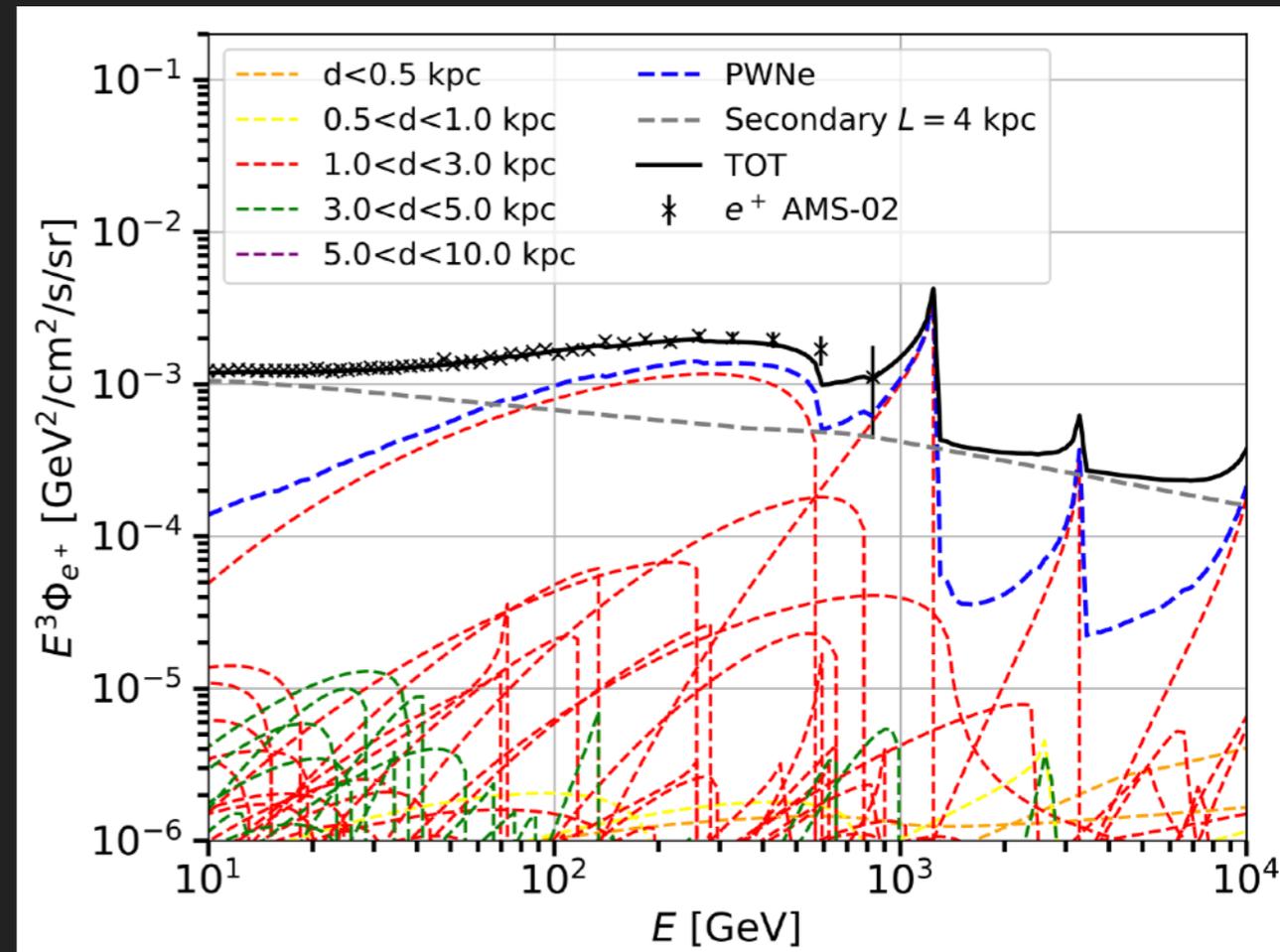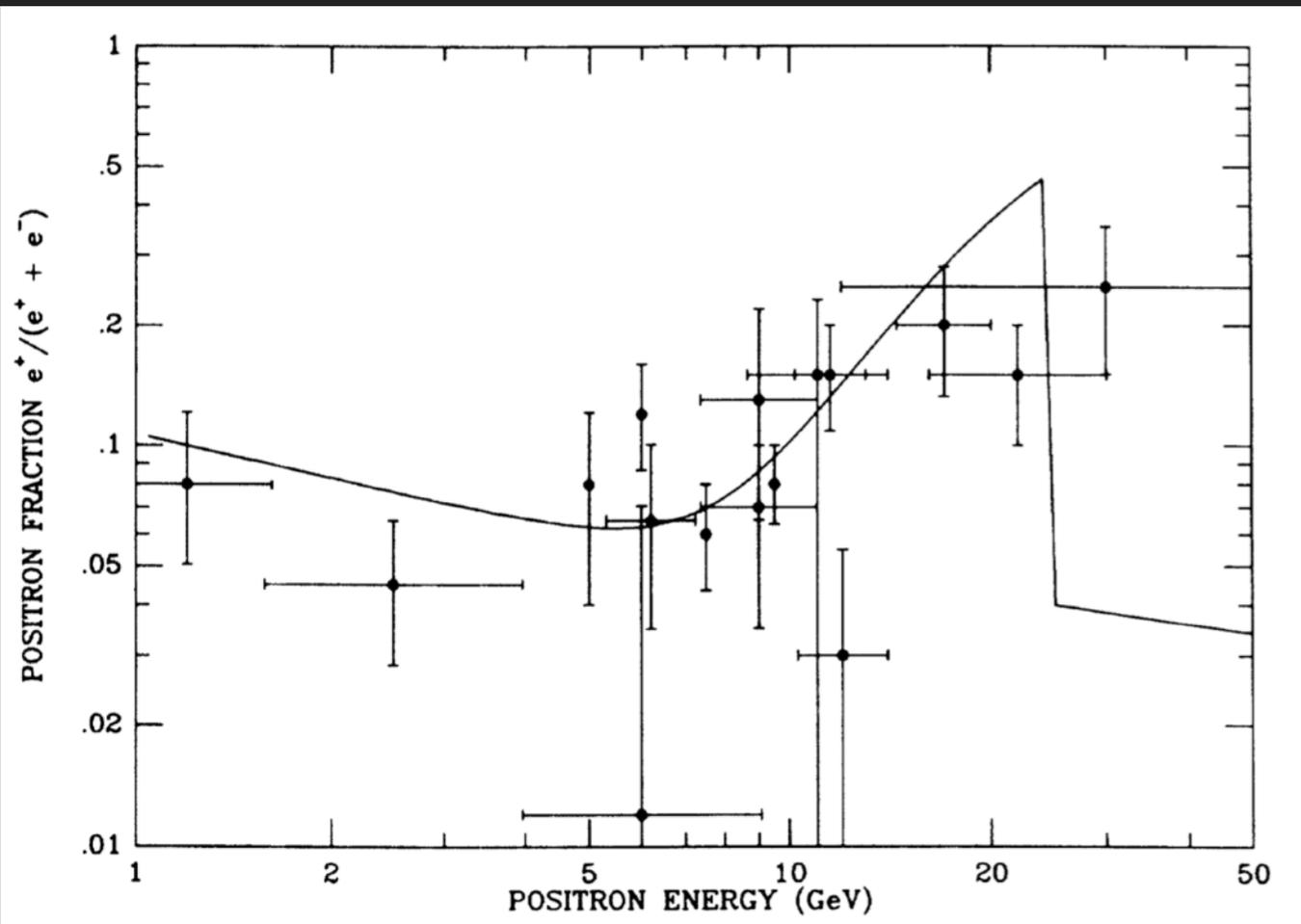


- Previously believed that sharp spectral features in the positron spectrum could be produced by either dark matter or pulsars.

▸ For pulsars, there is a key error: Studies generally use a continuous approximation for electron energy losses:

$$\frac{dE}{dt} = -\frac{4}{3}\sigma_T c \left(\frac{E}{m_e}\right)^2 \left[\rho_B + \sum_i \rho_i(\nu_i) S(E, \nu_i)\right]$$

▸ But ICS interactions are very rare and stochastic. The energy after a given time is not determined by the initial energy.

John & Linden (2022; 2206.04699)





$E_0 = 10$ TeV, t = 342 kyr

▸ For dark matter, the spectral cutoff is not produced by ICS cooling, but from the dark matter mass.

▸ The stochasticity of cooling instead means that some particles don't cool at all, enhancing the peak.

▸ Correctly accounting for ICS energy losses makes it possible to differentiate dark matter and pulsars via their positron spectrum.
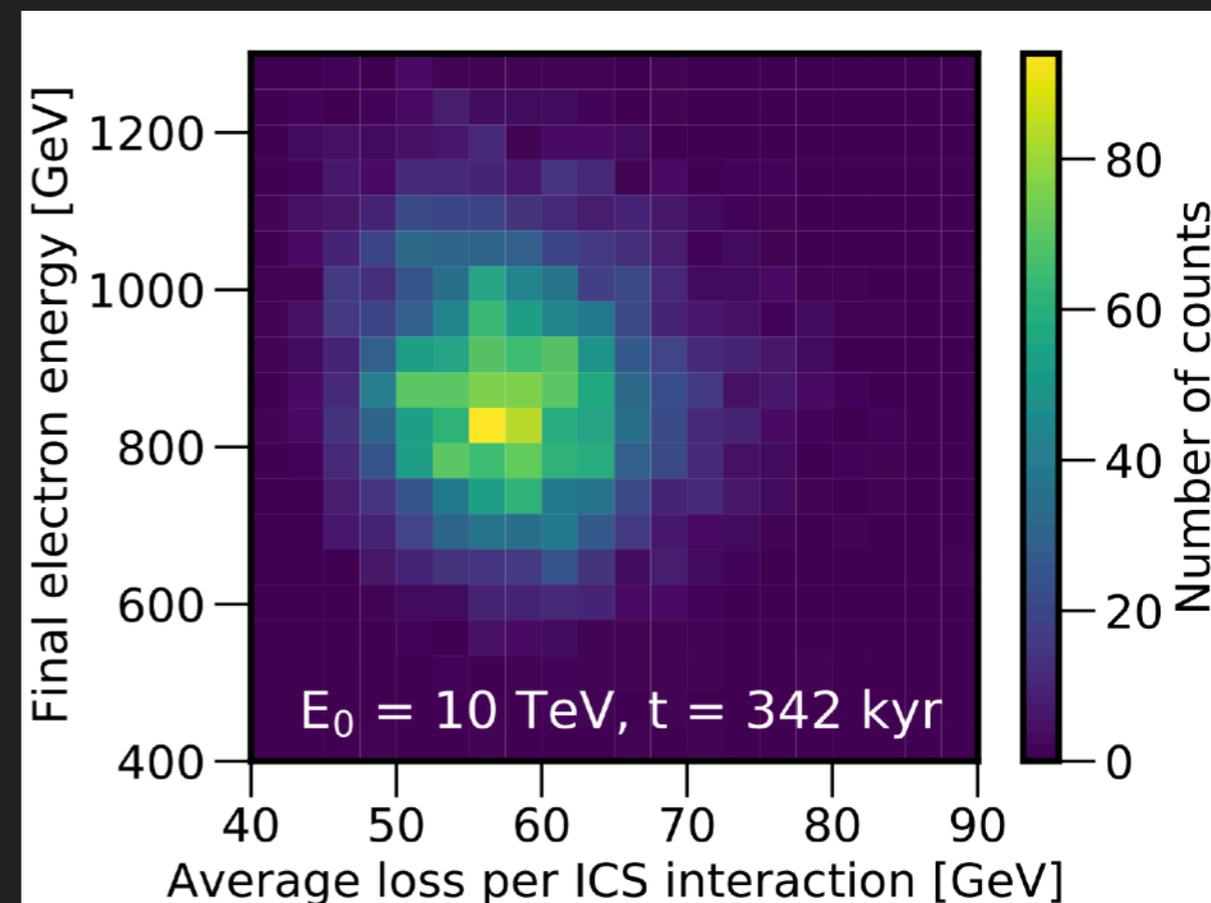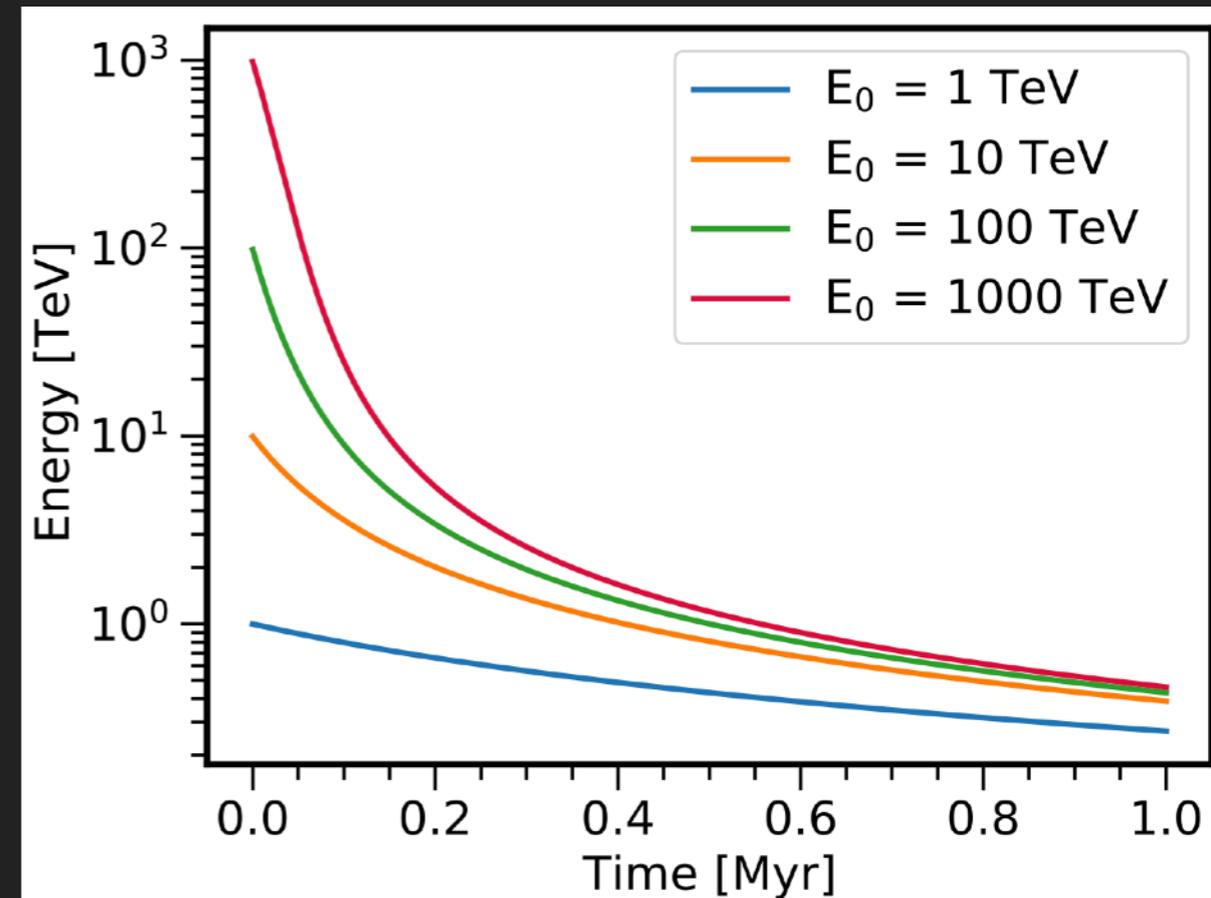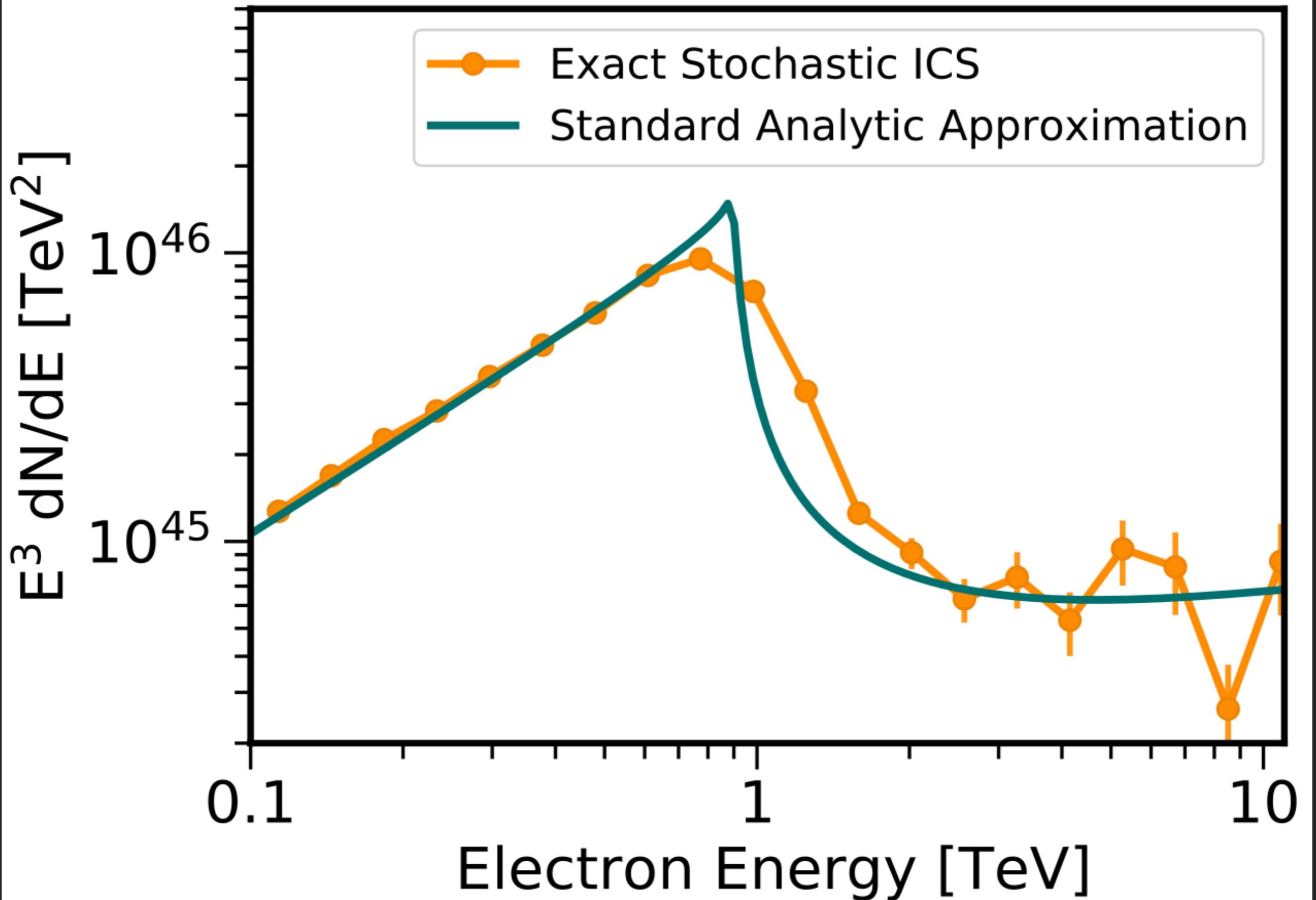
John & Linden (2023; 2304.07317)
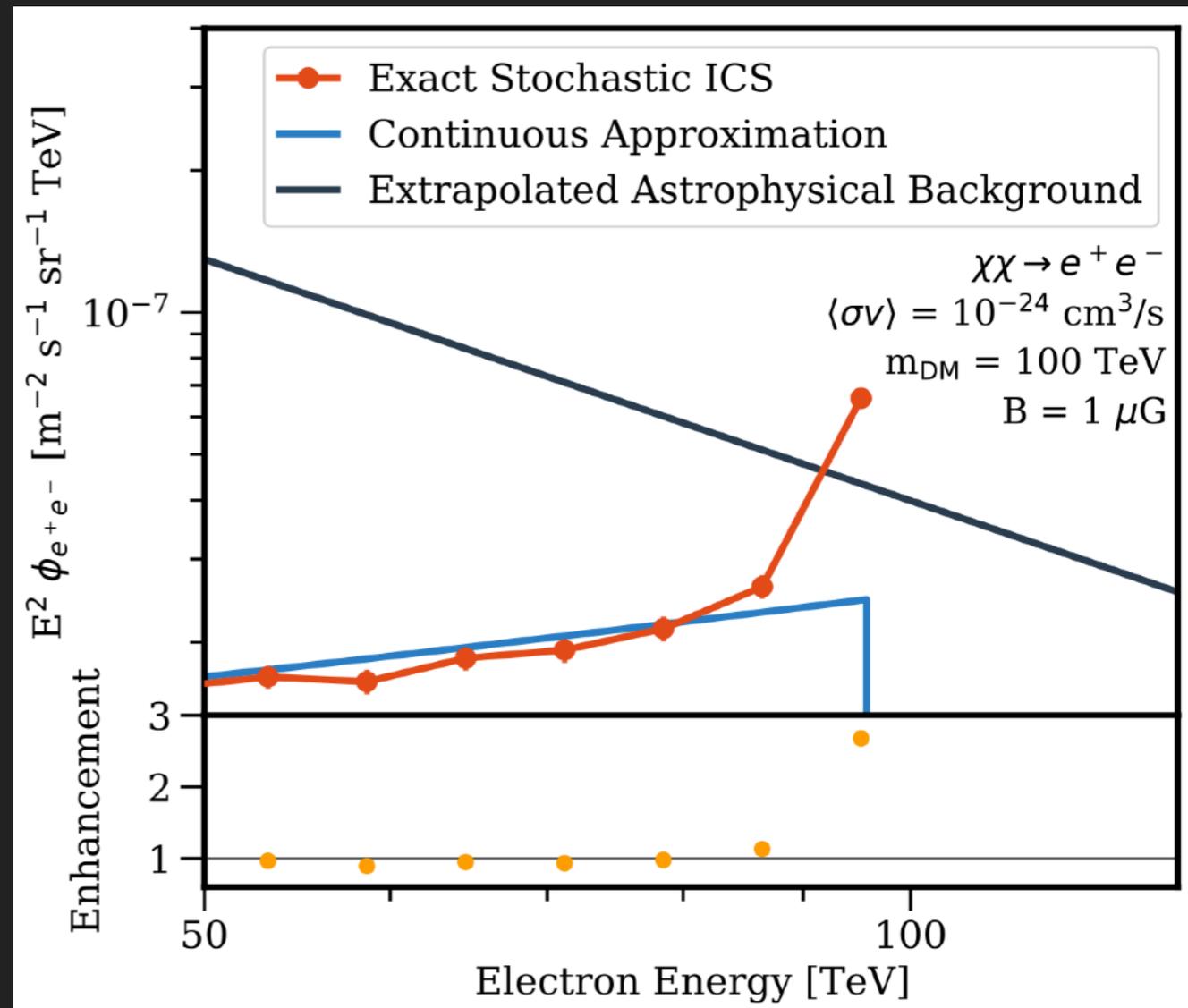
Moon (To Scale)

Geminga

PSR B0656+14
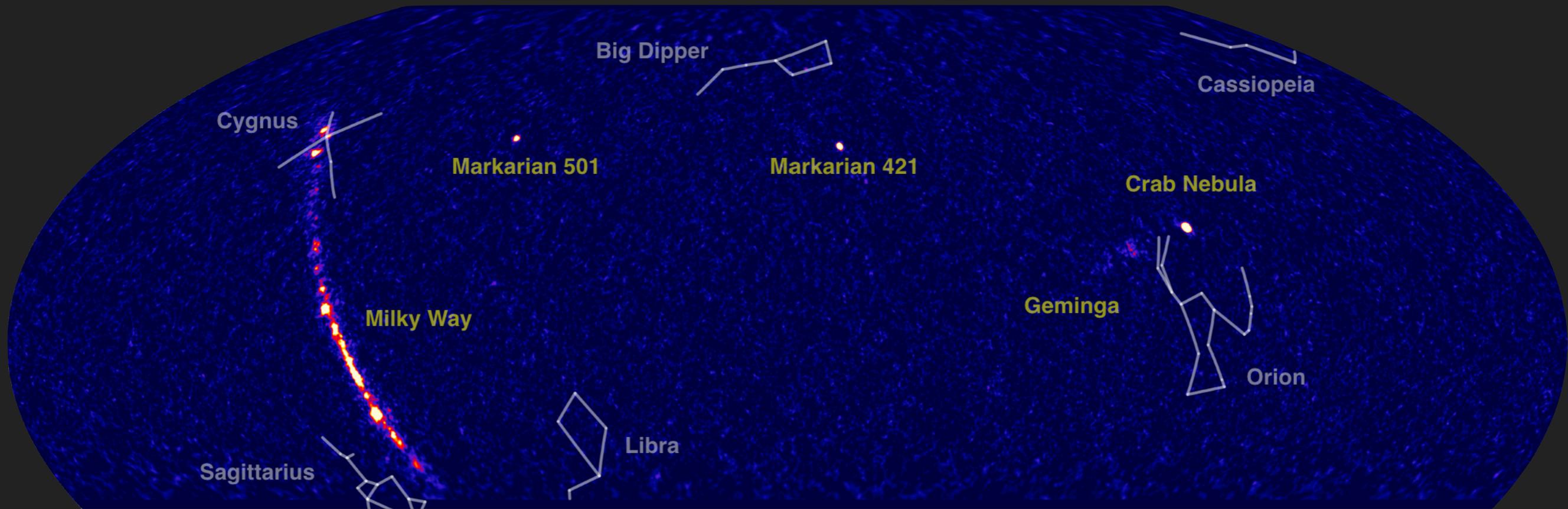
- There is bright diffuse gamma-ray emission across the galactic plane.

- Ratio of point source emission to diffuse emission is a powerful marker of emission mechanisms and local propagation.
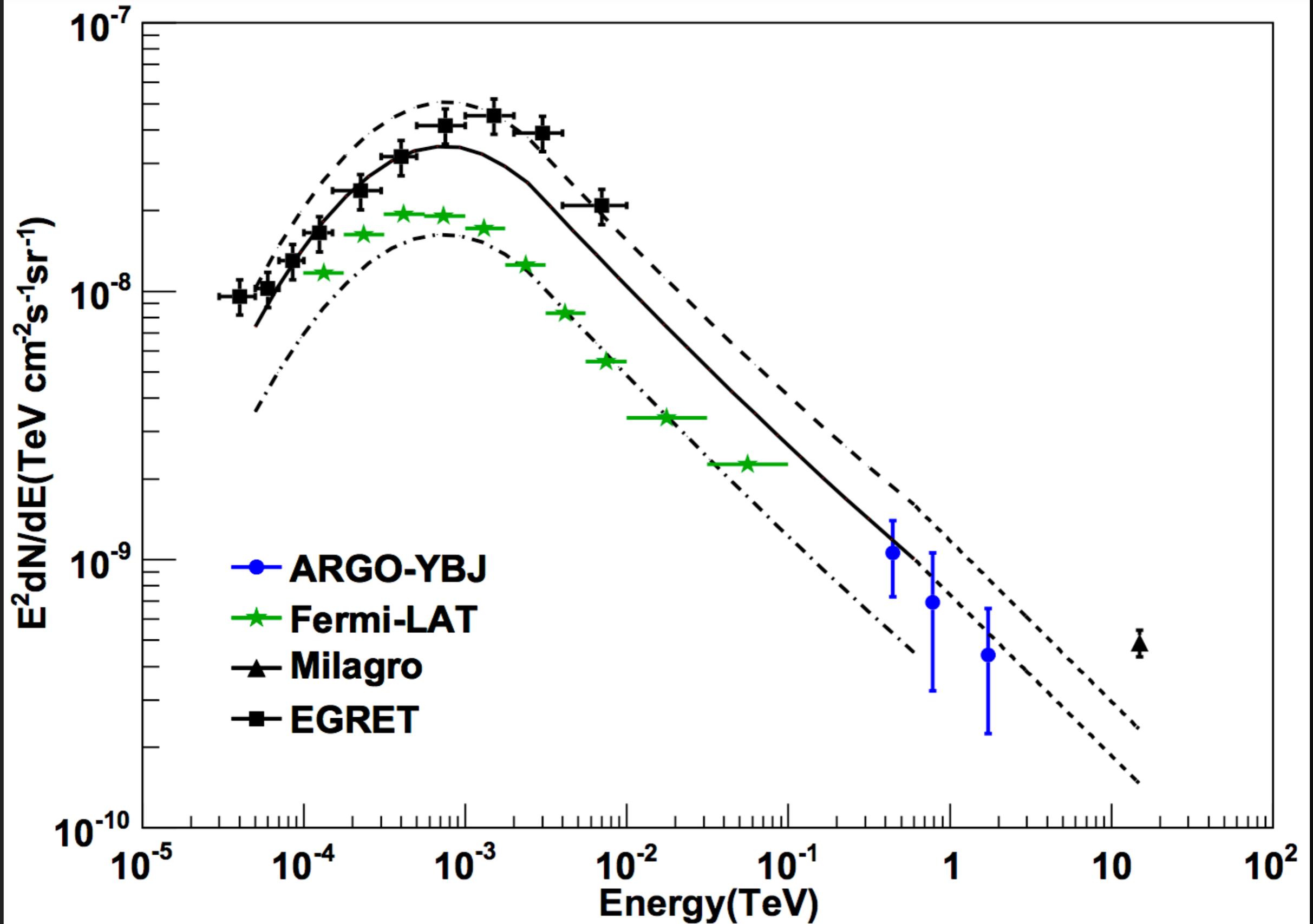
- TeV halos naturally explain the spectrum and intensity of this emission.

- Multiple halos observed with $E^{-2.0}$ spectra.

- Note - "Halo" is not needed

  - Pulsar efficiency ~10%

  - Power must escape PWN



Linden & Buckman (2017; 1707.01905)

- TeV halos naturally explain the spectrum and intensity of this emission.

- Multiple halos observed with E$^{-2.0}$ spectra.

- Note - "Halo" is not needed

  - Pulsar efficiency ~10%

  - Power must escape PWN

  - Recently extend to 100 TeV energies.
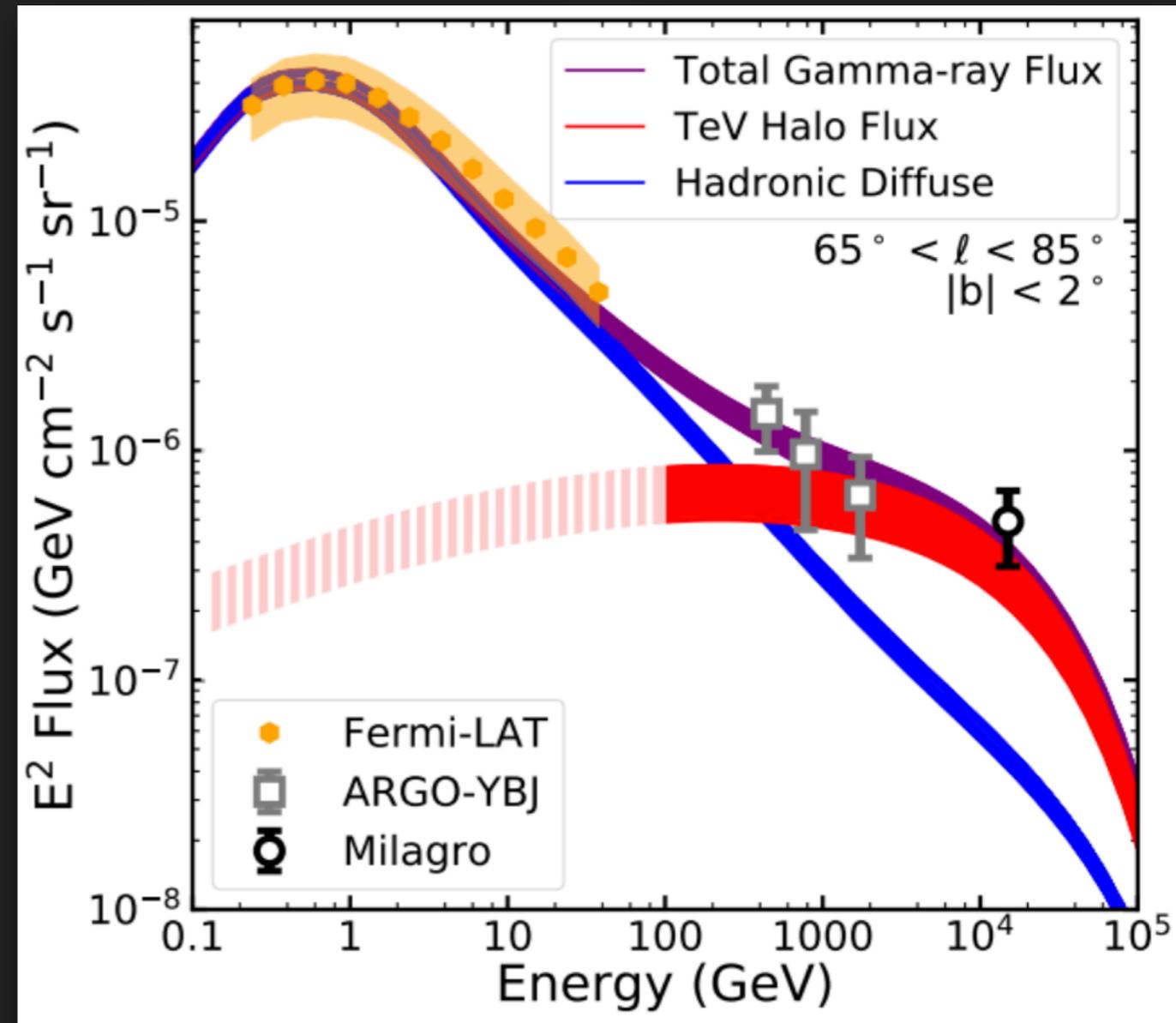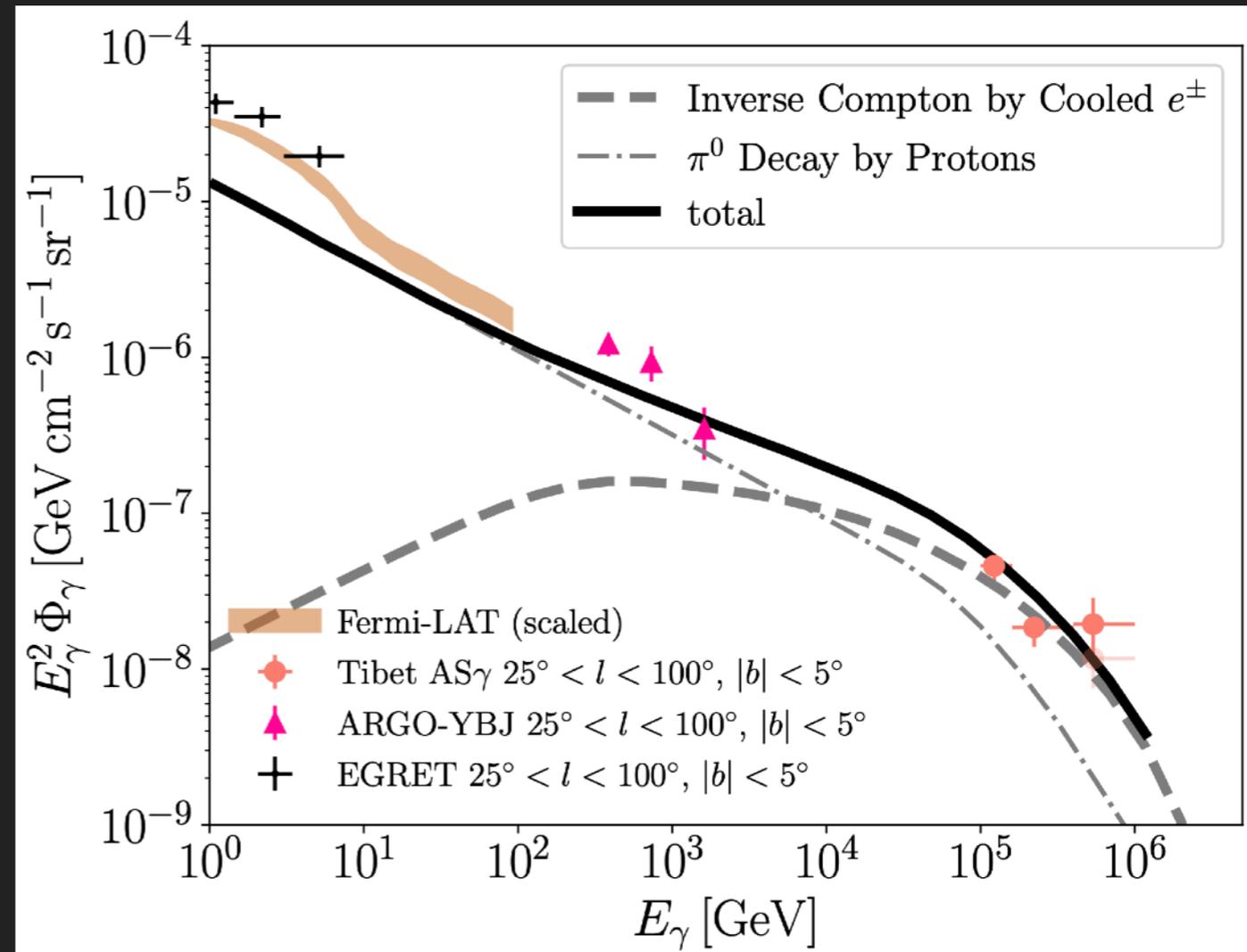
Fang & Murase (2021; 2104.09491)
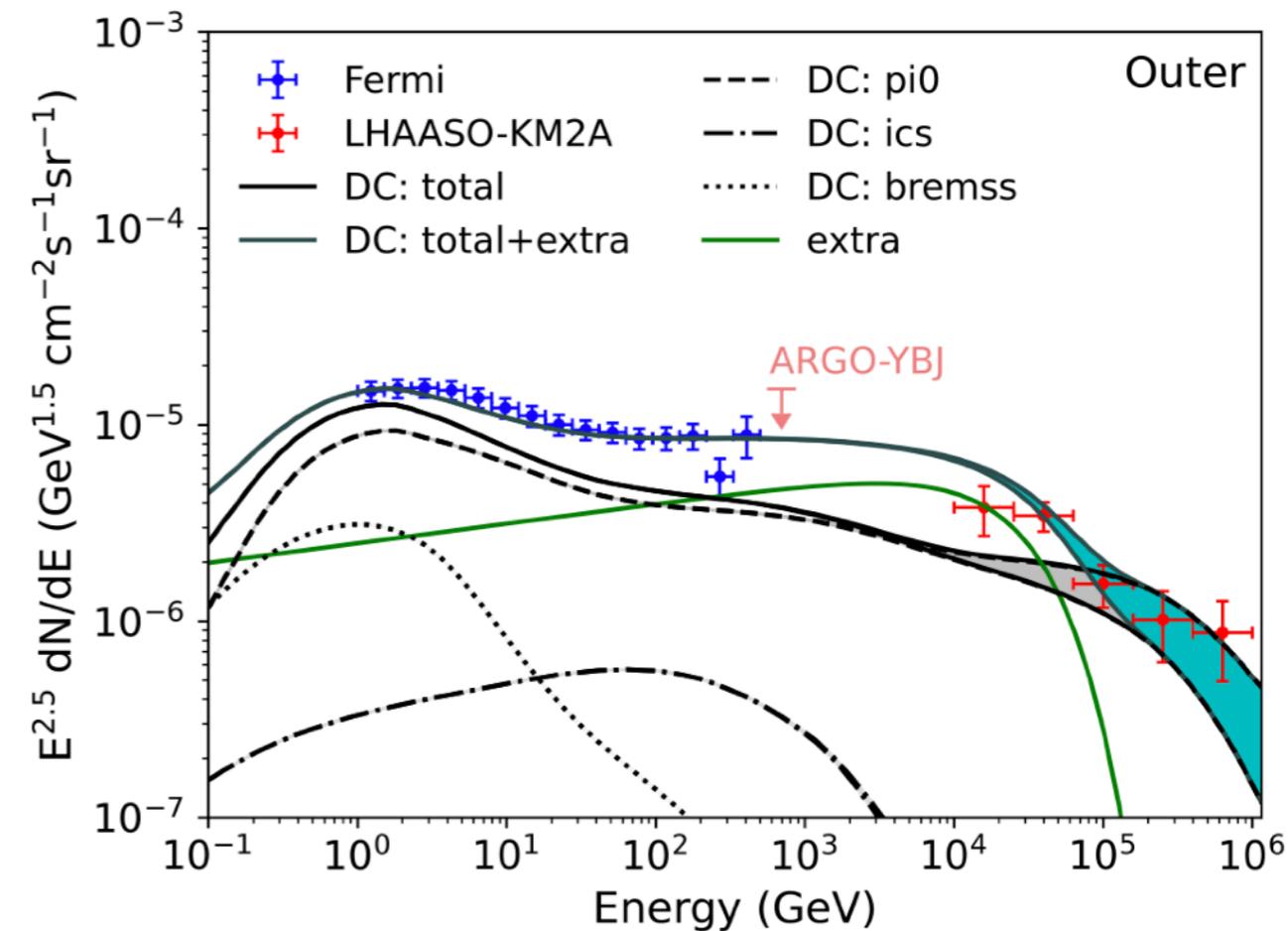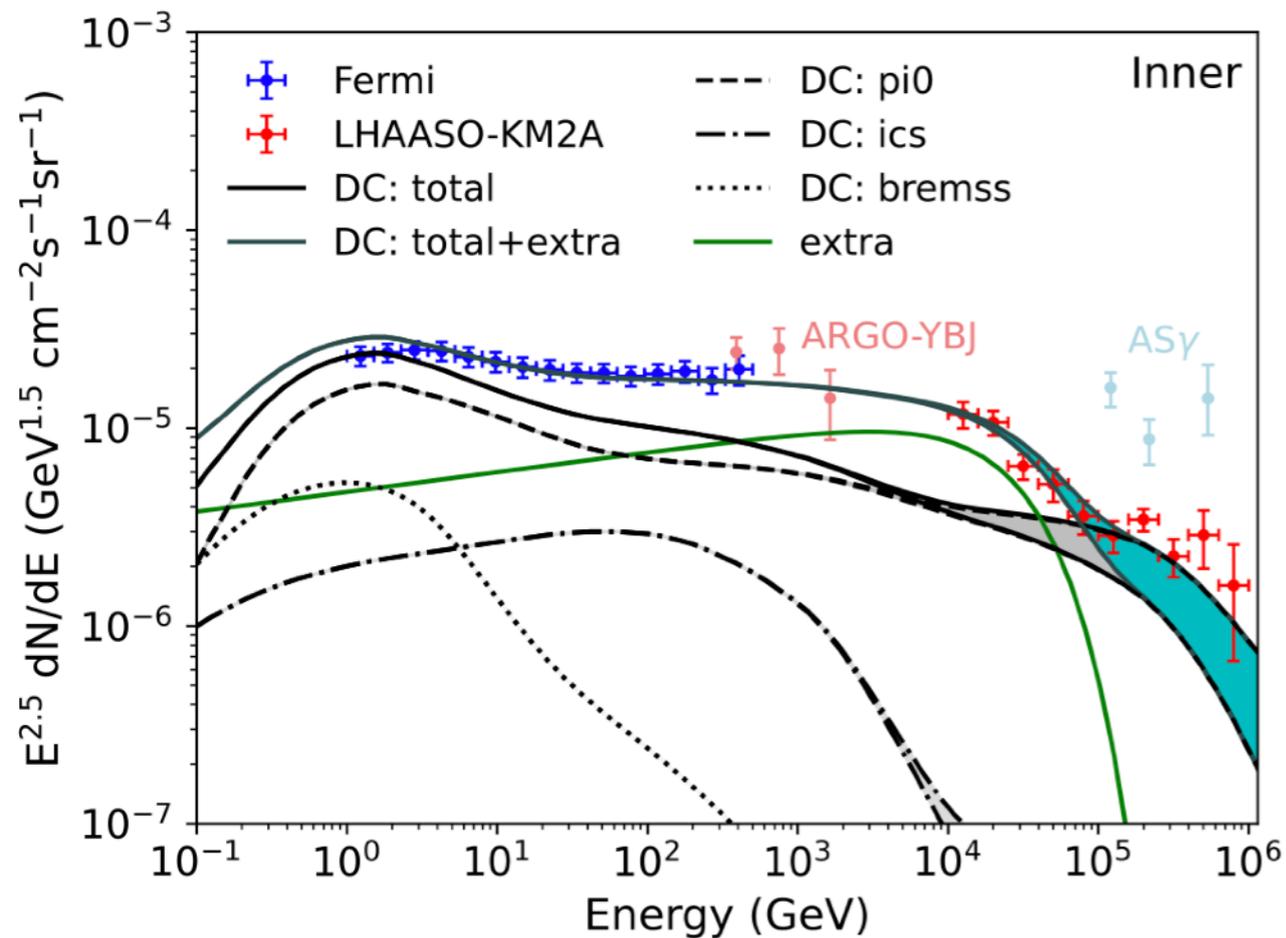
- Harder spectrum leptonic emission also improves the fit to LHASSO diffuse gamma-ray observations
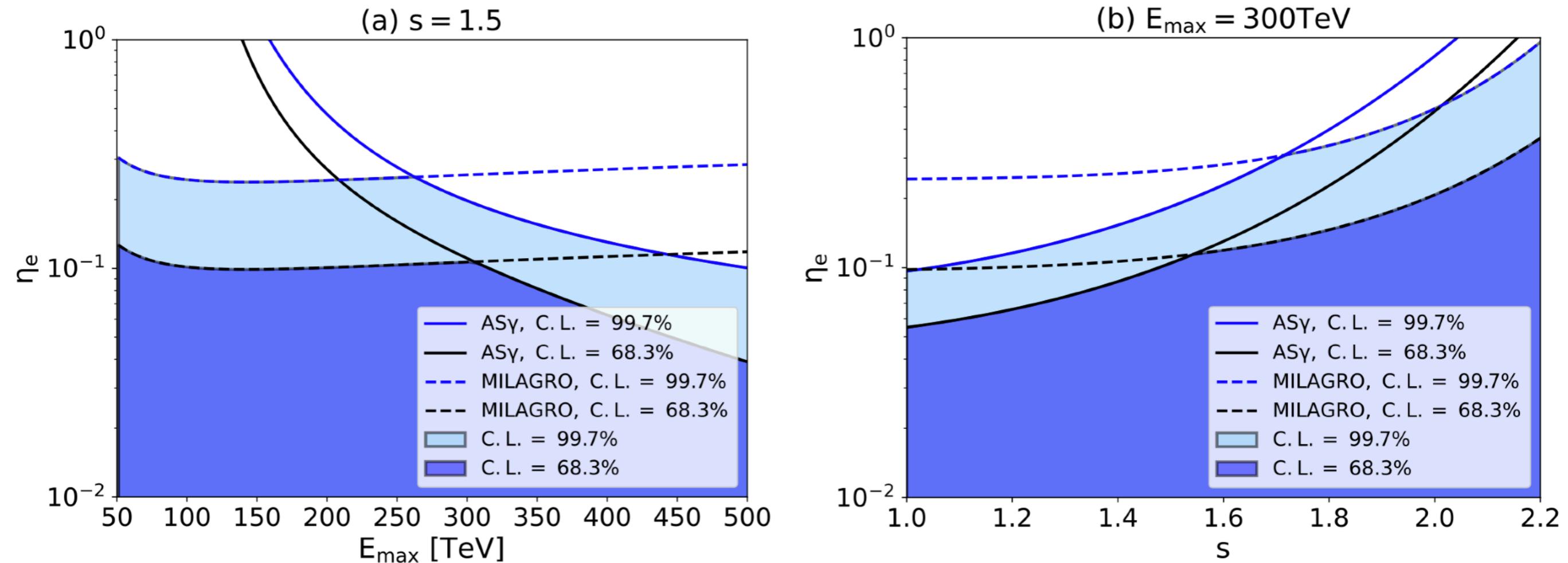
- This process can also be invested to place constraints on the electron injection efficiency, maximum energy, and electron injection spectrum from Milagro and AS$\gamma$ observations.

ANTARES and IceCube Collaboration (2018; 1808.03581)

- On the other hand, observations of a bright diffuse IceCube neutrino flux along the galactic plane (hint hint?), would place limits on the leptonic contribution.
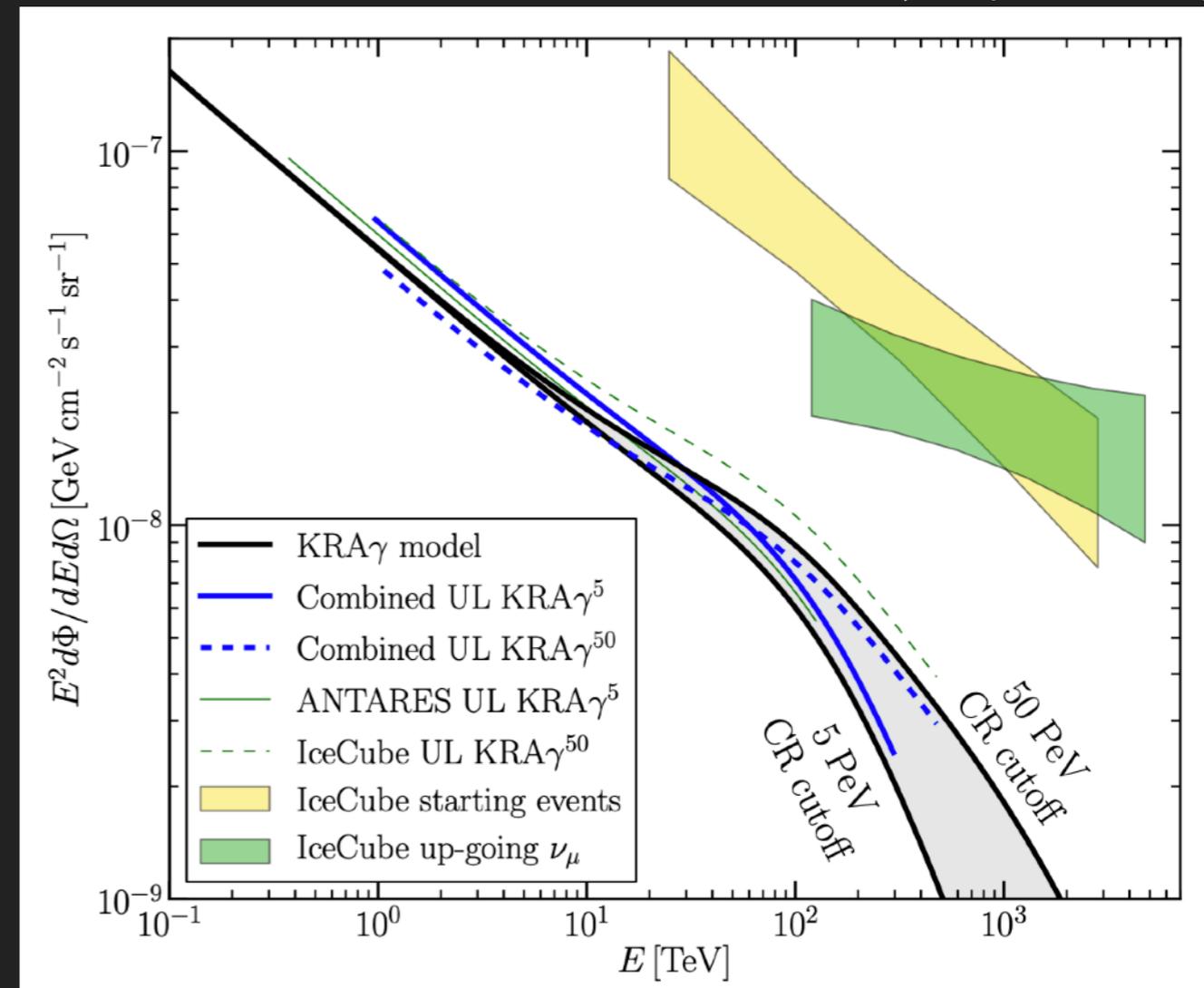


- Current limits are consistent with a hadronic flux up to 10x brighter than Galprop expectations, which would produce a significant fraction of the diffuse TeV emission.

- Current predictions for dark matter searches with TeV telescopes use extrapolations of the Fermi-LAT diffuse background.



Diffuse Model Template (p6v11) - Log

- Likely to be inaccurate if leptonic emission becomes dominant.

- More worrisome: GeV diffuse maps based on cosmic-ray propagation models where the local cosmic-ray density provides valuable information about the galactic cosmic-ray density. Unlikely to be true for TeV electrons.
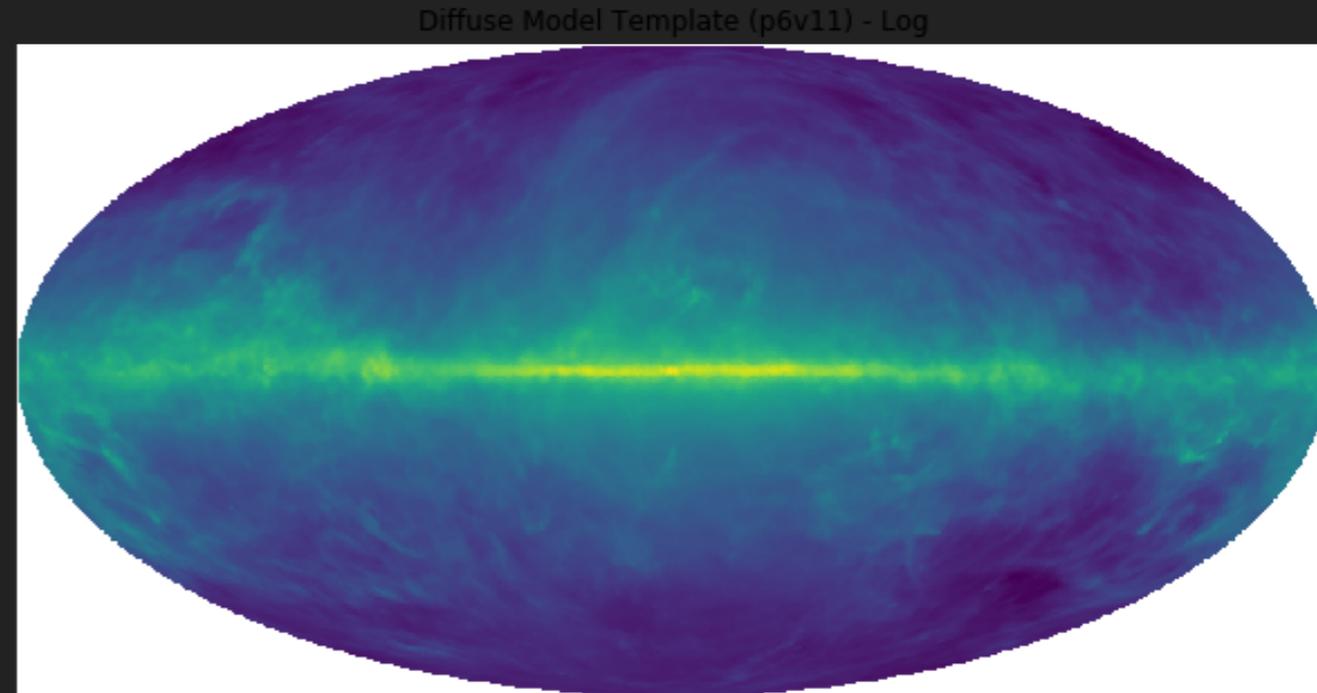
# The GALPROP Cosmic-ray Propagation and Nonthermal Emissions Framework: Release v57

T. A. Porter[1] , G. Jóhannesson[2] , and I. V. Moskalenko[1]

[1] W.W. Hansen Experimental Physics Laboratory and Kavli Institute for Particle Astrophysics and Cosmology, Stanford University, Stanford, CA 94305, USA

tporter@stanford.edu

[2] Science Institute, University of Iceland, IS-107 Reykjavik, Iceland

## Abstract

The past decade has brought impressive advances in the astrophysics of cosmic rays (CRs) and multiwavelength astronomy, thanks to the new instrumentation launched into space and built on the ground. Modern technologies employed by those instruments provide measurements with unmatched precision, enabling searches for subtle signatures of dark matter and new physics. Understanding the astrophysical backgrounds to better precision than the observed data is vital in moving to this new territory. A state-of-the-art CR propagation code, called GALPROP, is designed to address exactly this challenge. Having 25 yr of development behind it, the GALPROP framework has become a de facto standard in the astrophysics of CRs, diffuse photon emissions (radio to $\gamma$-rays), and searches for new physics. GALPROP uses information from astronomy, particle physics, and nuclear physics to predict CRs and their associated emissions self-consistently, providing a unifying modeling framework. The range of its physical validity covers 18 orders of magnitude in energy, from sub-keV to PeV energies for particles and from $\mu$eV to PeV energies for photons. The framework and the data sets are public and are extensively used by many experimental collaborations and by thousands of individual researchers worldwide for interpretation of their data and for making predictions. This paper details the latest release of the GALPROP framework and updated cross sections, further developments of its initially auxiliary data sets for models of the interstellar medium that grew into independent studies of the Galactic structure—distributions of gas, dust, radiation, and magnetic fields—as well as the extension of its modeling capabilities. Example applications included with the distribution illustrating usage of the new features are also described.

*Unified Astronomy Thesaurus concepts:* Galactic cosmic rays (567); Gamma-rays (637); Diffuse radiation (383); Gamma-ray astronomy (628); Non-thermal radiation sources (1119)
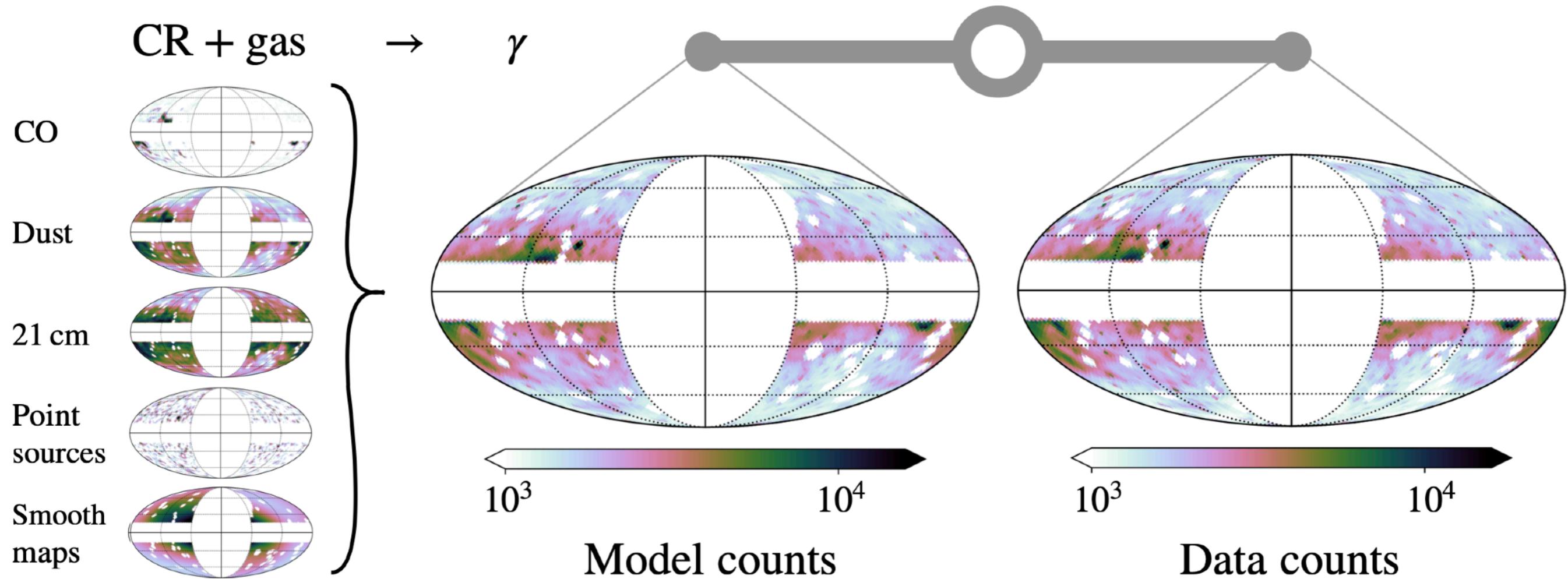
- Target models come from gas and dust tracers.

- CR density comes from Galprop simulations.

Korsmeier & Cuoco (2016; 1607.06093)

| Fit parameters | | (uni-PHe) | (uni-PHePbar) | (P) | (PHe) | (main) | (diMauro) | (1GV) | (noVc-1GV) | (noVc-5GV) |
|---|---|---|---|---|---|---|---|---|---|---|
| $\gamma_{1,p}$ | | - | - | $1.52^{+0.21}_{-0.32}$ | $1.27^{+0.11}_{-0.07}$ | $1.36^{+0.07}_{-0.10}$ | $1.38^{+0.07}_{-0.10}$ | $1.32^{+0.05}_{-0.12}$ | $1.61^{+0.06}_{-0.10}$ | $1.76^{+0.07}_{-0.04}$ |
| $\gamma_{2,p}$ | | - | - | $2.52^{+0.12}_{-0.45}$ | $2.069^{+0.098}_{-0.069}$ | $2.493^{+0.010}_{-0.026}$ | $2.499^{+0.026}_{-0.014}$ | $2.455^{+0.014}_{-0.007}$ | $2.421^{+0.010}_{-0.014}$ | $2.454^{+0.026}_{-0.014}$ |
| $\gamma_1$ | | $1.92^{+0.08}_{-0.14}$ | $1.50^{+0.07}_{-0.12}$ | - | $1.53^{+0.24}_{-0.11}$ | $1.29^{+0.04}_{-0.09}$ | $1.26^{+0.10}_{-0.06}$ | $1.32^{+0.06}_{-0.12}$ | $1.65^{+0.07}_{-0.11}$ | $1.70^{+0.06}_{-0.07}$ |
| $\gamma_2$ | | $2.582^{+0.010}_{-0.034}$ | $2.404^{+0.006}_{-0.022}$ | - | $2.003^{+0.094}_{-0.003}$ | $2.440^{+0.006}_{-0.018}$ | $2.451^{+0.018}_{-0.010}$ | $2.412^{+0.012}_{-0.006}$ | $2.381^{+0.010}_{-0.010}$ | $2.407^{+0.022}_{-0.014}$ |
| $R_0$ | [GV] | $8.16^{+1.22}_{-1.54}$ | $8.79^{+1.17}_{-1.55}$ | $4.38^{+3.23}_{-1.54}$ | $10.5^{+1.40}_{-1.59}$ | $5.54^{+0.76}_{-0.54}$ | $5.44^{+0.54}_{-0.54}$ | $5.52^{+0.33}_{-0.83}$ | $7.01^{+0.98}_{-0.54}$ | $8.63^{+0.98}_{-0.76}$ |
| $s$ | | $0.32^{+0.08}_{-0.02}$ | $0.41^{+0.09}_{-0.07}$ | $0.48^{+0.16}_{-0.31}$ | $0.59^{+0.16}_{-0.04}$ | $0.50^{+0.02}_{-0.04}$ | $0.50^{+0.05}_{-0.03}$ | $0.43^{+0.04}_{-0.03}$ | $0.31^{+0.03}_{-0.03}$ | $0.32^{+0.04}_{-0.05}$ |
| $\delta$ | | $0.16^{+0.03}_{-0.03}$ | $0.36^{+0.04}_{-0.03}$ | $0.29^{+0.46}_{-0.18}$ | $0.72^{+0.01}_{-0.11}$ | $0.28^{+0.03}_{-0.01}$ | $0.27^{+0.02}_{-0.04}$ | $0.32^{+0.03}_{-0.02}$ | $0.40^{+0.01}_{-0.01}$ | $0.36^{+0.02}_{-0.02}$ |
| $D_0$ | $[10^{28}$ cm$^2$/s] | $2.77^{+2.95}_{-0.53}$ | $2.83^{+0.90}_{-0.50}$ | $4.78^{+5.22}_{-3.49}$ | $5.95^{+0.83}_{-1.37}$ | $9.30^{+0.70}_{-5.48}$ | $9.04^{+0.96}_{-3.95}$ | $8.19^{+1.81}_{-4.68}$ | $4.92^{+1.12}_{-2.36}$ | $4.60^{+2.71}_{-2.04}$ |
| $v_A$ | [km/s] | $6.80^{+1.18}_{-2.73}$ | $29.2^{+2.80}_{-1.47}$ | $21.2^{+38.8}_{-21.2}$ | $1.84^{+2.36}_{-1.08}$ | $20.2^{+3.26}_{-6.33}$ | $18.2^{+3.15}_{-5.91}$ | $25.0^{+0.92}_{-2.30}$ | $22.8^{+1.46}_{-1.05}$ | $20.7^{+1.14}_{-3.43}$ |
| $v_{0,c}$ | [km/s] | $40.9^{+59.1}_{-5.89}$ | $40.2^{+38.1}_{-25.2}$ | $5.82^{+94.2}_{-5.82}$ | $87.8^{+12.2}_{-7.57}$ | $69.7^{+22.0}_{-24.7}$ | $57.3^{+41.1}_{-12.3}$ | $44.0^{+8.4}_{-16.5}$ | - | - |
| $z_h$ | [kpc] | $3.77^{+3.23}_{-1.77}$ | $2.04^{+0.40}_{-0.04}$ | $4.22^{+2.78}_{-2.22}$ | $6.55^{+0.45}_{-1.63}$ | $5.43^{+1.57}_{-3.43}$ | $5.84^{+1.16}_{-3.84}$ | $6.00^{+1.00}_{-4.00}$ | $5.05^{+1.95}_{-3.05}$ | $4.12^{+2.88}_{-2.12}$ |
| $\phi_{AMS}$ | | $300^{+60}_{-80}$ | $780^{+80}_{-40}$ | $620^{+180}_{-195}$ | $580^{+45}_{-115}$ | $400^{+90}_{-40}$ | $360^{+115}_{-45}$ | $700^{+20}_{-50}$ | $640^{+20}_{-20}$ | $340^{+45}_{-125}$ |
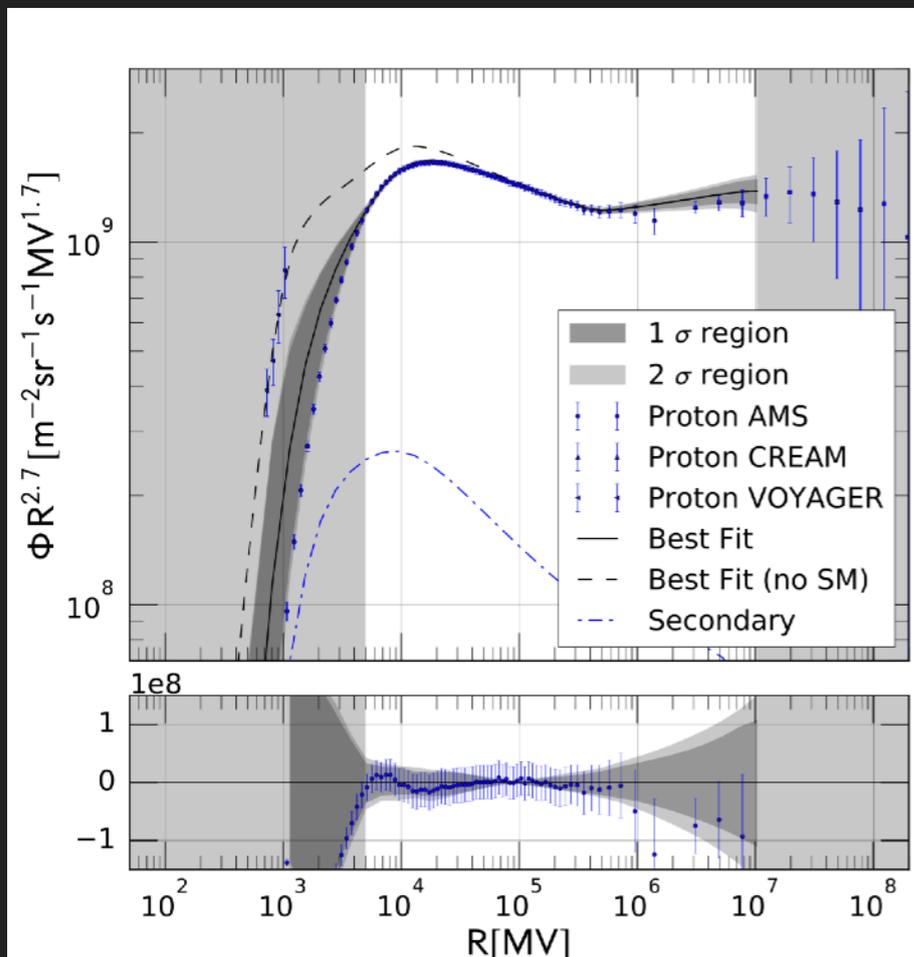


- Assume CR propagation is homogeneous.

- Fit data to local AMS-02 observables.

- But propagation is not homogeneous.

- Local TeV electrons might not tell you anything!
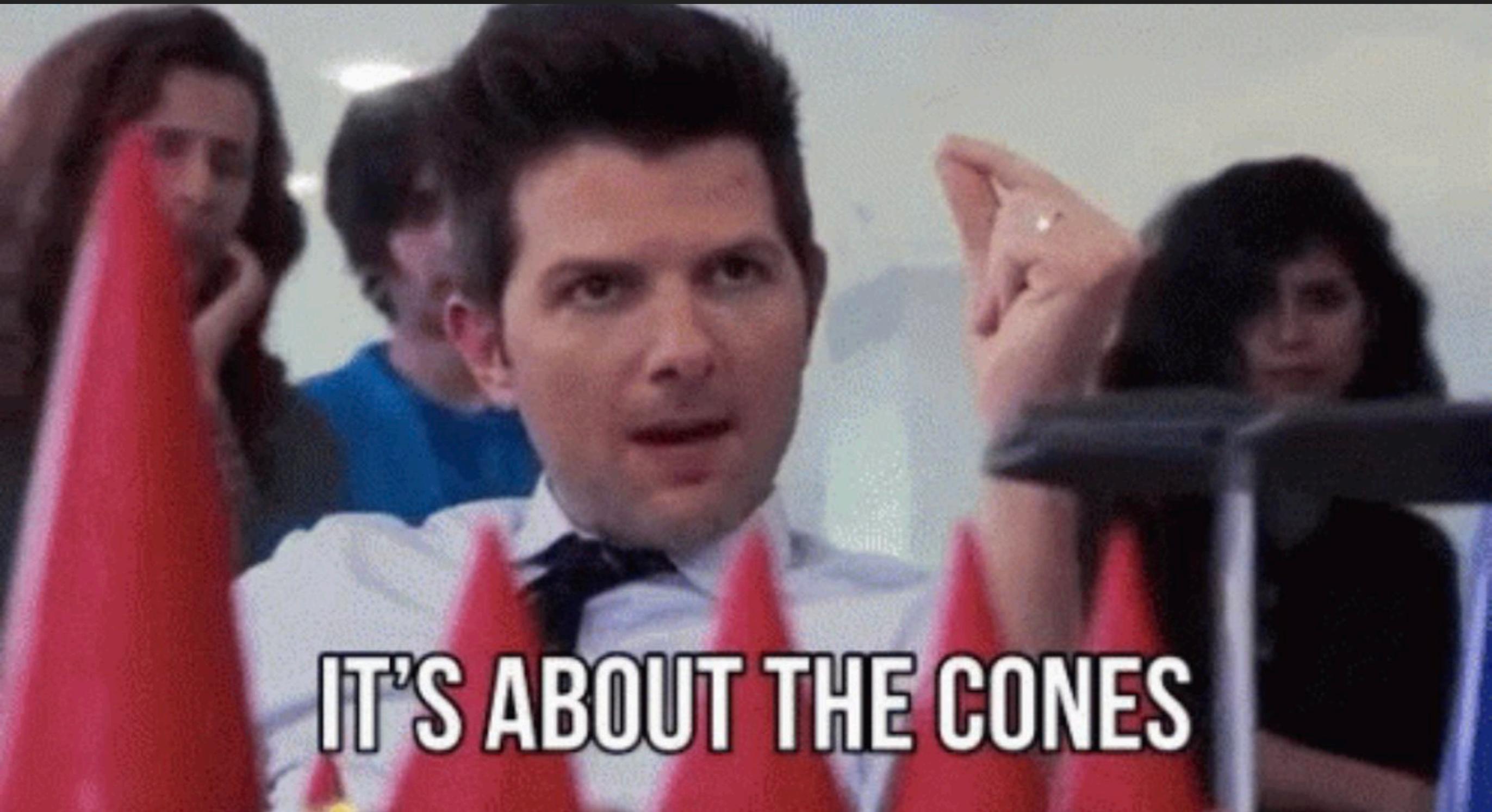
IT'S ABOUT THE CONES

# Pulsar searches and timing with the square kilometre array

R. Smits[1], M. Kramer[1], B. Stappers[1], D. R. Lorimer[2,3], J. Cordes[4], and A. Faulkner[1]

[1] Jodrell Bank Centre for Astrophysics, University of Manchester, UK
e-mail: Roy.Smits@manchester.ac.uk
[2] Department of Physics, 210 Hodges Hall, West Virginia University, Morgantown, WV 26506, USA
[3] National Radio Astronomy Observatory, Green Bank, USA
[4] Astronomy Department, Cornell University, Ithaca, NY, USA

## ABSTRACT

The square kilometre array (SKA) is a planned multi purpose radio telescope with a collecting area approaching 1 million square metres. One of the key science objectives of the SKA is to provide exquisite strong-field tests of gravitational physics by finding and timing pulsars in extreme binary systems such as a pulsar-black hole binary. To find out how three preliminary SKA configurations will affect a pulsar survey, we have simulated SKA pulsar surveys for each configuration. We estimate that the total number of pulsars the SKA will detect, is around 14 000 normal pulsars and 6000 millisecond pulsars, using only the 1-km core and 30-mn integration time. We describe a simple strategy for follow-up timing observations and find that, depending on the configuration, it would take 1–6 days to obtain a single timing point for 14 000 pulsars. Obtaining one timing point for the high-precision timing projects of the SKA, will take less than 14 h, 2 days, or 3 days, depending on the configuration. The presence of aperture arrays will be of great benefit here. We also study the computational requirements for beam forming and data analysis for a pulsar survey. Beam forming of the full field of view of the single-pixel feed 15-m dishes using the 1-km core of the SKA requires about $2.2 \times 10^{15}$ operations per second. The corresponding data rate from such a pulsar survey is about $4.7 \times 10^{11}$ bytes per second. The required computational power for a deep real time analysis is estimated to be $1.2 \times 10^{16}$ operations per second. For an aperture array or dishes equipped with phased array feeds, the survey can be performed faster, but the computational requirements and data rates will go up.

‣ Radio pulsars are beamed!

‣ Beaming fraction is small

$$f = \left[ 1.1 \ \left( \log_{10} \left( \frac{\tau}{100 \ \mathrm{Myr}} \right) \right)^2 + 15 \right] \ \%$$

Tauris & Manchester (1998)

‣ This varies between 15-30%.

‣ Most pulsars are unseen in radio!
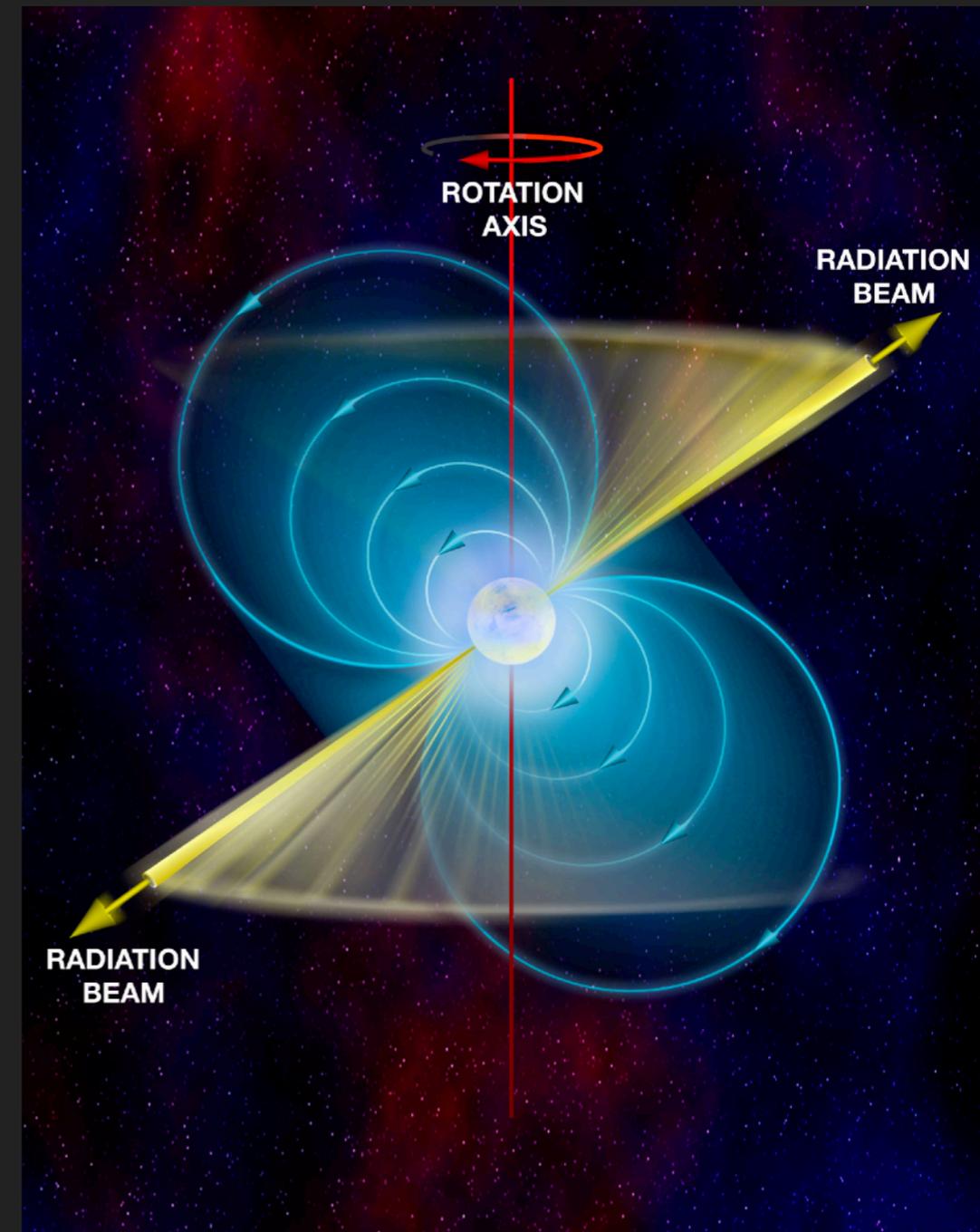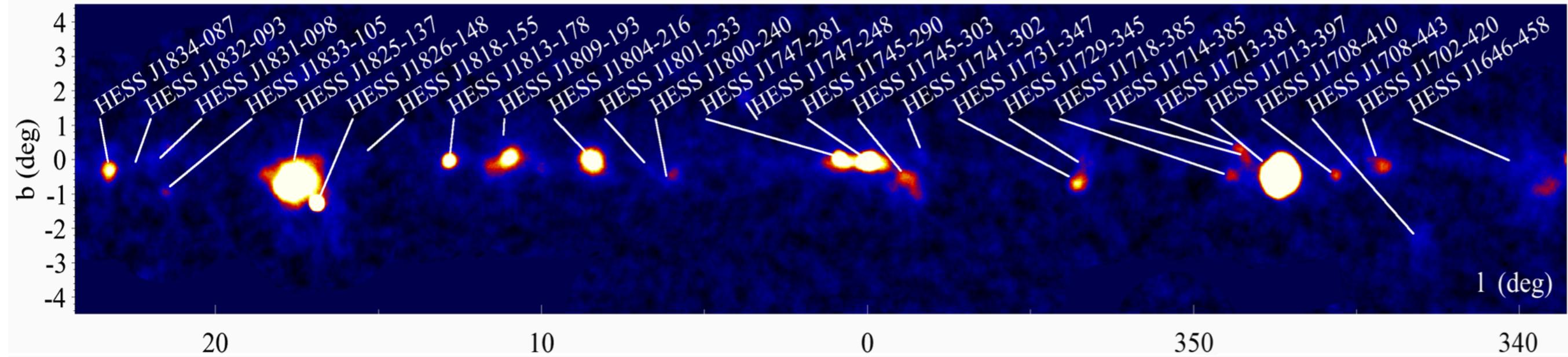
## The H.E.S.S. Galactic plane survey

H.E.S.S. Collaboration, H. Abdalla[1], A. Abramowski[2], F. Aharonian[3,4,5], F. Ait Benkhali[3], E.O. Angüner[21], M. Arakawa[43], M. Arrieta[15], P. Aubert[24], M. Backes[8], A. Balzer[9], M. Barnard[1], Y. Becherini[10], J. Becker Tjus[11], D. Berge[12], S. Bernhard[13], K. Bernlöhr[3], R. Blackwell[14], M. Böttcher[1], C. Boisson[15], J. Bolmont[16], S. Bonnefoy[37], P. Bordas[3], J. Bregeon[17], F. Brun*[26], P. Brun[18], M. Bryan[9], M. Büchele[36], T. Bulik[19], M. Capasso[2], S. Carrigan[3,48], S. Caroff[30], A. Carosi[24], S. Casanova[21,3], M. Cerruti[16], N. Chakraborty[3], R.C.G. Chaves*[17,22], A. Chen[23], J. Chevalier[24], S. Colafrancesco[23], B. Condon[26], J. Conrad[27,28], I.D. Davids[8], J. Decock[18], C. Deil*[3], J. Devin[17], P. deWilt[14], L. Dirson[2], A. Djannati-Ataï[31], W. Domainko[3], A. Donath*[3], L.O'C. Drury[4], K. Dutson[33], J. Dyks[34], T. Edwards[3], K. Egberts[35], P. Eger[3], G. Emery[16], J.-P. Ernenwein[20], S. Eschbach[36], C. Farnier[27,10], S. Fegan[30], M.V. Fernandes[2], A. Fiasson[24], G. Fontaine[30], A. Förster[3], S. Funk[36], M. Füßling[37], S. Gabici[31], Y.A. Gallant[17], T. Garrigoux[1], H. Gast[3,49], F. Gaté[24], G. Giavitto[37], B. Giebels[30], D. Glawion[25], J.F. Glicenstein[18], D. Gottschall[29], M.-H. Grondin[26], J. Hahn[3], M. Haupt[37], J. Hawkes[14], G. Heinzelmann[2], G. Henri[32], G. Hermann[3], J.A. Hinton[3], W. Hofmann[3], C. Hoischen[35], T. L. Holch[7], M. Holler[13], D. Horns[2], A. Ivascenko[1], H. Iwasaki[43], A. Jacholkowska[16], M. Jamrozy[38], D. Jankowsky[36], F. Jankowsky[25], M. Jingo[23], L. Jouvin[31], I. Jung-Richardt[36], M.A. Kastendieck[2], K. Katarzyński[39], M. Katsuragawa[44], U. Katz[36], D. Kerszberg[16], D. Khangulyan[43], B. Khélifi[31], J. King[3], S. Klepser[37], D. Klochkov[29], W. Kluźniak[34], Nu. Komin[23], K. Kosack[18], S. Krakau[11], M. Kraus[36], P.P. Krüger[1], H. Laffon[26], G. Lamanna[24], J. Lau[14], J.-P. Lees[24], J. Lefaucheur[15], A. Lemière[31], M. Lemoine-Goumard[26], J.-P. Lenain[16], E. Leser[35], T. Lohse[7], M. Lorentz[18], R. Liu[3], R. López-Coto[3], I. Lypova[37], V. Marandon*[3], D. Malyshev[29], A. Marcowith[17], C. Mariaud[30], R. Marx[3], G. Maurin[24], N. Maxted[14,45], M. Mayer[7], P.J. Meintjes[40], M. Meyer[27], A.M.W. Mitchell[3], R. Moderski[34], M. Mohamed[25], L. Mohrmann[36], K. Morâ[27], E. Moulin[18], T. Murach[37], S. Nakashima[44], M. de Naurois[30], H. Ndiyavala[1], F. Niederwanger[13], J. Niemiec[21], L. Oakes[7], P. O'Brien[33], H. Odaka[44], S. Ohm[37], M. Ostrowski[38], I. Oya[37], M. Padovani[17], M. Panter[3], R.D. Parsons[3], M. Paz Arribas[7], N.W. Pekeur[1], G. Pelletier[32], C. Perennes[16], P.-O. Petrucci[32], B. Peyaud[18], Q. Piel[24], S. Pita[31], V. Poireau[24], H. Poon[3], D. Prokhorov[10], H. Prokoph[12], G. Pühlhofer[29], M. Punch[31,10], A. Quirrenbach[25], S. Raab[36], R. Rauth[13], A. Reimer[13], O. Reimer[13], M. Renaud[17], R. de los Reyes[3], F. Rieger[3,41], L. Rinchiuso[18], C. Romoli[4], G. Rowell[14], B. Rudak[34], C.B. Rulten[15], S. Safi-Harb[50], V. Sahakian[6,5], S. Saito[43], D.A. Sanchez[24], A. Santangelo[29], M. Sasaki[36], M. Schandri[36], R. Schlickeiser[11], F. Schüssler[18], A. Schulz[37], U. Schwanke[7], S. Schwemmer[25], M. Seglar-Arroyo[18], M. Settimo[16], A.S. Seyffert[1], N. Shafi[23], I. Shilon[36], K. Shiningayamwe[8], R. Simoni[9], H. Sol[15], F. Spanier[1], M. Spir-Jacob[31], Ł. Stawarz[38], R. Steenkamp[8], C. Stegmann[35,37], C. Steppa[35], I. Sushch[1], T. Takahashi[44], J.-P. Tavernet[16], T. Tavernier[31], A.M. Taylor[37], R. Terrier[31], L. Tibaldo[3], D. Tiziani[36], M. Tluczykont[2], C. Trichard[20], M. Tsirou[17], N. Tsuji[43], R. Tuffs[3], Y. Uchiyama[43], D.J. van der Walt[1], C. van Eldik[36], C. van Rensburg[1], B. van Soelen[40], G. Vasileiadis[17], J. Veh[36], C. Venter[1], A. Viana[3,46], P. Vincent[16], J. Vink[9], F. Voisin[14], H.J. Völk[3], T. Vuillaume[24], Z. Wadiasingh[1], S.J. Wagner[25], P. Wagner[7], R.M. Wagner[27], R. White[3], A. Wierzcholska[21], P. Willmann[36], A. Wörnlein[36], D. Wouters[18], R. Yang[3], D. Zaborov[30], M. Zacharias[1], R. Zanin[3], A.A. Zdziarski[34], A. Zech[15], F. Zefi[30], A. Ziegler[36], J. Zorn[3], and N. Żywucka[38]

(Affiliations can be found after the references)

**ABSTRACT**

We present the results of the most comprehensive survey of the Galactic plane in very high-energy (VHE) γ-rays, including a public release of Galactic sky maps, a catalog of VHE sources, and the discovery of 16 new sources of VHE γ-rays. The High Energy Spectroscopic System (H.E.S.S.) Galactic plane survey (HGPS) was a decade-long observation program carried out by the H.E.S.S. I array of Cherenkov telescopes in Namibia from 2004 to 2013. The observations amount to nearly 2700 h of quality-selected data, covering the Galactic plane at longitudes from $\ell = 250°$ to 65° and latitudes $|b| \leqslant 3°$. In addition to the unprecedented spatial coverage, the HGPS also features a relatively high angular resolution $(0.08° \approx 5$ arcmin mean point spread function 68% containment radius), sensitivity $(\lesssim 1.5\%$ Crab flux for point-like sources), and energy range (0.2 to 100 TeV). We constructed a catalog of VHE γ-ray sources from the HGPS data set with a systematic procedure for both source detection and characterization of morphology and spectrum. We present this likelihood-based method in detail, including the introduction of a model component to account for unresolved, large-scale emission along the Galactic plane. In total, the resulting HGPS catalog contains 78 VHE sources, of which 14 are not reanalyzed here, for example, due to their complex morphology, namely shell-like sources and the Galactic center region. Where possible, we provide a firm identification of the VHE source or plausible associations with sources in other astronomical catalogs. We also studied
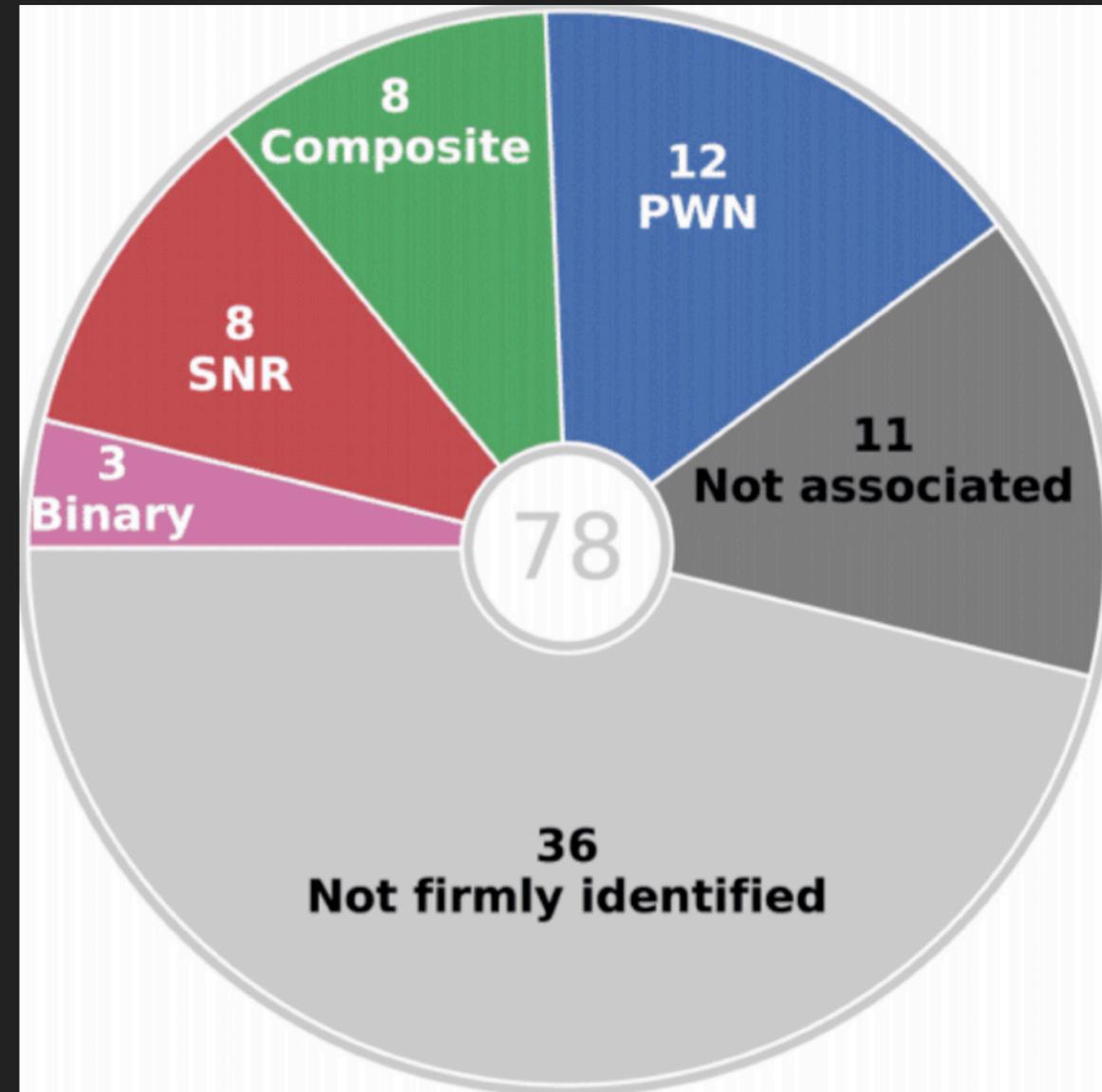
▸ Observations expect HAWC to find between 50-100 sources.

▸ Only ~1/3 of these will surround known radio pulsars.

# LHAASO Sky @ >100 TeV



Significance (σ)

240°    G.C.    0°    -120°

Crab Nebula

Dec=60°    Dec=50°    Dec=40°    Dec=30°    Dec=20°    Dec=10°    Dec=0°    Dec=-10°

LHAASO J2226+6057    LHAASO J2032+4102    LHAASO J1956+2845    LHAASO J1908+0621    LHAASO J1843-0338    LHAASO J1825-1326

LHAASO J2108+5157    LHAASO J2018+3651    LHAASO J1929+1745    LHAASO J1849-0003    LHAASO J1839-0545

Galactic latitude (deg)

Galactic longitude (deg)

Hooper, TL (2021; 2104.00014)
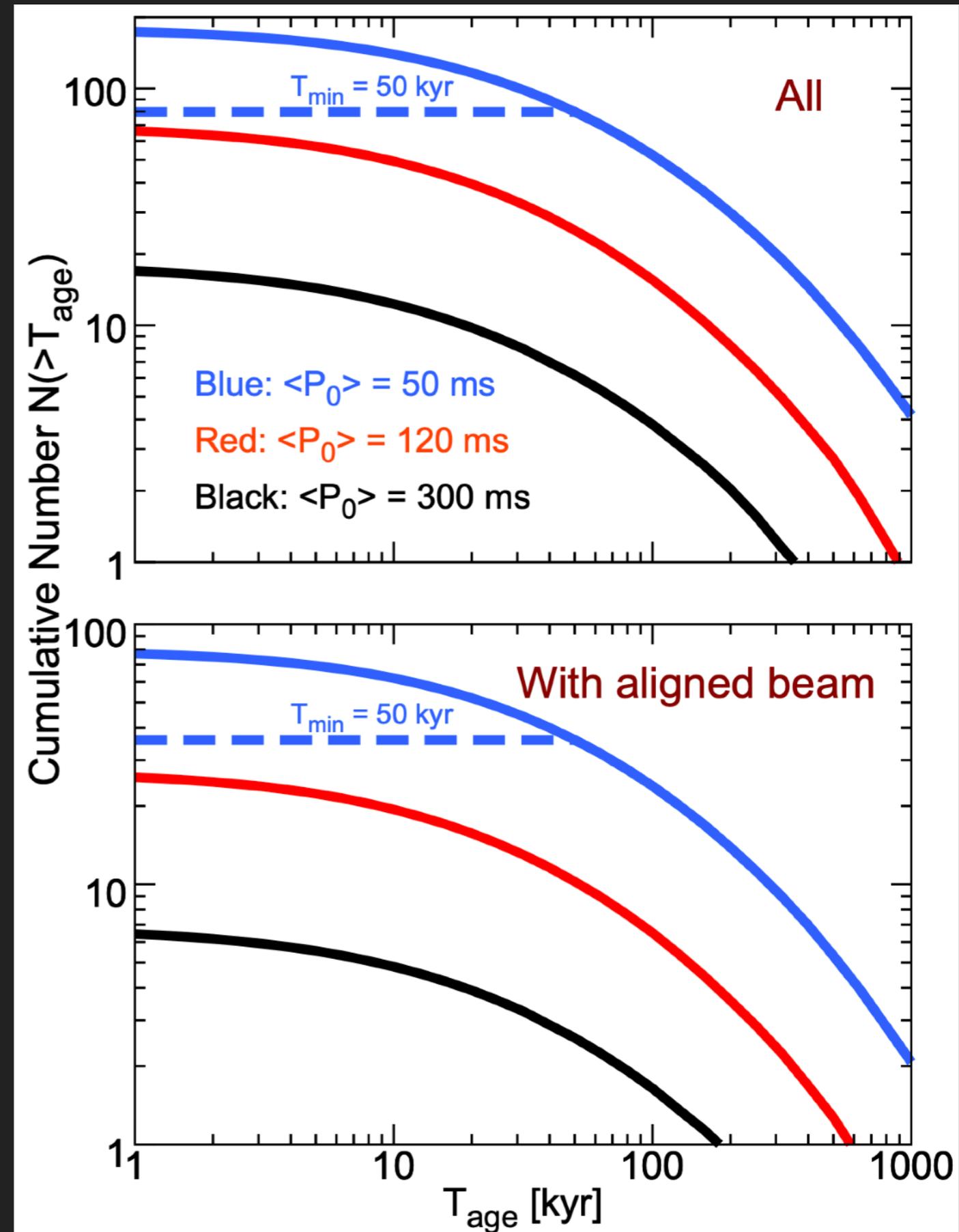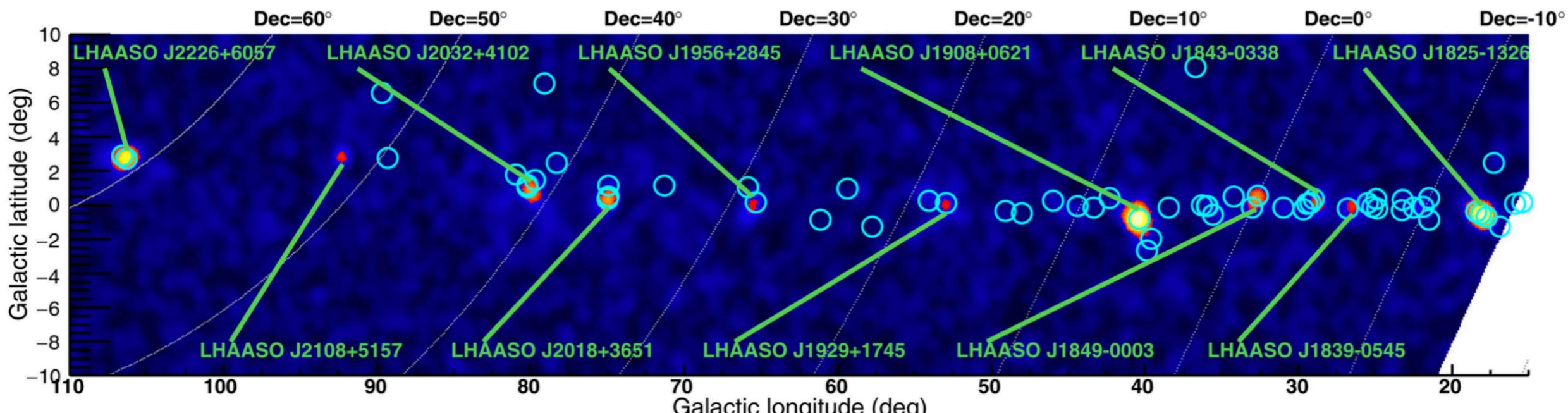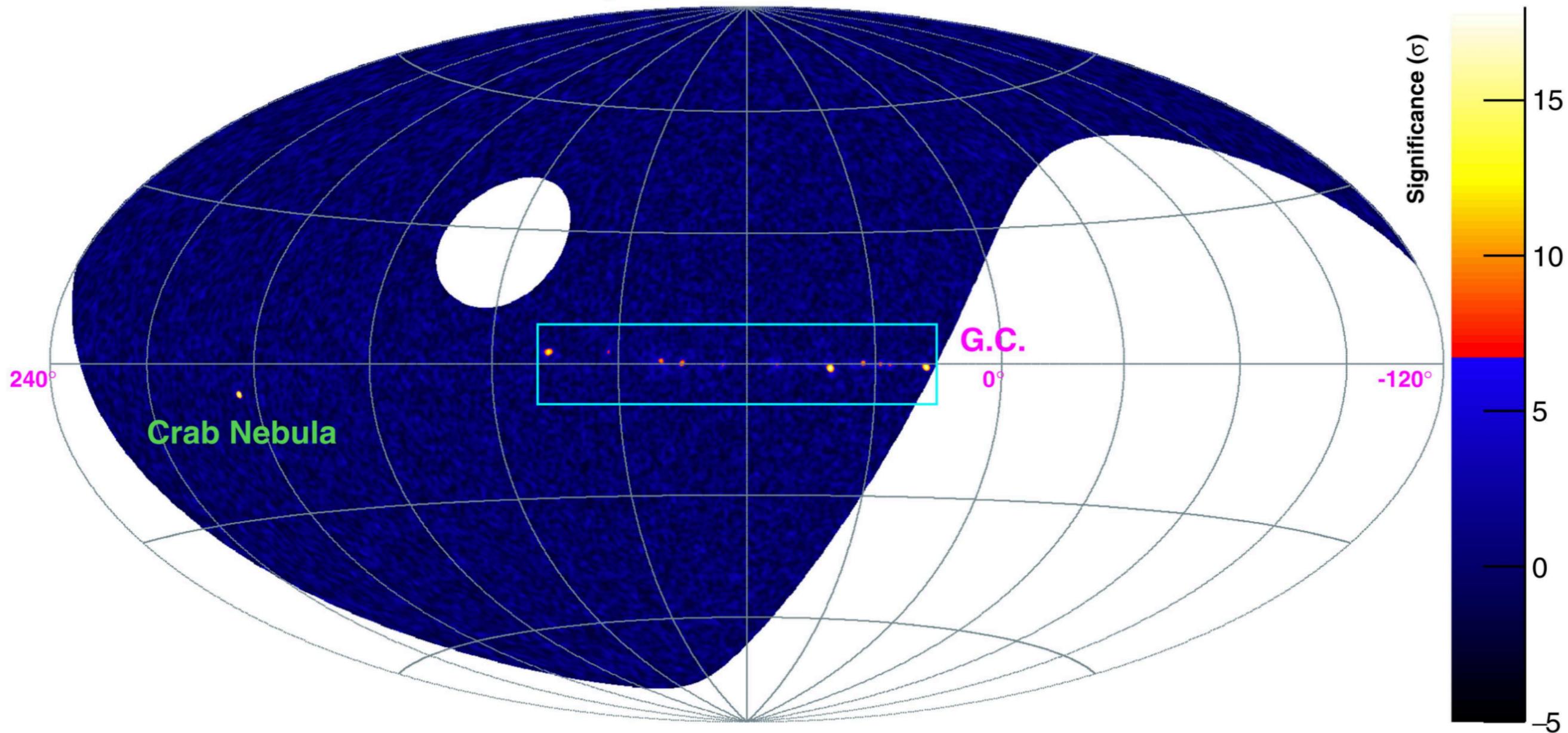
▸ Do MSPs Have TeV Halos?

▸ Tentative: **4.24σ** evidence from a HAWC stacking analysis,

▸ Using blank sky locations to test the non-Poissonian nature of the background, we still find that fewer than 1% of locations yielded the same significance as the MSP population.
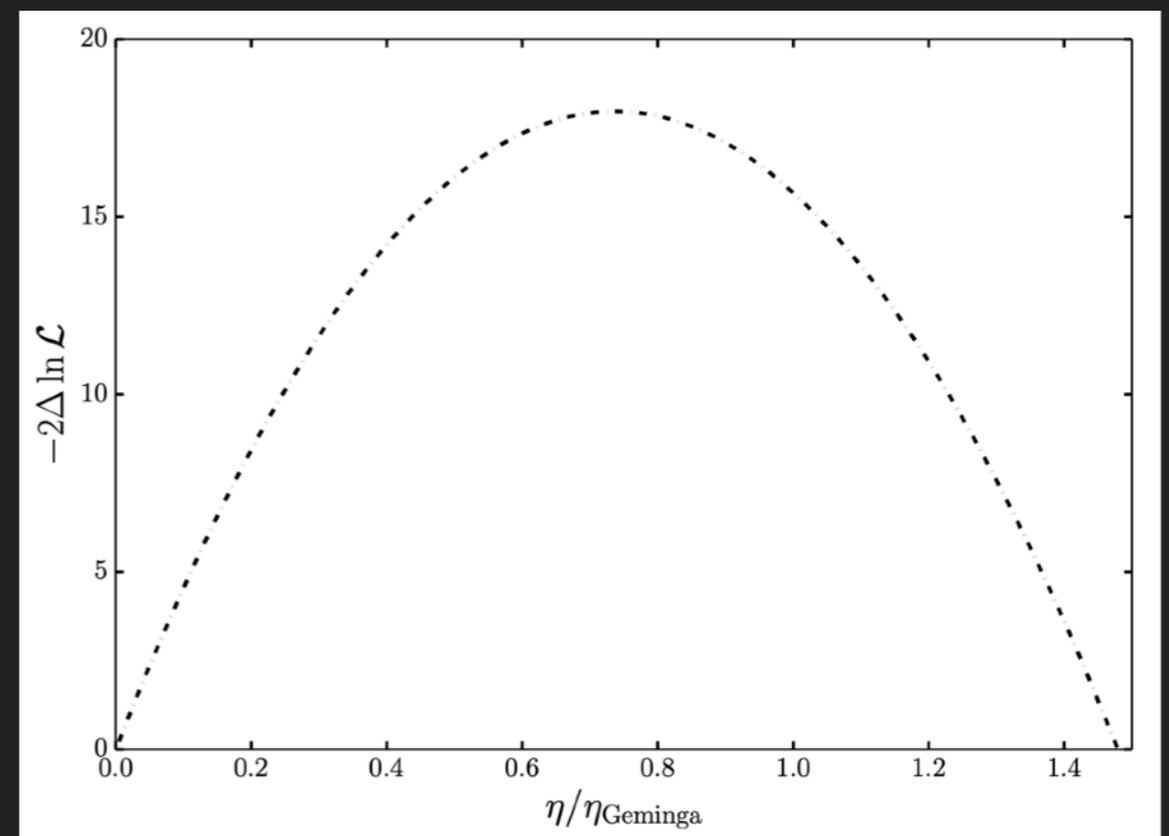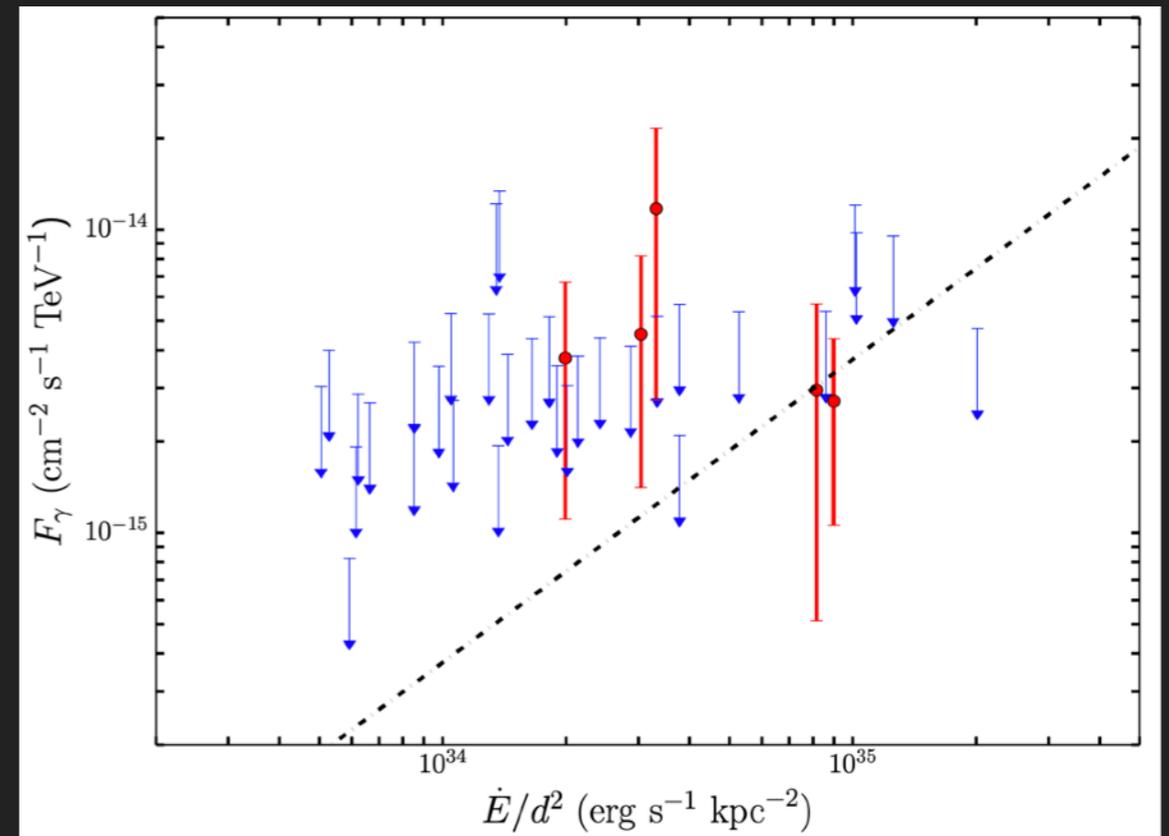
‣ Important theoretical implications:

   ‣ MSPs are a cleaner system than young pulsars

      ‣ Cosmic-Ray confinement driven by pulsar only?

   ‣ New Insights into cosmic-ray diffusion at high latitudes

      ‣ Does a high latitude pulsar produce a larger halo?

Hooper, TL (2018; 1803.08046)

- Assume MSPs in the galactic center produce a similar fraction of TeV/GeV emission

- Any MSP pulsar population bright enough to produce the GCE would overproduce the TeV diffuse gamma-ray emission observed by HESS



- Constraint likely even stricter. MSPs in the Galactic center would not have to confine the electrons to produce diffuse ICS emission.

Keith et al. (2022; 2212.08080)

‣ With HESS, you might be able to model build around this:

   ‣ MSP emission only a factor of a few too high

   ‣ Only within 0.5 degrees, which may have unusual dynamics.
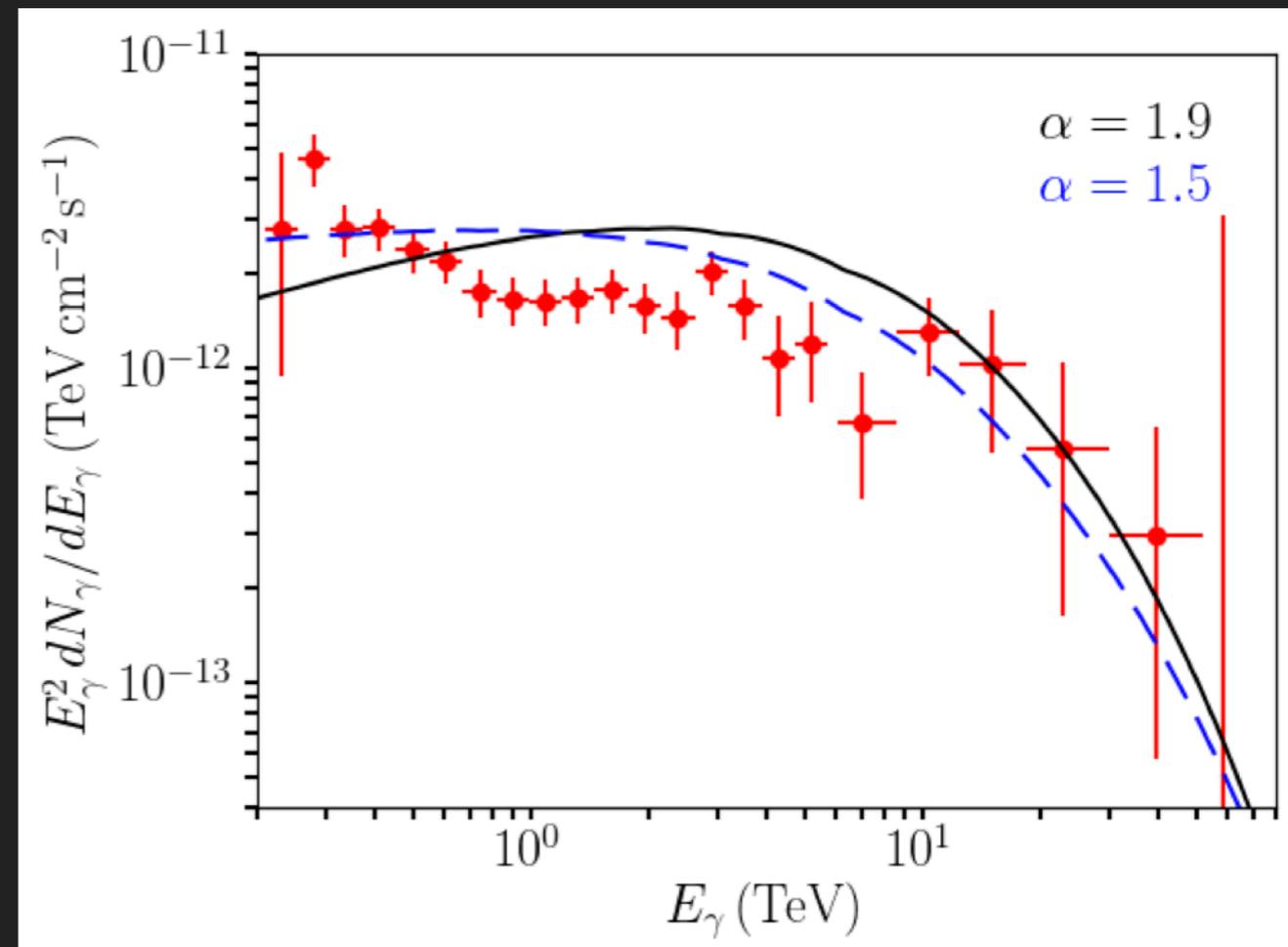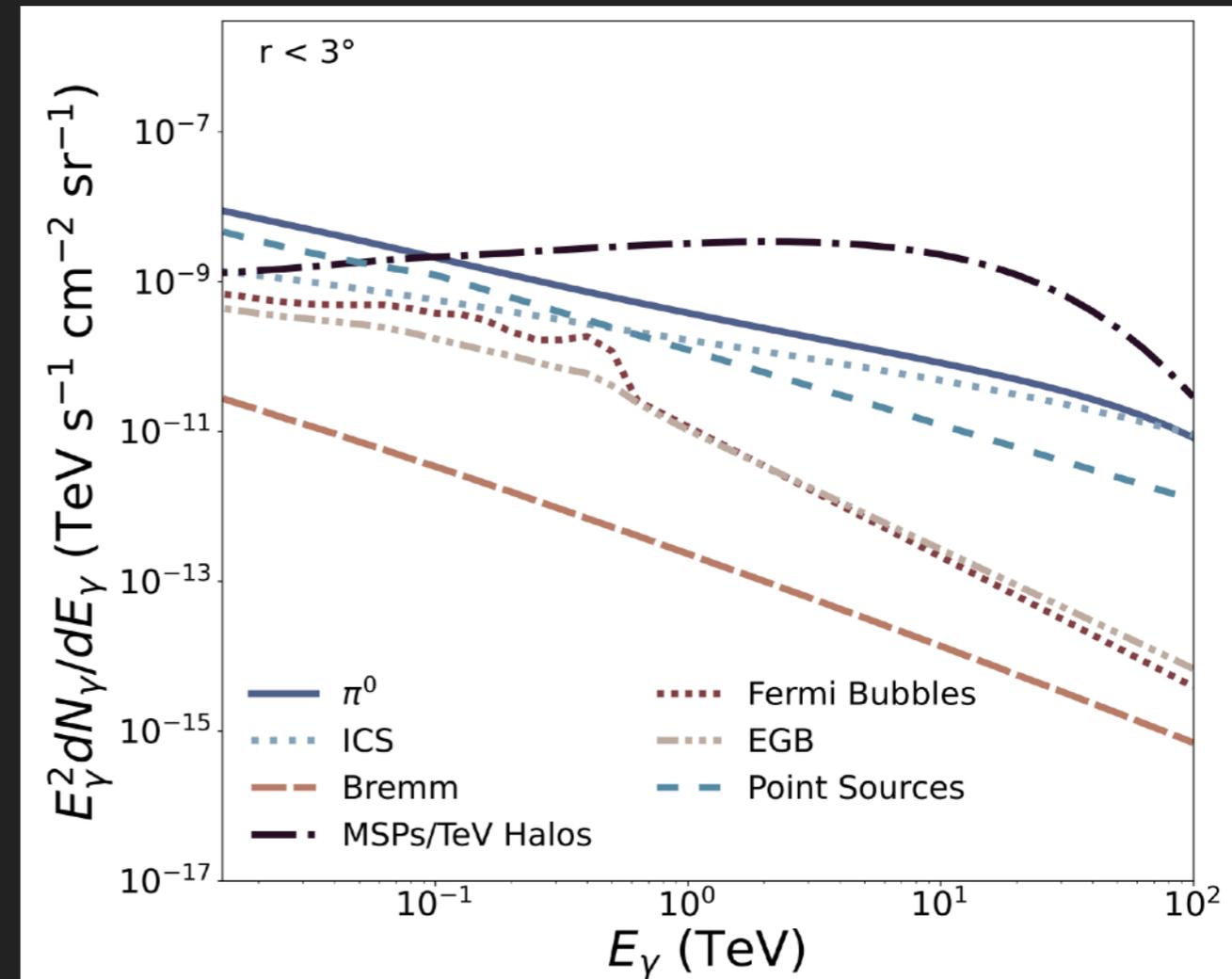


‣ CTA will definitively test an MSP origin of the galactic center excess in models where MSPs produce bright TeV emission.

Abeysekara et al. (2017; 1711.06223)

▸ Models to Explain Inhibited Diffusion:

    ▸ Diffusion Coefficient in TeV halos: $\sim 10^{28}$ cm$^2$ s$^{-1}$ at 10 TeV

    ▸ Average diffusion coefficient in Milky Way: $\sim 10^{30}$ cm$^2$s$^{-1}$ at 10 TeV
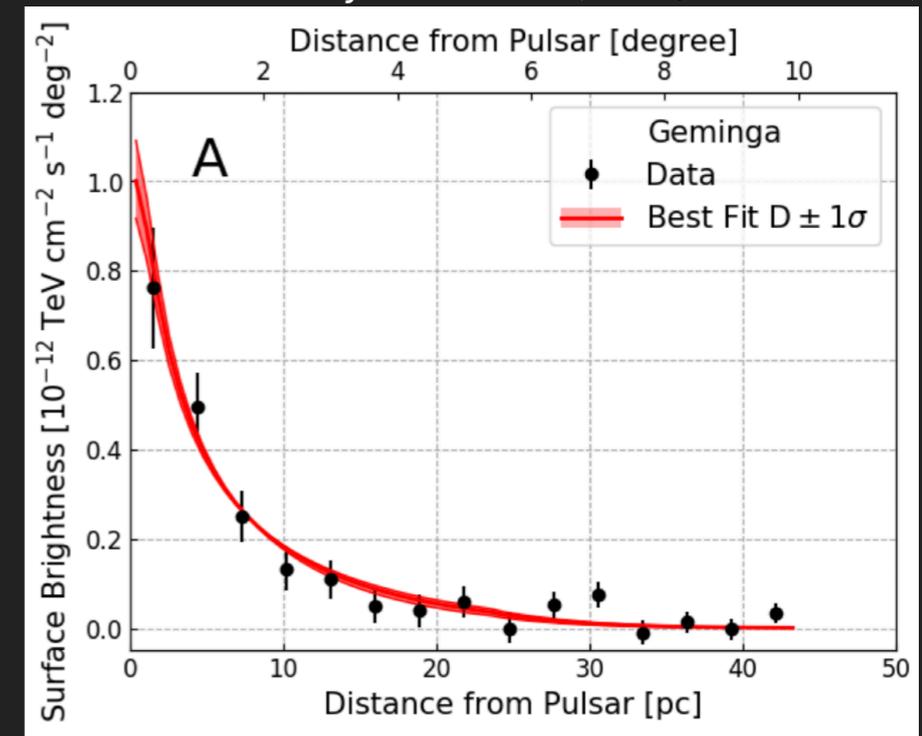
Trotta et al. (2010, 1011.0037)
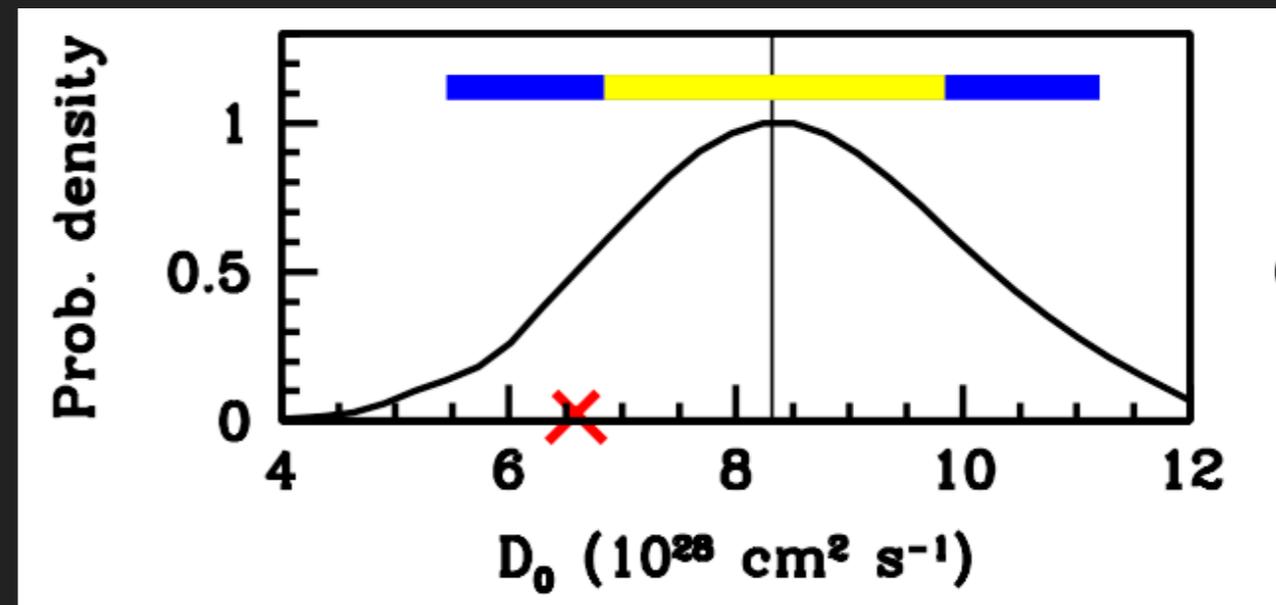
Abeysekara et al. (2017; 1711.06223)

▸ Models to Explain Inhibited Diffusion:



▸ Pre-Existing Regions of Low Diffusion

▸ Reasonable when only Geminga and Monogem were detected - but not now.



Abeysekara et al. (2017; 1711.06223)
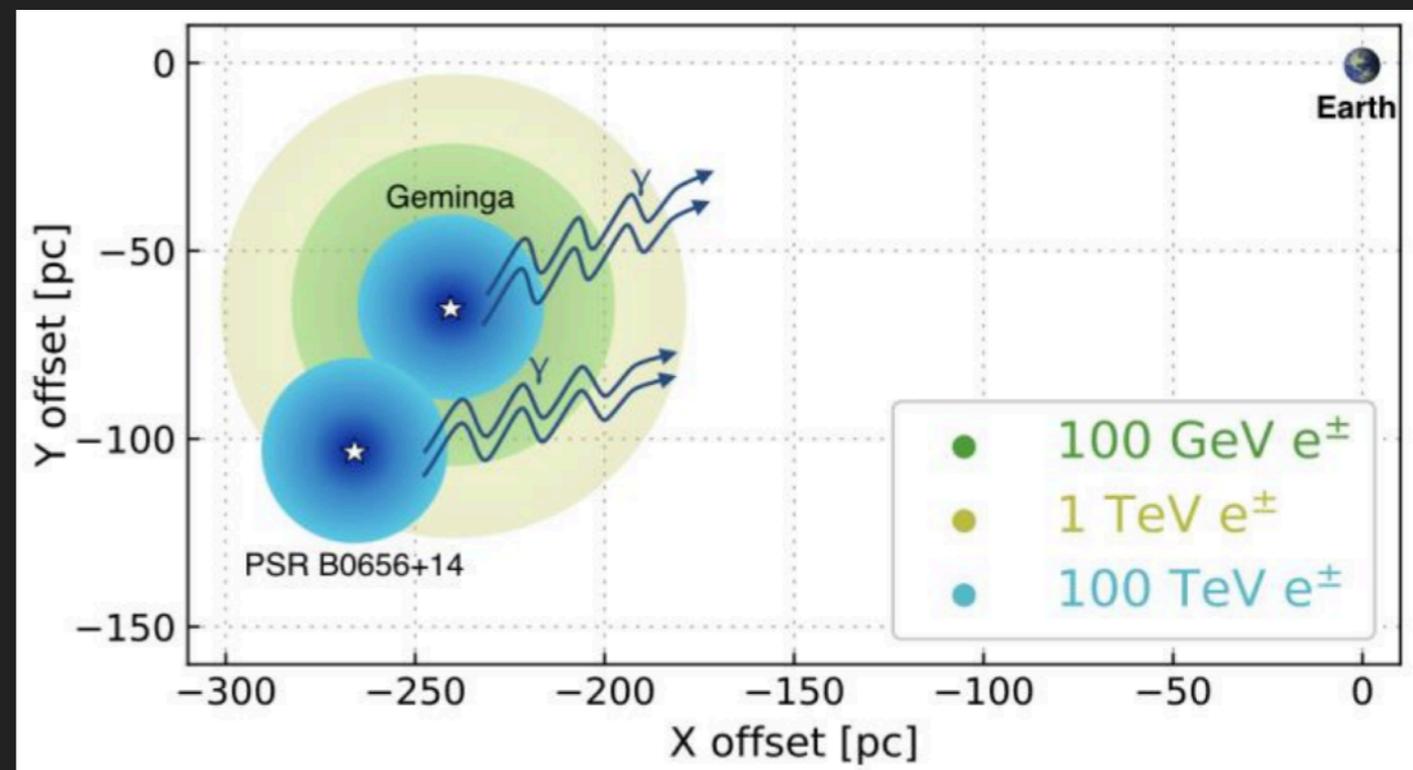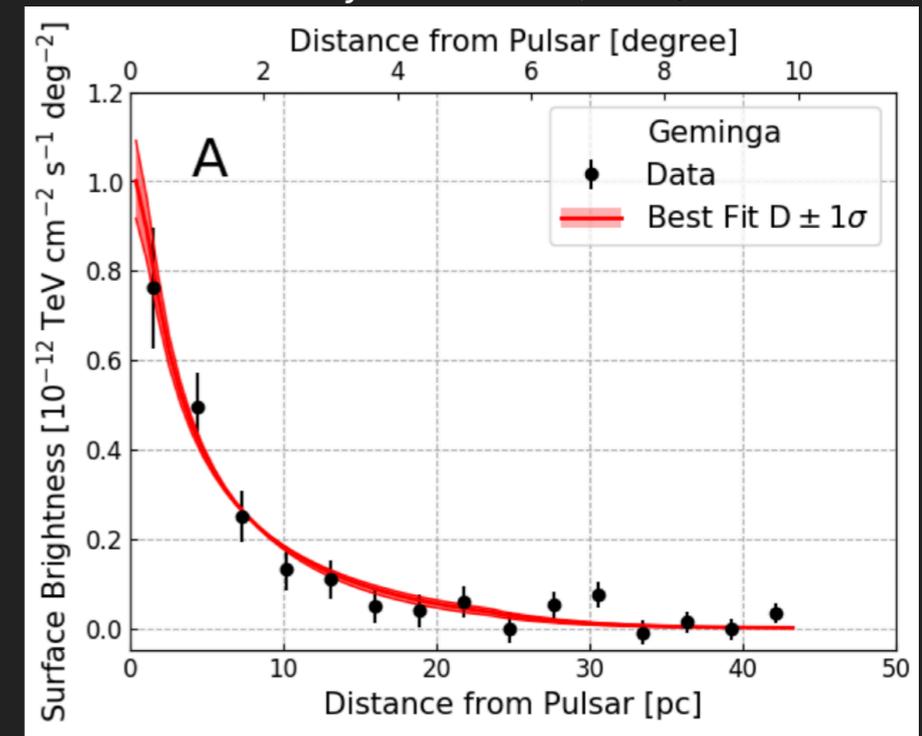
▸ Models to Explain Inhibited Diffusion:

▸ One-Dimensional Diffusion

  ▸ If magnetic field were pointed towards Earth, then you would not see significant transverse diffusion. Diffusion would "look" inhibited.

▸ Models to Explain Inhibited Diffusion:

De la Torre Luque et al. (2022; 2205.08544)
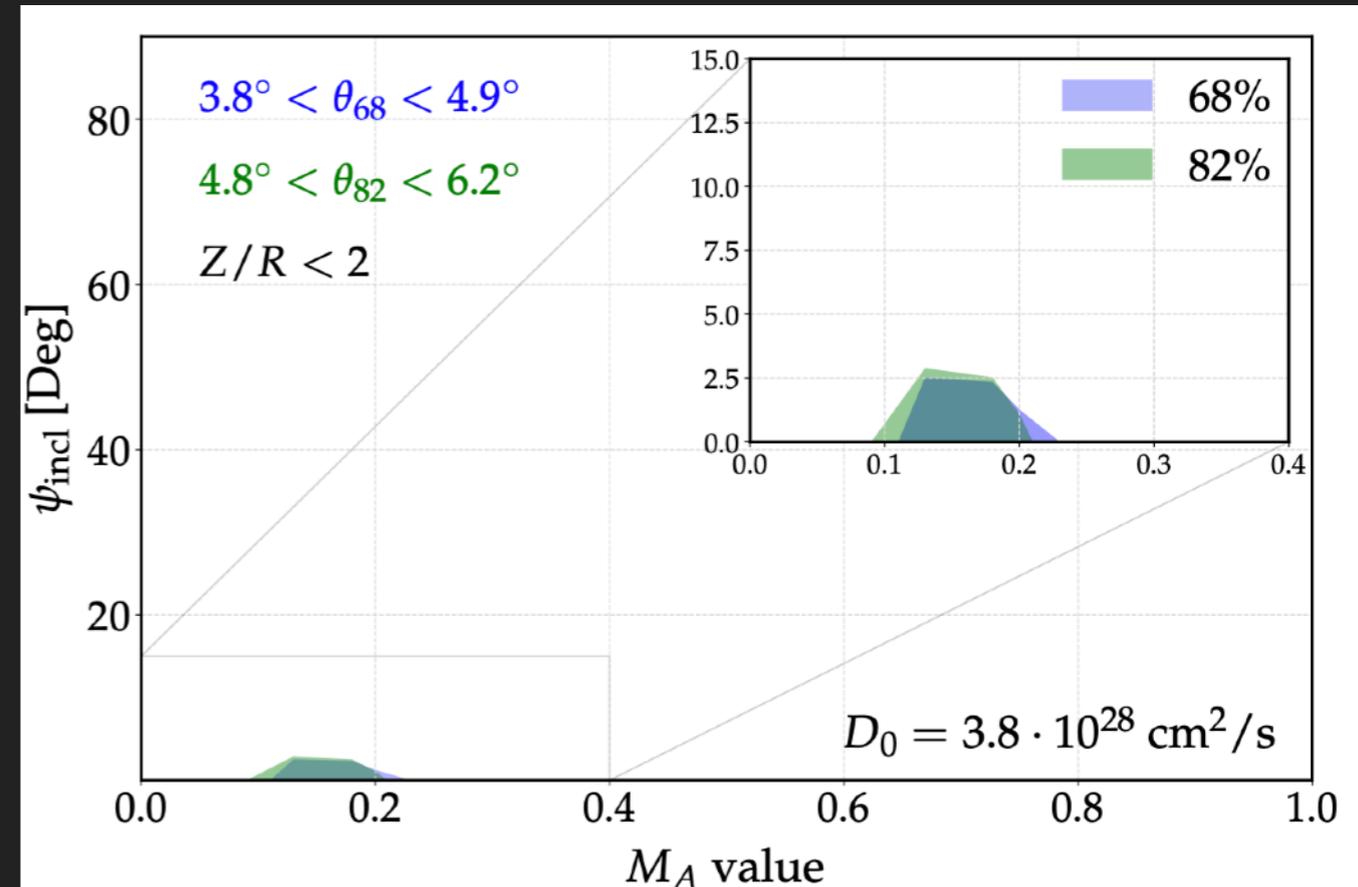


▸ One-Dimensional Diffusion

▸ Magnetic fields must be pointed along line of sight - unlikely if many halos detected.

Recchia et al. (2021; 2106.02275)
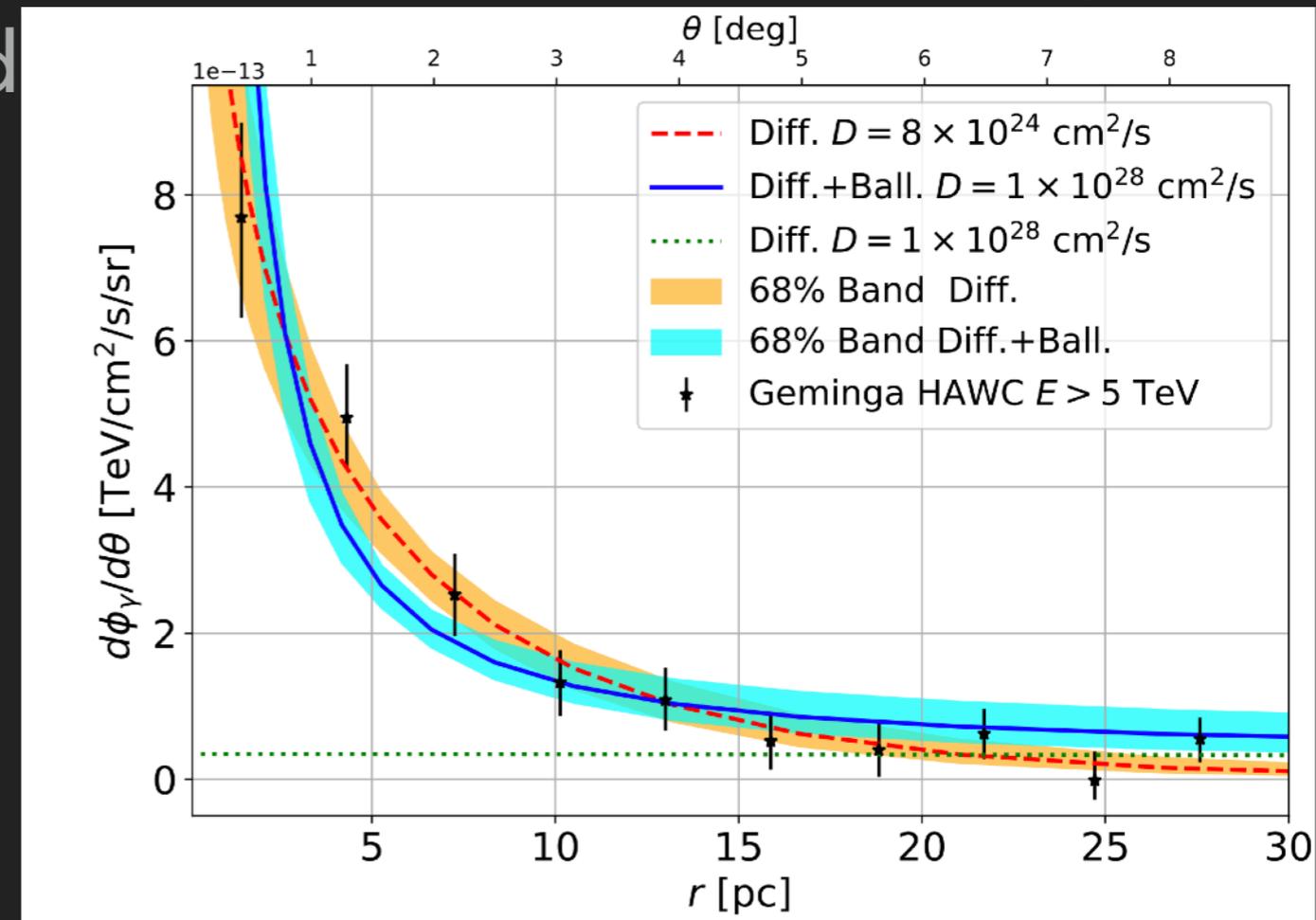
▸ # Models to Explain Inhibited Diffusion:

▸ # Transition from Ballistic Propagation

▸ If particles are moving in direct line towards us - parallel diffusion appears suppressed.

Bao, Fang & Bi (2021; 2107.07395)

Recchia et al. (2021; 2106.02275)

▸ Models to Explain Inhibited Diffusion:

▸ Transition from Ballistic Propagation

▸ However, necessary efficiency for conversion of spin down power to e+e- is much higher than 100%.

Bao, Fang & Bi (2021; 2107.07395)
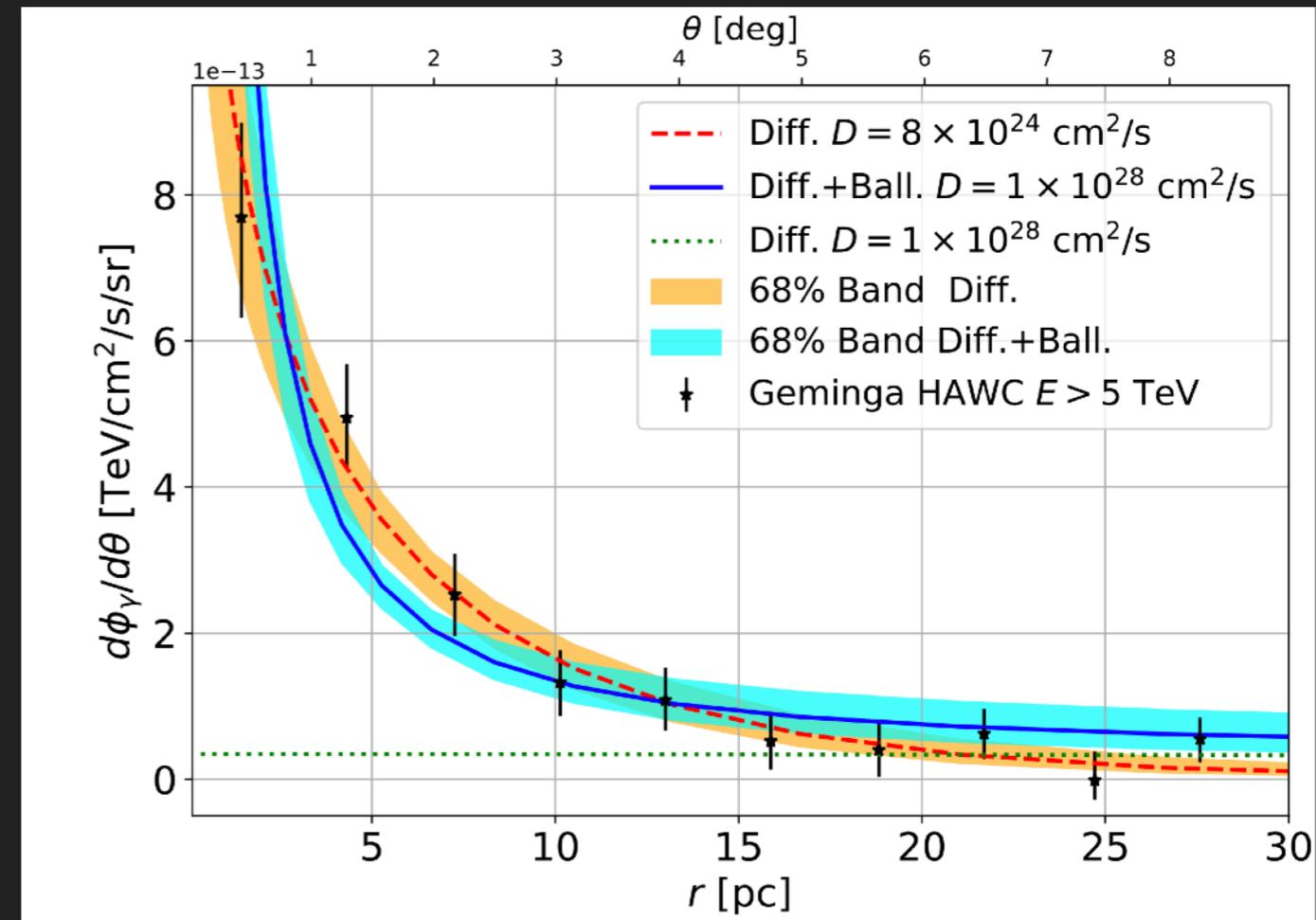
▸ Models to Explain Inhibited Diffusion:

▸ The Pulsar/SNR could actively inhibit local diffusion
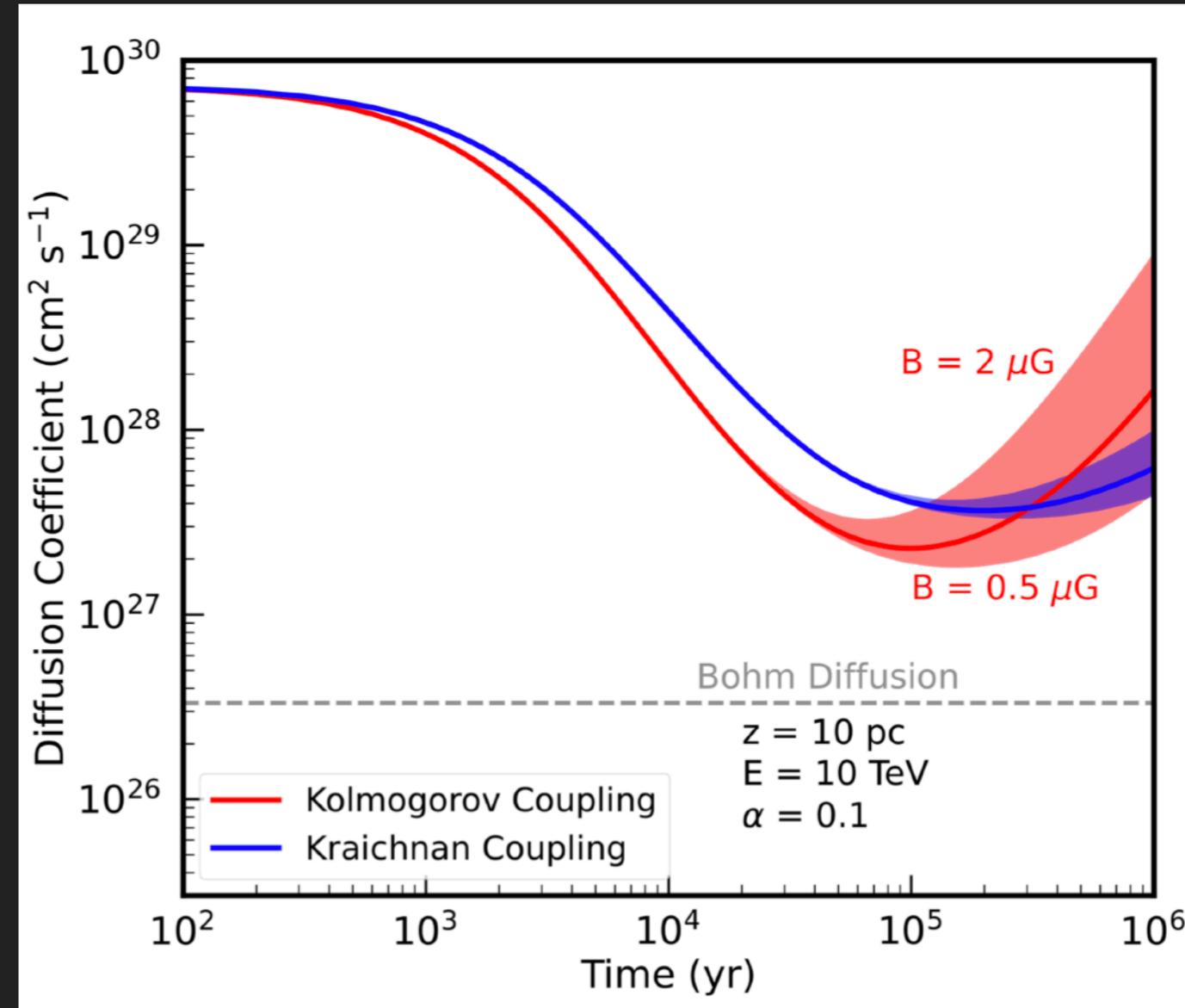


$$\frac{\partial \mathcal{W}}{\partial t} + v_A \frac{\partial \mathcal{W}}{\partial z} = (\Gamma_{\mathrm{CR}} - \Gamma_{\mathrm{D}})\mathcal{W}(k, z, t)$$

$$\Gamma_{\mathrm{CR}}(k) = \frac{2\pi}{3} \frac{c|v_A|}{k\mathcal{W}(k)\,U_0} \left[ p^4 \frac{\partial f}{\partial z} \right]_{p_{\mathrm{res}}}$$

▸ Many uncertainties in these models:

  ▸ Role of Supernova Remnant

  ▸ Disruption by molecular gas/ magnetic fields

  ▸ Pulsar Proper Motion

  ▸ 1D vs. 3D diffusion

  ▸ non-Resonant Terms

  ▸ Halos in close proximity
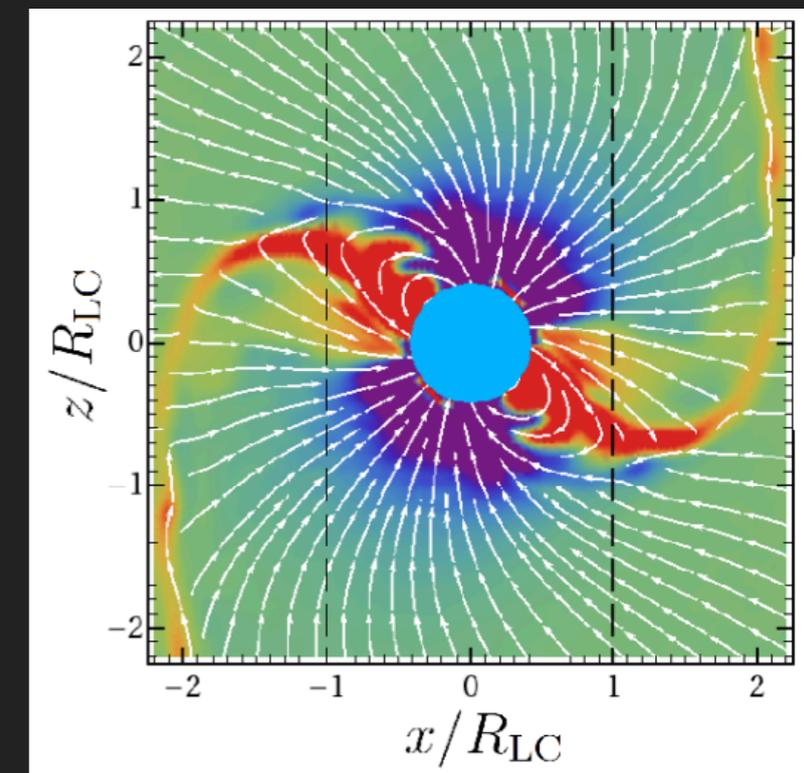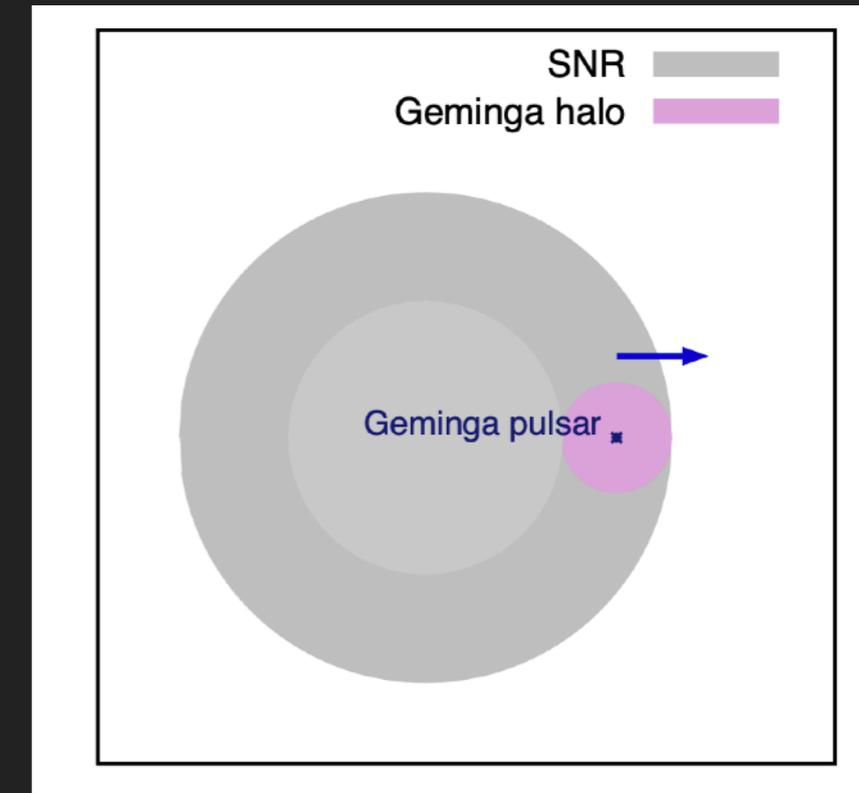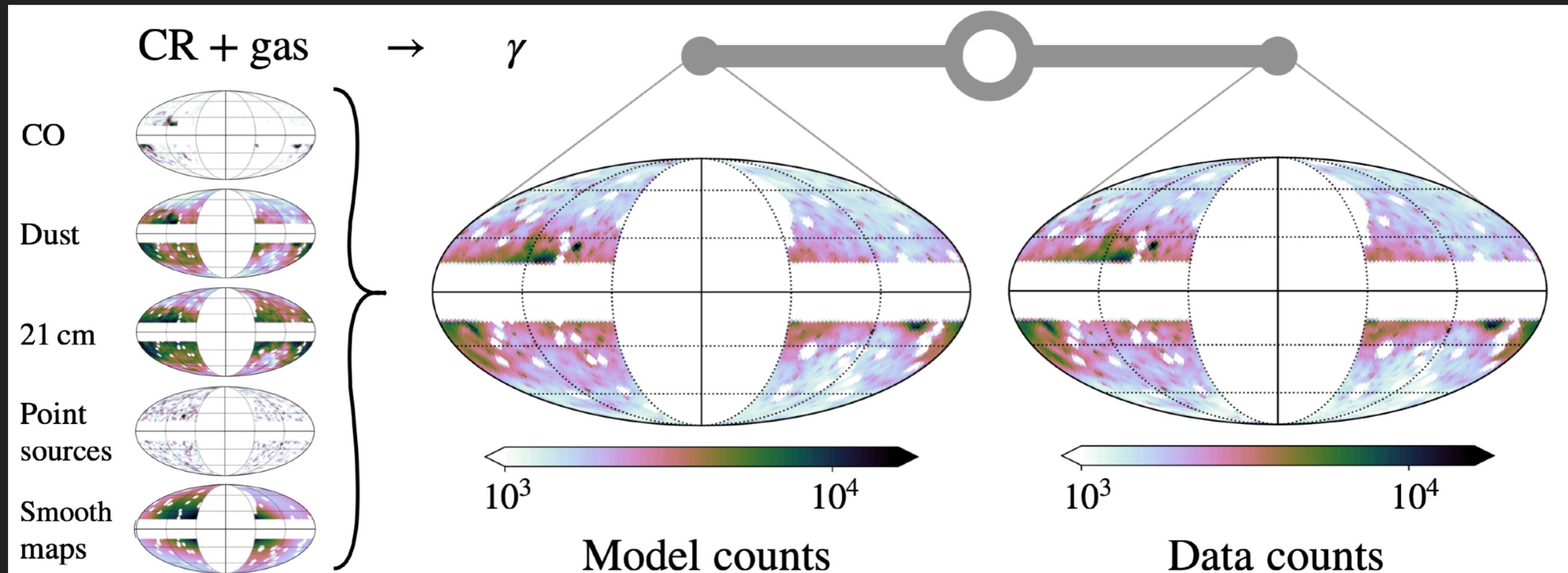
▸ Dark matter studies require accurate diffuse emission models.

▸ TeV models are expected to be very different than GeV models.

▸ Pulsar catalogs provide an answer:

    ▸ >3000 pulsars (>15000 expected from SKA)

    ▸ Specific locations, ages, and spin down powers

    ▸ Translates directly into local diffusion model in streaming instability models.

| # | PSRJ | P0 (s) | P1 | DIST (kpc) | AGE (Yr) | BSURF (G) | EDOT (ergs/s) |
|---|------|--------|-----|-----------|----------|-----------|---------------|
| 1 | J0537-6910 | 0.016122 | 5.18e-14 | 49.700 | 4.93e+03 | 9.25e+11 | 4.88e+38 |
| 2 | J0534+2200 | 0.033392 | 4.21e-13 | 2.000 | 1.26e+03 | 3.79e+12 | 4.46e+38 |
| 3 | J0540-6919 | 0.050570 | 4.79e-13 | 49.700 | 1.67e+03 | 4.98e+12 | 1.46e+38 |
| 4 | J1813-1749 | 0.044741 | 1.27e-13 | 4.700 | 5.58e+03 | 2.41e+12 | 5.60e+37 |
| 5 | J1400-6325 | 0.031182 | 3.89e-14 | 7.000 | 1.27e+04 | 1.11e+12 | 5.07e+37 |
| 6 | J1747-2809 | 0.052153 | 1.56e-13 | 8.141 | 5.31e+03 | 2.88e+12 | 4.33e+37 |
| 7 | J1833-1034 | 0.061884 | 2.02e-13 | 4.100 | 4.85e+03 | 3.58e+12 | 3.37e+37 |
| 8 | J2022+3842 | 0.048579 | 8.61e-14 | 10.000 | 8.94e+03 | 2.07e+12 | 2.96e+37 |
| 9 | J0205+6449 | 0.065716 | 1.94e-13 | 3.200 | 5.37e+03 | 3.61e+12 | 2.70e+37 |
| 10 | J2229+6114 | 0.051624 | 7.83e-14 | 3.000 | 1.05e+04 | 2.03e+12 | 2.25e+37 |
| 11 | J1513-5908 | 0.151582 | 1.53e-12 | 4.400 | 1.57e+03 | 1.54e+13 | 1.73e+37 |
| 12 | J1617-5055 | 0.069357 | 1.35e-13 | 4.743 | 8.13e+03 | 3.10e+12 | 1.60e+37 |
| 13 | J1124-5916 | 0.135477 | 7.53e-13 | 5.000 | 2.85e+03 | 1.02e+13 | 1.19e+37 |
| 14 | J1930+1852 | 0.136855 | 7.51e-13 | 7.000 | 2.89e+03 | 1.03e+13 | 1.16e+37 |
| 15 | J1023-5746 | 0.111472 | 3.84e-13 | 2.080 | 4.60e+03 | 6.62e+12 | 1.09e+37 |
| 16 | J1420-6048 | 0.068180 | 8.32e-14 | 5.632 | 1.30e+04 | 2.41e+12 | 1.04e+37 |
| 17 | J1410-6132 | 0.050052 | 3.20e-14 | 13.510 | 2.48e+04 | 1.28e+12 | 1.01e+37 |
| 18 | J1849-0001 | 0.038523 | 1.42e-14 | * | 4.31e+04 | 7.47e+11 | 9.78e+36 |
| 19 | J1402+13 | 0.005890 | 4.83e-17 | * | 1.93e+06 | 1.71e+10 | 9.34e+36 |
| 20 | J1846-0258 | 0.326571 | 7.11e-12 | 5.800 | 7.28e+02 | 4.88e+13 | 8.06e+36 |
| 21 | J0835-4510 | 0.089328 | 1.25e-13 | 0.280 | 1.13e+04 | 3.38e+12 | 6.92e+36 |
| 22 | J1811-1925 | 0.064667 | 4.40e-14 | 5.000 | 2.33e+04 | 1.71e+12 | 6.42e+36 |
| 23 | J1111-6039 | 0.106670 | 1.95e-13 | * | 8.66e+03 | 4.62e+12 | 6.35e+36 |
| 24 | J1813-1246 | 0.048072 | 1.76e-14 | 2.635 | 4.34e+04 | 9.30e+11 | 6.24e+36 |
| 25 | J1838-0537 | 0.145708 | 4.72e-13 | * | 4.89e+03 | 8.39e+12 | 6.02e+36 |
| 26 | J1838-0655 | 0.070498 | 4.92e-14 | 6.600 | 2.27e+04 | 1.89e+12 | 5.55e+36 |
| 27 | J1418-6058 | 0.110573 | 1.69e-13 | 1.885 | 1.03e+04 | 4.38e+12 | 4.95e+36 |
| 28 | J1935+2025 | 0.080118 | 6.08e-14 | 4.598 | 2.09e+04 | 2.23e+12 | 4.66e+36 |
| 29 | J1856+0245 | 0.080907 | 6.21e-14 | 6.318 | 2.06e+04 | 2.27e+12 | 4.63e+36 |
| 30 | J1112-6103 | 0.064962 | 3.15e-14 | 4.500 | 3.27e+04 | 1.45e+12 | 4.53e+36 |
| 31 | J1640-4631 | 0.206443 | 9.76e-13 | 12.750 | 3.35e+03 | 1.44e+13 | 4.38e+36 |
| 32 | J1844-0346 | 0.112855 | 1.55e-13 | * | 1.16e+04 | 4.23e+12 | 4.25e+36 |
| 33 | J1952+3252 | 0.039531 | 5.84e-15 | 3.000 | 1.07e+05 | 4.86e+11 | 3.74e+36 |
| 34 | J1826-1256 | 0.110224 | 1.21e-13 | 1.550 | 1.44e+04 | 3.70e+12 | 3.58e+36 |
| 35 | J1709-4429 | 0.102459 | 9.30e-14 | 2.600 | 1.75e+04 | 3.12e+12 | 3.41e+36 |
| 36 | J2021+3651 | 0.103741 | 9.57e-14 | 1.800 | 1.72e+04 | 3.19e+12 | 3.38e+36 |
| 37 | J1524-5625 | 0.078219 | 3.90e-14 | 3.378 | 3.18e+04 | 1.77e+12 | 3.21e+36 |
| 38 | J1357-6429 | 0.166108 | 3.60e-13 | 3.100 | 7.31e+03 | 7.83e+12 | 3.10e+36 |
| 39 | J1913+1011 | 0.035909 | 3.37e-15 | 4.613 | 1.69e+05 | 3.52e+11 | 2.87e+36 |
| 40 | J1826-1334 | 0.101487 | 7.53e-14 | 3.606 | 2.14e+04 | 2.80e+12 | 2.84e+36 |
| 41 | J1907+0602 | 0.106633 | 8.68e-14 | 2.370 | 1.95e+04 | 3.08e+12 | 2.83e+36 |
| 42 | J1801-2451 | 0.124924 | 1.28e-13 | 3.803 | 1.55e+04 | 4.04e+12 | 2.59e+36 |
| 43 | J1016-5857 | 0.107386 | 8.08e-14 | 3.163 | 2.10e+04 | 2.98e+12 | 2.58e+36 |
| 44 | J1747-2958 | 0.098814 | 6.13e-14 | 2.520 | 2.55e+04 | 2.49e+12 | 2.51e+36 |
| 45 | J1105-6107 | 0.063202 | 1.58e-14 | 2.360 | 6.32e+04 | 1.01e+12 | 2.48e+36 |
| 46 | J1119-6127 | 0.407963 | 4.02e-12 | 8.400 | 1.61e+03 | 4.10e+13 | 2.34e+36 |
| 47 | J1824-2452A | 0.003054 | 1.62e-18 | 5.500 | 2.99e+07 | 2.25e+09 | 2.24e+36 |
| 48 | J1803-2137 | 0.133667 | 1.34e-13 | 4.400 | 1.58e+04 | 4.29e+12 | 2.22e+36 |
| 49 | J1135-6055 | 0.114943 | 7.93e-14 | * | 2.30e+04 | 3.05e+12 | 2.06e+36 |
| 50 | J1048-5832 | 0.123725 | 9.61e-14 | 2.900 | 2.04e+04 | 3.49e+12 | 2.00e+36 |

Gaggero et al. (2014; 1411.7623)

▸ First attempts at this approach.

▸ Decreasing diffusion in the spiral arms produces better fits to GeV gamma-ray data



Jóhannesson et al. (2019.1903.05509)
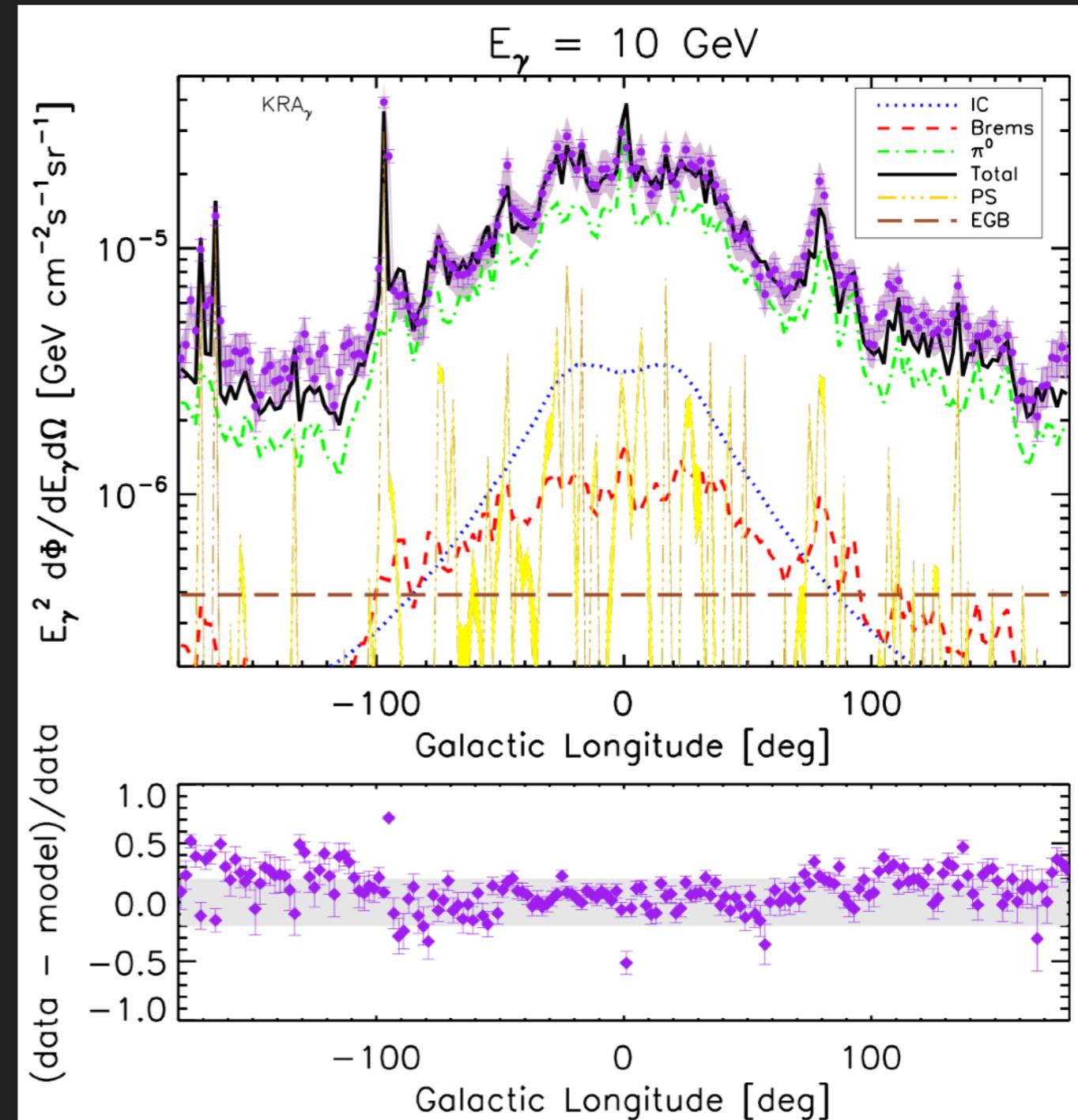
▸ Galprop models illustrate the problem.

  ▸ Adding sources produces huge residuals in TeV leptonic maps.

  ▸ Need to know where the sources go and how they work to solve this.

Porter et al. (2019; 1909.02223)
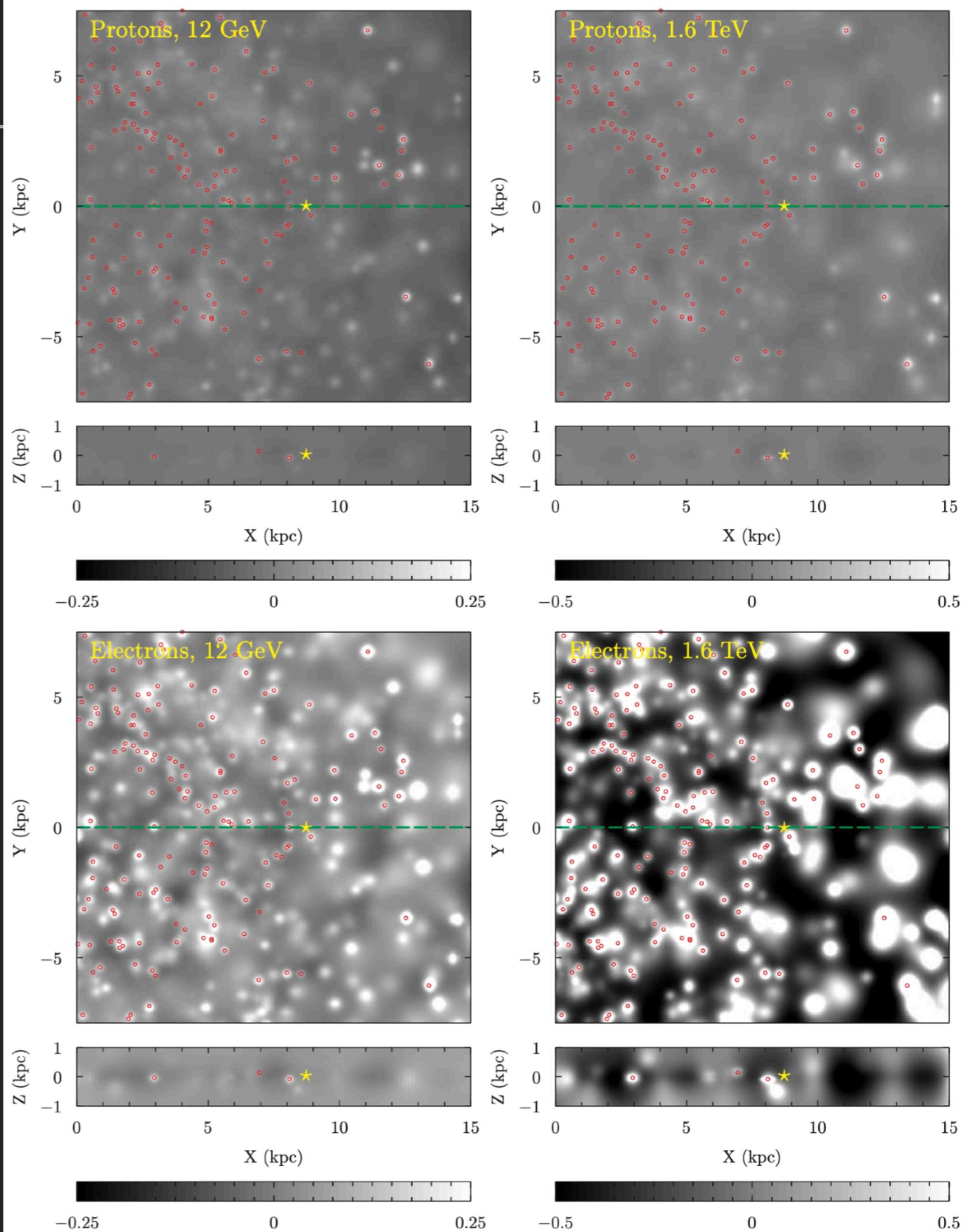
▸ Leptons are likely a dominant diffuse emission component at TeV energies.

▸ Standard methods of building a diffuse model fail for TeV leptons.

▸ The solution is the sources

   ▸ Radio/Gamma-Ray Observations of Pulsars

   ▸ Theoretical models to transfer information about pulsar age/spindown power/environment into information about local diffusion.

# Extra Slides